Effect of ultraviolet/visible radiation processing on the quality of fruit juices

Karla Aguilar Lara

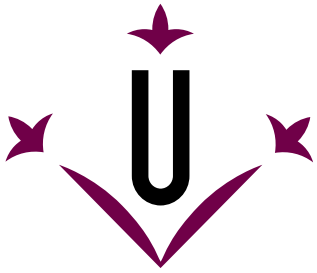

Universitat de Lleida

DOCTORAL THESIS

Effect of ultraviolet/visible radiation processing on the quality of fruit juices

Karla Aguilar Lara

Dissertation presented to fulfil the requirements to obtain the degree of
Doctor by The University of Lleida
Doctoral Program of Agricultural and Food Science and Technology

Directors
Albert Ibarz Ribas
Alfonso Garvín Arnés

2017

A los mexicanos que trabajan
por una vida mejor

¿En perseguirme, mundo, qué interesas?
¿En qué te ofendo, cuando sólo intento
poner bellezas en mi entendimiento
y no mi entendimiento en las bellezas?

Sor Juana Inés de la Cruz

This thesis was undertaken in the Department of Food Technology of the Technical Superior School of Agricultural Engineering at the University of Lleida (Lleida, Catalonia, Spain). The research was funded by the Ministry of Science and Innovation of the Spanish Government in the CTQ2011-26569 project. Part of the research was performed with the Group of Studies on Processing and Engineering (Ge^2P) in the Department of Agrifood Industry, Food and Nutrition (LAN) of the Luiz de Queiroz College of Agriculture (ESALQ) at the University of São Paulo (USP, Brazil). This piece of work was part of project no.º 2014/16998-3, funded by the São Paulo Research Foundation (FAPESP, Brazil), and project no.° 401004/2014-7, funded by The National Council for Scientific and Technological Development (CNPq, Brazil).

My doctoral studies were sponsored by the National Council of Science and Technology of the Mexican Government (CONACyT, Mexico) by means of a fellowship for post-graduate foreign studies. The stay at the University of São Paulo was supported by the Research Vice-chancellor's Office of the University of Lleida.

Finally, this thesis has received a grant for its linguistic revision from the Language Institute of the University of Lleida (2017 call).

SUMMARY

Fresh fruit juices are nutritious refreshing beverages. For commercialization, they need to be submitted to a process to inactivate microorganisms and enzymes. Thermal pasteurization, commonly used for this purpose, alters the organoleptic and nutritional quality of food. Besides, it does not eliminate mycotoxins and induces the formation of the potentially toxic 5-hydroxymethylfurfural (HMF). Ultraviolet irradiation is an alternative for fruit juice pasteurization due to its effectiveness at inactivating microorganisms and enzymes as well as destroying mycotoxins. This work studied the effect of ultraviolet-visible (UV-Vis) irradiation processing on the quality attributes of clarified fruit juices.

The results showed that UV irradiation does not produce HMF and is capable of degrading it. A three-stage mechanism related to the radiation absorbed by the liquid sample was proposed to describe the photo-degradation of this compound. From this mechanism, three kinetic models were developed to describe this process: first-order, zero-order and/or pseudo-first-order. The fitness to the model depended on the initial concentration of HMF. On applying the kinetic and thermodynamic compensation theory, it was concluded that the HMF photo-degradation process is entropically controlled and can be speeded up by changing non-thermal parameters such as agitation. On the contrary, when a multi-wavelenght emission lamp was used, the photo-degradation of L-ascorbic acid was insignificant.

After the UV-Vis treatments, most of the physicochemical parameters of the fruit juices were practically unaltered. The enzymes polyphenoloxidase and peroxidase were totally or partially inactivated, the higher the temperature the higher the inactivation. To sum up, UV-Vis processing combined with mild-heating for fruit juice pasteurization is an alternative to traditional methods, since it is effective inactivating enzymes, preserves quality attributes of the product and does not produce HMF.

RESUM (Catalan)

Els sucs frescs són begudes refrescants i nutritives. Per a la seva comercialització, els sucs acabats de fer necessiten ser sotmès a un procés per a la inactivació de microorganismes i enzims. La pasteurització tèrmica, comunament utilitzada per aquest propòsit, altera la qualitat organolèptica i nutricional dels aliments. A més, no elimina les micotoxines i indueix la formació del potencialment tòxic 5-hidroximetil-furfural (HMF). La irradiació ultraviolada és una alternativa per a la pasteurització de suc de fruita a causa de la seva eficàcia inactivant microorganismes i enzims, així com la destrucció de les micotoxines. En aquest treball es va estudiar l'efecte de la irradiació ultraviolada-visible (UV-Vis) en els atributs de qualitat de sucs clarificats.

Els resultats van mostrar que la irradiació UV no produeix HMF i és capaç de degradar-lo. Per descriure la reacció de degradació de HMF és va proposar un mecanisme de tres etapes, relacionat amb la radiació absorbida per la mostra líquida. A partir d'aquest mecanisme, tres models cinètics van ser desenvolupats per a descriure aquest procés: primer ordre, d'ordre zero i/o de pseudo-primer ordre. L'aptitud per al model va dependre de la concentració inicial de HMF. Aplicant la teoria de la compensació cinètica i termodinàmica es va concloure que el procés de foto-degradació de HMF es controlat entròpicament i pot ser accelerat canviant paràmetres no tèrmics com agitació. Per contra, amb el us d'una làmpada de emissió múltiple la foto-degradació de l'àcid L-ascòrbic va ser insignificant.

Després dels tractaments d'UV-Vis, la majoria dels paràmetres fisicoquímics dels sucs de fruita van ser pràcticament inalterats. Els enzims polifenol oxidasa i peroxidasa van ser totalment o parcialment inactivades; a major temperatura major inactivació. Per resumir, el processament d'UV-Vis combinat amb lleu escalfament per a la pasteurització de sucs és una alternativa als mètodes tradicionals, ja que és efectiu inactivant enzims, conserva els atributs de qualitat del producte i no produeix HMF.

RESUMEN (Spanish)

Los zumos frescos son bebidas refrescantes nutritivas. Para su comercialización, los jugos recién extraídos deben someterse a un proceso para inactivar microorganismos y enzimas. La pasteurización térmica, comúnmente usada con este propósito, altera la calidad organoléptica y nutricional del alimento. Además, no elimina las micotoxinas e induce la formación del potencialmente tóxico 5-hidroximetilfurfural (HMF). La irradiación con ultravioleta es una alternativa para la pasteurización de zumos debido a su efectividad inactivando microorganismos y enzimas así com destruyendo micotoxinas. Este trabajo estudió el efecto de la irradiación ultravioleta-visible (UV-Vis) en atributos de calidad de zumos clarificados.

Los resultados mostraron que la irradiación UV no produce HMF y es capaz de degradarlo. Para describir la reacción se propuso un mecanismo de degradación en tres etapas, relacionado con la radiación absorbida por la muestra líquida. A partir de este mecanismo se desarrollaron tres modelos cinéticos: primer orden, orden cero y pseudo-primer orden. El modelo apropiado dependió de la concentración inicial de HMF. Aplicando la teoría de la compensación cinética y termodinámica, se concluyó que el proceso de foto-degradación está controlado entrópciamente y puede ser acelerado cambiando parámetros no térmicos como la agitación. Por el contrario, al usar una lámpara de emisión múltiple la foto-degradación del ácido L-ascórbico fue insignificante.

Después de los tratamientos UV-Vis, la mayoría de los parámetros fisicoquímicos de los zumos fueron prácticamente inalterados. Las enzimas polifenoloxidasa y peroxidasa fueron totalmente o parcialmente inactivadas; a mayor temperatura, mayor inactivación. En resumen, el procesamiento UV-Vis combinado con calentamiento suave para la pasteurización de zumos es una alternativa a los tratamientos térmicos convencionales ya que es efectivo inactivando enzimas, preserva los atributos de calidad del producto y no produce HMF.

RESUMO (Portuguese)

Os sucos frescos são bebidas nutritivas e refrescantes. Para sua comercialização, eles precisam de ser submetidos a um processo para inativar microrganismos e enzimas. A pasteurização térmica, comunamente utilizada para este fim, altera a qualidade organoléptica e nutricional dos alimentos. Além disso, não elimina as micotoxinas e induz a formação do potencialmente tóxico 5-hidroximetilfurfural (HMF). A irradiação ultravioleta é uma alternativa para a pasteurização de sucos devido à sua eficácia inativando microrganismos e enzimas, bem como destruindo micotoxinas. Este trabalho estudou o efeito da irradiação ultravioleta-visível (UV-Vis) sobre os atributos de qualidade dos sucos clarificados.

Os resultados mostraram que a irradiação UV não produz HMF e é capaz de degradá-la. Um mecanismo de três fases, relacionado com a radiação absorvida pela amostra líquida, foi proposto para descrever a reação de degradação de HMF. A partir desse mecanismo, três modelos cinéticos foram desenvolvidos para descrever esse processo: primeira ordem, ordem zero e/ou pseudo-primeira ordem. A adequação ao modelo dependia da concentração inicial de HMF. Aplicando a teoria da compensação cinética e termodinâmica, concluiu-se que o processo de fotodegradação de HMF é controlado entropicamente e pode ser acelerado pela alteração de parâmetros não-térmicos como a agitação. Pelo contrário, utilizando uma lâmpada de emissão de multi-comprimento de onda a fotodegradação do ácido L-ascórbico foi insignificante.

Após os tratamentos UV-Vis, a maioria dos parâmetros físico-químicos dos sucos de frutas foram praticamente inalterados. As enzimas polifenoloxidase e peroxidase foram inativadas total ou parcialmente, quanto maior a temperatura, maior a inativação. Resumindo, o processamento UV-Vis combinado com o aquecimento suave para a pasteurização de suco de frutas é uma alternativa aos tratamentos de calor convencionais, uma vez que é eficaz inativando enzimas, preserva os atributos de qualidade do produto e não produz HMF.

TABLE OF CONTENTS

NOMENCLATURE AND MAIN ABREVIATIONS

Nomenclature

UV irradiation

A	Reactor dimension on the x axis
B	Reactor dimension on the y axis
C	Reactor dimension on the z axis
$A(\lambda)$	Absorbance of the solution at wavelength λ
$A_{10}(\lambda)$	10-base logarithm absorbance at wavelength λ
$A_e(\lambda)$	e-base logarithm absorbance at wavelength λ
C_A	Concentration of the absorber substance present in the solution
D	Radius of the sphere defined by both the emitting lamp point as the sphere centre and the solution point considered
D_r	UV dose expressed in $J \cdot cm^{-2}$
D_S	Path length of light through the solution
D_{UV}	UV dose expressed in $J \cdot L^{-1}$
i	Each layer of the reactor
L	Lamp length
n	Number of layers of the reactor
P_{abs}	Total spectral radiant power absorbed by the whole solution and the whole lamp per volume unit
P_{emit}	Real power emitted by the lamp
$P_{emit,\lambda}$	Real power emitted by the lamp at wavelength λ
$P(0)$	Incident spectral radiant power on the surface of the reactor for this whole surface
$P(C)$	Incident spectral radiant power at the bottom of the reactor for this whole surface
$P(x,y,z)$	Total radiant power reaching the specific point (x,y,z) in the solution from a specific point in the lamp
$P_\lambda(x,y,z)$	Spectral radiant power reaching the specific point (x,y,z) in the solution from a specific point in the lamp at wavelength λ
$P(z)$	Incident spectral radiant power for a specific depth of the reactor for its whole surface
P_λ	Spectral radiant power at wavelength λ transmitted by the solution
P_λ^0	Spectral radiant power emitted at wavelength λ from a specific point in the lamp
t	Exposure time
V	Reaction volume
$\overline{V}$	Volumetric flow rate
x	Position on the x axis for the point inside the solution where the absorption energy is considered
y	Position on the y axis for the point inside the solution where the absorption energy is considered
z	Position on the z axis for the point inside the solution where the absorption energy is considered
x_0	Lamp position on the x axis
y_0	Lamp's starting point position on the y axis
y_L	Coordinate that defines each specific point of the lamp
z_0	Lamp position on the z axis
β	Angle defined by both the emitting point in the lamp and the solution point receiving the radiation
ε_λ	Molar extinction coefficient at wavelength λ
φ	Quantum yield
λ	Wavelength
λ_{max}	Wavelength at which a compound has its maximum value of molar absorption coefficient
μ_λ	Absorption coefficient at wavelength λ

Photo-degradation of HMF

a	Origin ordinate resulting from the linear regression between P_{abs} and C_{HMF} data
b	Slope resulting from the linear regression between P_{abs} and C_{HMF} data
C_{HMF}	HMF concentration
C_{HMF}^0	Initial HMF concentration

C_{HMF*}	Concentration of the excited HMF molecule
k	Kinetic constant for the photo-product formation step
HMF	HMF molecule
HMF*	Excited HMF molecule
k_D	Kinetic constant for the declining step
k_R	Constant in the relation between C_{HMF} and P_{abs}
K_{HMF}	Kinetic constant for the global HMF photo-degradation reaction (quantum yield)
m_{HMF}	Constant in the relation between C_{HMF} and time
r_{HMF}	Intensive reaction rate for the HMF degradation
t	Time
Kinetic/thermodynamic compensation	
E_a	Activation energy
h	Planck's constant
k_{eq}	Equilibrium kinetic constant
K_0	Frequency factor
K_B	Boltzmann's constant
N	Total number of treatments
R	Universal gas constant
T	Absolute temperature
T_B	Isokinetic temperature
T_{hm}	Harmonic mean temperature
ΔG_B	Change in Gibbs free energy at the isoequilibrium point
ΔH	Change in enthalpy
ΔS	Change in entropy
Enzymatic inactivation	
A^0	Initial absorbance at 420 nm
$A(t_{an})$	Absorbance at 420 nm of the sample at any analysis time t_{an}
A^∞	Asymptotic value for the absorbance at 420 nm
C_E	Concentration of the enzyme
C_E^0	Initial concentration of the enzyme
C_{EI}	Concentration of the intermediate form of the enzyme
C_{EI}^0	Initial concentration of the intermediate form of the enzyme
C_{EN}	Concentration of the native form of the enzyme
C_{EN}^0	Initial concentration of the native form of the enzyme
C_P	Concentration of the product of the analytical enzymatic reaction
C_R	Concentration of the reactant of the analytical enzymatic reaction
C_R^0	Initial concentration of the product of the analytical enzymatic reaction
$EA(t_{UV})$	Enzymatic activity for any sample after t_{UV} irradiation time
E_D	Denatured form of the enzyme
E_I	Intermediate form of the enzyme
E_N	Native form of the enzyme
k	First-order kinetic constant of the enzyme inactivation
k_1	Kinetic constant for the formation of the intermediate form of the enzyme
k_2	Kinetic constant for the intermediate enzyme denaturation
k_{an}	Kinetic constant of the analytical reaction used to determine the enzymatic activity
k_{cat}	Kinetic constant for the product formation from the complex enzyme-substrate for the analytical reaction
k_N	Kinetic constant for the product formation from the complex native enzyme-substrate
k_I	Kinetic constant for the product formation from the complex intermediate enzyme-substrate
L	Optical path of the beam to measure the absorbance (width of the quartz cell)
M	Kinetic value of the Michaelis-Menten kinetic equation
M_I	Kinetic value of the Michaelis-Menten kinetic equation for the intermediate form of the enzyme
M_N	Kinetic value of the Michaelis-Menten kinetic equation for the native form of the enzyme
$REA(t_{UV})$	Relative enzymatic activity at a specific inactivation time
r_P	Intensive reaction rate for the formation of the product from the analytical enzymatic reaction

t_{an}	Analysis time
t_{UV}	Irradiation time
ε_P	Extinction molar coefficient of the product of the analytical enzymatic reaction
ε_R	Extinction molar coefficient of the reactant of the analytical enzymatic reaction
Λ	Ratio between the kinetic constants of the intermediate and native enzyme forms for the analytical enzymatic reaction
AA degradation	
AA	L-ascorbic acid molecule
AA*	Excited L-ascorbic acid molecule
C_{AA}	Concentration of the L-ascorbic acid molecule
C_{AA*}	Concentration of the excited L-ascorbic acid molecule
C_{AA}^{0}	Initial concentration of ascorbic acid
C_{AA}^{∞}	Concentration of ascorbic acid at infinite time
K_{AA}	Kinetic constant for the global photo-degradation reaction (quantum yield)
k_D	Kinetic constant for the formation of photo-products
k_O	Kinetic constant for the oxidation of AA
k_R	Constant in the relation between C_{AA} and P_{abs}
m_{AA}	Constant in the relation between C_{AA} and time
r_{AA}	Intensive reaction rate for the AA degradation

Main abreviations

AA	L-ascorbic acid
ANOVA	Analysis of variance
E	Einsteins
EU	European Union
HMF	5-hydroxymethylfurfural
MJ	Mandarin juice
OJ	Orange juice
PPO	Polyphenol oxidase
POD	Peroxidase
US	Ultrasound
UV	Ultraviolet
Vis	Visible

LIST OF FIGURES

LIST OF TABLES

CHAPTER 1. INTRODUCTION

1.1 Basic concepts of fruit juices

1.1.1 Definition

Fruit juice is the unfermented but fermentable liquid from the edible part of sound, appropriately mature and fresh fruit or of fruit maintained in sound condition by suitable means including post-harvest surface treatments. It should not have added ingredients, except minerals and vitamins for the purpose of fortification and permitted additives (CODEX STAN 247-2005; AIJN, 2016). Flavour, pulp, and cells obtained by suitable physical means from the same species of fruit may be restored to the juice. The addition of sugars is no longer authorized, and neither is the addition of preservatives, aromas, and colouring agents (Horváth-Kerkai and Stéger-Máté, 2012; Official Journal of the European Union, 2012).

1.1.2 Classification

Fruit juices can be classified regarding the flavour, appearance, obtaining method, as well as storage conditions (Table 1). If the product is obtained from one kind of fruit it is called as *single juice*; if it is obtained by blending two or more juices, it is called as *mixed juice* (CODEX STAN 247-2005). According to the appearance, juices can be clear or cloudy (constituted by colloids, e.g. citrus-based juices). Products belonging to this latter group may contain fruit fibres (Horváth-Kerkai and Stéger-Máté, 2012).

Table 1. Classification of fruit juices.

Criteria	Name
Flavour	Single
	Mixed
Appearance	Clear
	Cloudy
Obtaining method	From concentrate
	Not from concentrate
Storage conditions	Chilled
	Ambient

Fruit juice may be obtained directly expressed by mechanical extraction processes or by reconstituting concentrated fruit juice with potable water (CODEX STAN 247-2005). The majority of fruit juice is made by reconstituting concentrated juice with water to a composition similar to that of its original state. Reconstituted juices are often packed in aseptic long-life containers such as Tetra Pack. On the other hand, there is a growing market for fresh ‘single strength’ juice made by squeezing fruit, subjecting it to some processing, i.e. pasteurization, packaging it and selling it within a cold chain distribution

system. Such juice is usually referred to as *not from concentrate* and will have a shelf life that varies from 1 or 2 weeks to 2 or 3 months (Ashurst, 1999). Thus, the product may also be marketed, according to the conditions of the distribution chain, as *chilled* or *ambient* (AIJN, 2016).

1.1.3 Processing technology

The technology to obtain fruit juices varies depending on many factors, such as the nature of the raw material, final product desired, size of plant, etc. In general terms, the process to obtain fruit juices involves the following steps (McLellan and Padilla-Zakour, 2005; Belitz *et al.*, 2009; Horváth-Kerkai and Stéger-Máté, 2012):

Preparation of the fruit. - The process starts with sound fruit, freshly harvested from the field or taken from refrigerated or frozen storage. Thorough washing removes dirt and foreign objects and may be followed by a sanitation step to decrease the load of contaminants. Sorting to remove decayed and mouldy fruit is also necessary to make sure the final juice will not have a high microbial load, undesirable flavours, or mycotoxins contamination. If necessary, other operations (e.g. trimming or pitting) are applied to remove stone seeds, stems or calyx. After that, fruit is disintegrated mechanically or thermally by heating (at about 80 ºC) or by freezing (less than -5ºC). The yield can be increased by enzymatic pectin degradation (particularly of stone fruits and of berries) or by applying procedures such as ultrasound or electropermeabilization.

Juice extraction. - Separation of the juice is achieved by different methods such as pressing, diffusion, centrifugal procedures, and reverse-osmosis. The type of equipment applied depends on the fruit species, production line, and economy of scale. The most widely used solution is pressing. This step should be done as rapidly as possible so as to minimize its oxidation by naturally present enzymes.

Clarification. - Extracted fruit juices are usually turbid, due to insoluble plant particles (fibres, cellulose, hemicellulose, protopectin, starch, and lipids) and colloid macromolecules (pectin, proteins, soluble-starch fractions, certain polyphenols, and their oxidized or condensed derivatives). For cloudy juices, further clarification might not be necessary or may involve a coarse filtration or a controlled centrifugation to remove only larger insoluble particles.

Clarified juices are real solutions that should not contain dissolved colloid substances, and these compounds therefore have to be eliminated. Juice clarification can

be performed by physico-chemical methods, mechanical procedures, and their combination. The former involves treatment with enzymes, mostly pectinolytic, and, if necessary, removal of starch and polyphenols using gelatine, alone or together with colloidal silicic acid or tannin, or polyvinylpyrrolidone. Finally, proteins are removed by adsorption on bentonite. Mechanical clarification is achieved by filtration or by centrifugation.

Deaeration. - Since juices contain oxygen-sensitive compounds, a deaeration is performed to remove dissolved gas particles. This is achieved by an evacuation step or by purging the juice with an inert gas such as N_2 or CO_2.

Filling. - Fruit-based beverages are filled into glass and plastic bottles or carton boxes made of combined layers.

Pasteurization. - The juice is pasteurized to control spoilage microorganisms and to inactivate enzymes that occur naturally in fruit. In the traditional way, liquids are heated to 82-85 ºC, filled at this temperature, and then pasteurized in water bath at 84-88 ºC for 15-40 minutes depending on the size of the packaging container. After the heat treatment, products are cooled to room temperature.

With aseptic filling technology, the liquid is pasteurized at 94-112 ºC for 30-60 seconds in a closed, flow-through system. Then the fluid is cooled to 25-30 ºC and filled into containers that have already been sterilized. The aseptic filling-closing system is a closed unit under overpressure, which hinders the post-contamination of heat-treated products.

The juices obtained can also be transformed into concentrates. In that case, the fresh squeezed juices are transferred to an evaporator to remove water to the desired concentration level. Other processes used for water removal include reverse osmosis and freeze concentration. The concentrate is then ready for final processing, packaging and storage (McLellan and Padilla-Zakour, 2005; Horváth-Kerkai and Stéger-Máté, 2012).

A general diagram of the process for clear juices not from concentrate is shown in Figure 1.

1.1.4 Nutritional value

Fresh juices are important in human nutrition far beyond their use as refreshing sources of liquid. They have a water content similar to that of the fruits themselves, the removal of the plant cell wall material having only a minor effect overall. Since the

clarification step removes all the plant cell wall polysaccharides (dietary fibre), clear juices are very low in non-starch polysaccharides and the carbohydrates present are limited to mixtures of the free sugars which are characteristic of the fruit and the processing conditions (Southgate *et al.*, 1995).

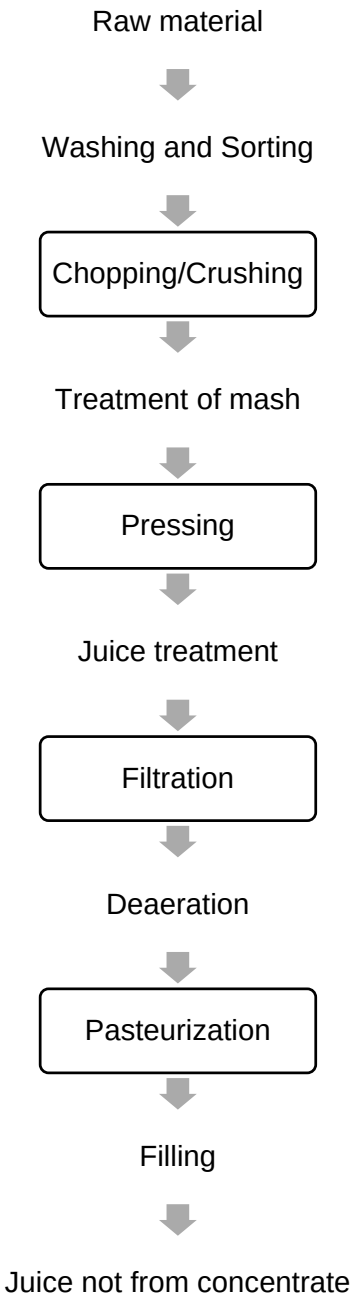

Figure 1. Diagram of process for clear juice not from concentrate.

Like whole fruits and vegetables, these products are rich in potassium, magnesium, folate, vitamin A and vitamin C. They also contain other bioavailable plant components, such as polyphenols -compounds that have strong antioxidant and anti-

inflammatory activity (Brauns, 2014). Overall, fruit juices can play a significant part in a healthy diet because they offer good taste and a variety of nutrients found naturally in fruits. However, it should be noted that changes occur, particularly to the minor components of juice during storage, e.g. Vitamin C, especially under adverse conditions (light, increasing temperature, long storage, etc.) (Ashurst, 1999).

1.1.5 Quality parameters

The Codex Alimentarius (CODEX STAN 247-2005) establishes that juice must be prepared by suitable processes, which maintain the essential physical, chemical, organoleptic and nutritional characteristics of the fruit from which it comes. Since product selection by consumers greatly depends on these characteristics, systemic activities are necessary to obtain juice of the highest quality. Moreover, the final product needs to be characterized to ensure that it fulfil the pertinent regulations as well as consumer expectances. With the purpose of juice characterization, the European Fruit Juice Association publishes a compilation of methods of analysis (http://www.ifu-fruitjuice.com/list-of-methods).

Among the physicochemical features, the soluble solids content is the first parameter characterizing a fruit juice. These solids are mostly sugars naturally occurring in fruits (i.e. glucose, fructose and sucrose) and organic acids in second place. The soluble solids content is determined by means of the refractive index and is generally expressed as Brix. However, this measurement is only an estimate which considers that everything in solution has the same refractive index as sucrose. Furthermore, it is common to check the levels of the individual sugars in the product to assess its authenticity and quality (Hammond, 1999). The basic characterization of a juice is complemented with the total acidity obtained by titration, which is a measure of the content of mineral and organic acids. In addition, the pH value detects the acids that easily or totally ionizate.

Organoleptic attributes shall also be evaluated, since the food-purchasing consumer assesses a product using his/her senses. Taste, flavour and colour play the most important roles among the sensory characteristics affecting consumer acceptance and/or preferences (Kraus and Popek, 2013). The former two are generally controlled by sensory assessments involving trained panellists. The colour may be determined in a number of ways including measurement of the absorbance of the product at one or more wavelength –only in clear products- or by tristimulus colour measurements (Hammond, 1999).

Regarding the nutritional quality of liquid fruit products, the most significant factor is their content of vitamins that are vital for preserving health, the growth of living organisms, as well as for the correct functioning of body cells (Kraus and Popek, 2013). Vitamin C, mainly found in the form of L-ascorbic acid, plays an important role in human nutrition because of its antioxidant capacity, cell protection, immune response and iron absorption. It is present in collagen synthesis and stimulates the production of some hormones. This substance cannot be synthetized by our organism, and thus we depend entirely on dietary sources to meet our needs. Ascorbic acid is naturally occurring in fruits and vegetables and is also used as an additive in many foods because of its antioxidant capacity (Nagy, 1980; Gregory, 2008). This compound is unstable and easily degrades under several processing conditions such as high temperatures. Thereby, it is usually an indicator of the nutritional quality during processing and storage of foods, since it is generally observed that, if ascorbic acid is well retained, the other nutrients are also well retained (Sapei and Hwa, 2014).

Other compounds found in plant-based foods that are not considered nutrients but exhibit health-promoting biological functions can also be evaluated. Among them, phenolic compounds play an important role in plant-derived food quality, as they affect quality characteristics such as appearance, flavour and health-promoting properties (Tomás-Barberán and Espín, 2001).

Besides the characterization of the product, the changes induced by processing have to be taken into account to control the overall quality of juices. During squeezing, the cell tissue of fresh fruits breaks, releasing several cell compounds that can interact with each other as well as with the environment. As a consequence, a number of detrimental reactions -microbial fermentation, enzymatic and non-enzymatic browning, oxidation of ascorbic acid, loss of aromas, etc. - may occur during processing and storage. These adverse reactions should be avoided in order to preserve the natural attributes of the juices and prolong their shelf life.

For liquid foods preserving, thermal pasteurization is the most extended approach used to inactivate microorganisms and enzymes, thus inhibiting the associated detrimental reactions. The effectiveness of the treatment is evaluated by microbiological assays, usually counts of a target bacterium. For instance, *Salmonella* sp is considered a good target for orange juice, *E. coli* for apple juice and *L. monocytogenes* for various juices that have never been involved in outbreaks (Tribst *et al.*, 2009). An adequate pasteurization method should guarantee a reduction of the level of pathogen

microorganisms by at least 5-log cycles (FDA, 2000). The total inactivation of natural microbial load (mesophylls, yeasts and moulds) also indicates a successful disinfection.

Besides microorganisms, enzymes play an important role in fruit juice manufacturing. The most important enzymes affecting juice quality are (Falguera *et al.*, 2011c; Koutchma *et al.*, 2016):

(a) Polyphenol oxidase (PPO). This enzyme is responsible for enzymatic browning, transforming phenolic compounds into *o*-quinones, resulting in melanins after a polymerization stage.
(b) Peroxidase (POD) catalyzes the oxidation of a wide variety of compounds in the presence of hydrogen peroxide. When acting on phenolic compounds, POD contributes to enzymatic browning much like PPO.
(c) Amylases and pectic enzymes, e.g. pectinmethylesterase (PME). In the production of clarified and depectinated juices, it is essential to leave these enzymes to act in order to eliminate pectin and starch. Nevertheless, in purees and juices with suspended pulp (i.e. citrus juices), it is important to inactivate them to avoid cloud loss in the product. If they are not completely inactivated in the storage stage they may have a residual activity on pectic fractions resulting in sedimentation of the pulp due to destabilization of the system. Thus, in this kind of product it is imperative to ensure that there is no enzymatic activity, as it may adversely affect the quality of the juice.
(d) Lipoxygenase (LOX) is responsible for the generation of volatile flavour compounds and free radicals in many juices. It catalyzes the oxidation of polyunsaturated fatty acids into hydroperoxides. This process leads to loss of nutritional quality and colour.

Although thermal pasteurization inactivates microorganisms and enzymes in liquid fruit products, detrimental changes such as non-enzymatic browning reactions can take place. These browning reactions may occur in products with high-sugar content, being accelerated at high temperatures. Essentially, three kind of non-enzymatic browning reactions have been described (Ibarz *et al.*, 1989):

(a) Maillard reactions that take place between carbonyl and free amino groups.

(b) Caramelization reactions, when polyhydroxylated compounds are heated at relatively high temperatures in the absence of amino groups.
(c) Oxidation reactions that, for instance, convert ascorbic acid and polyphenols into di and polycarbonated compounds.

A number of assays can be performed to monitor the non-enzymatic browning. For instance, the formation of 5-hydroxymethylfurfural (HMF). This compound is intermediate in the aforementioned reactions, being formed as result of the dehydration of ketopentoses, particularly in acidic and high-temperature environments (Morales, 2009; EFSA, 2011; Lee *et al.*, 2014). High values of HMF in the product reveal excessive thermal treatment and inappropriate storage conditions. Moreover, the formation of this molecule is associated with other detrimental reactions, i.e. loss of L-ascorbic acid, changes in such physical properties as colour and sensorial characteristics (AIJN, 2001; Chen *et al.*, 2009).

Non-enzymatic browning also can be evaluated by means of colorimetric assays. The relative absorbance at 420 nm, also known as the browning index, is commonly measured since the final products of the browning reactions (enzymatic and non-enzymatic) absorb light at that wavelength. Other analyses such as the content of hexoses (glucose and fructose) give information about chemical changes occurring in the juice composition during processing. The formol index, which is an estimation of the content of free amino acids, reveals information about the participation of these compounds in the Maillard reaction.

Other detrimental reactions, like the oxidation of phytochemical compounds, can be prevented by deaerating the juices after squeezing, as well as using suitable packaging material that acts as a barrier to oxygen. The ascorbic degradation during the processing and storage of fruit juices will then be caused by the presence of residual oxygen. Once this gas has been consumed, the anaerobic degradation will start at a relatively slow rate (Nagy, 1980; Gregory, 2008). Polyphenols can also be decomposed in the presence of oxygen. Therefore, both ascorbic acid and phenolics should be determined before and after processing and during storage of fruit derivatives.

In addition to physicochemical, sensorial and nutritional attributes in fruit juices, another issue is the safety of the final product for consumers. This aspect is particularly important in order to prevent diseases caused by food. For that reason, the presence of pathogen microorganisms as well as toxic substances should be avoided in foodstuffs.

With that purpose, good manufacturing practice should be followed during processing. In other words, food processing has to be carried out under hygienic conditions that ensure final product safety. Furthermore, the product must be disinfected by means of a physical or chemical process capable of reducing the level of pathogen microorganisms.

Concerning toxicological safety, the levels of potential toxic compounds either proceeding from contaminated raw materials or formed during processing should be kept as low as possible. For example, the content of patulin is an indicator, which shows whether the juice was produced from windfalls or spoiled apples. The level of this compound is regulated in most countries, since it is carcinogenic and teratogen (Oke *et al.*, 2012).

Another potential toxic substance that has been identified in commercial fruit juices is 5-hydroxymethylfurfural (HMF) (Morales, 2009). As was already explained, this compound is formed during non-enzymatic browning reactions (Ibarz *et al.*, 1989). Thus, this molecule, which is not present in fresh fruits, is generated in sugar-containing food during heat treatments (Lee *et al*., 2014) or after long periods of storage. Given its probable genotoxicity, subchronic toxicity and carcinogenicity, the EFSA (2011) has considered that it would be prudent to reduce the HMF content as much as is technologically feasible. European producers recommend a maximum content of 10 $mg \cdot kg^{-1}$ in citrus juices and 20 $mg \cdot kg^{-1}$ in other commercial juices (AIJN, 2001).

1.1.6 Consumption trends

Fruit juices are consumed as such or are used as intermediary products, e.g., for the production of syrups, jellies, lemonades, fruit-juice liqueurs or fruit candies (Belitz *et al.*, 2009). According to the Liquid Fruit Market Report published by the European Fruit Juice Association (AIJN, 2016), global fruit juice and nectar consumption was 38.5 billion litres in 2015. In the same year, the consumption of these beverages in the European Union was 9.6 billion litres, 100% juice accounting almost two-thirds of this market. Other current trends reported in that document are the following:

a) A shift to consuming less in quantity, but better in quality. As a result, the volume of chilled and not from concentrate juices has been boosted at the expense of a general down-trade (Fig. 2).
b) Orange is the most popular flavour, followed by flavour mixes (Fig. 3).

c) For home consumption, the majority of fruit juices are sold in modern retail channels, such as hypermarkets, supermarkets and discounters.

d) Heritage and origin, including products made from regional fruits or allowing local farmers to participate in profits, have become more important to western consumers.

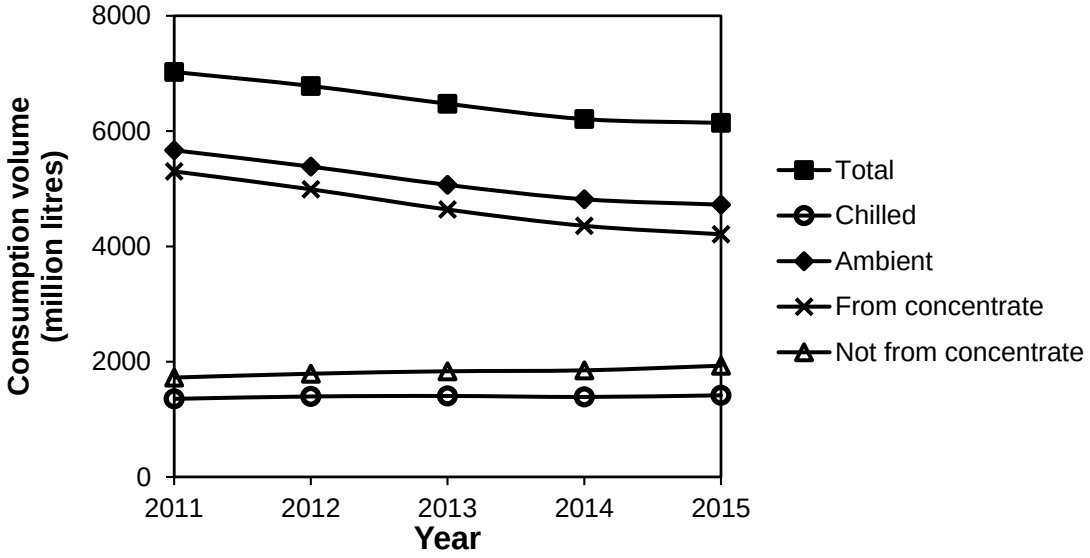

Figure 2. Consumption of 100% juice in The European Union (2011-2015). Data from The Liquid Fruit Market Report (AIJN, 2016).

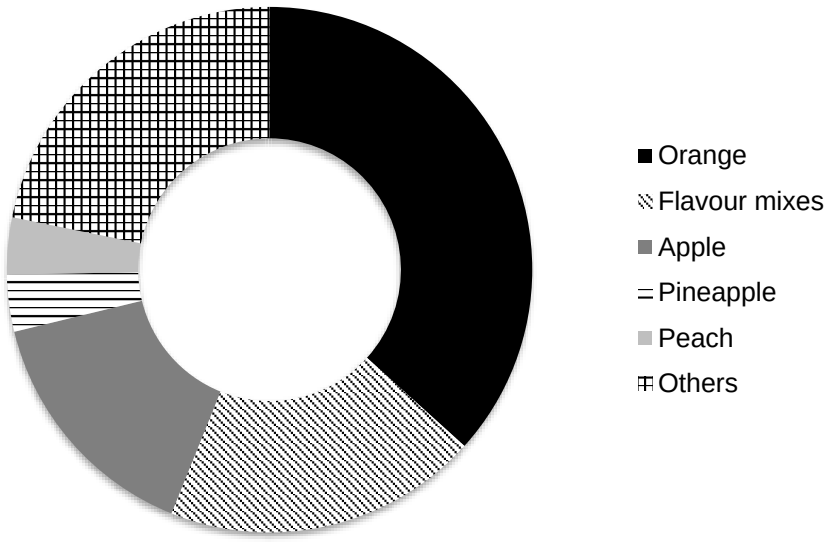

Figure 3. Fruit juices and nectar consumption by flavour in the EU in 2015. Data from The Liquid Fruit Market Report (AIJN, 2016).

The decline in fruit juice consumption both in the EU (Fig. 2) and in the United States of America (PBH, 2015) may be because these beverages have recently come under fire regarding sugar content, especially juices from concentrate (Brauns, 2014). On the contrary, the continuing growth in not from concentrate and chilled juice consumption is in line with consumer trends such as health awareness, wellness trends and the increasing consumer interest in "good for me" and functional products. These products are perceived as healthier and as more natural than ambient or from concentrate juices (AIJN, 2016).

1.1.7 Innovative technologies

Advances in food processing technologies mostly occur in response to consumer demands or improvement in the efficiency of technology. Consumers are increasingly looking for products which have a beneficial effect on their health and have attractive sensory characteristics, as well as exhibiting characteristics similar to fresh raw products. Recent demands for safe and minimally processed food with high-quality attributes have encouraged industry and scientific researchers to find innovative processing techniques to produce foods with a minimum of changes induced by the technologies themselves.

Over the years, fruit juice preservation has mainly relied on low pH, heat pasteurization, refrigeration and the addition of preservatives. Frequently two or three of the aforementioned methods were required to provide stability for ready-to-drink industrialized fruit juice (Tribst *et al.*, 2009). However, it is known that thermal pasteurization commonly used to inactivate microorganisms and enzymes may degrade organoleptic and nutritional quality of these foodstuffs (Ling *et al.*, 2015; Santhirasegaram *et al.*, 2013; Soares *et al.*, 2017). Other methods like chemical additives raise concerns about toxicity and undesirable residuals (Koutchma, 2009; Keklik *et al.*, 2012). Besides, in some cases, fruit derivatives can contain mycotoxins that come from mould-contaminated pieces of fruit. Such mycotoxins that have adverse effects on health are not eliminated with conventional processes (Falguera *et al.*, 2011b, c).

In this context, there is a continuous search for new methods of microbial and enzymatic inactivation that guarantee food stability and safety with minimum effects on its nutritional and sensorial characteristics (Tribst *et al.*, 2009; Falguera *et al.*, 2011b,c; Gayán *et al.*, 2011; Li and Farid, 2016). Consequently, several alternatives to conventional methods are being studied for the preservation of fruit juices. On the one hand, an effort is being made to improve current thermal treatment, trying to reduce heating lag phases and to improve the homogeneity and intensity of treatments (Gayán *et*

al., 2011). On the other hand, food scientists and industries have been investigating emerging food processing technologies, which do not rely on increasing temperature as the most important processing variable (Yi *et al.*, 2017).

In 2004, the National Advisory Committee on Microbiological criteria for Foods (NACMCF) for the USDA revised the definition of "pasteurization" for foods. It now includes any process, treatment, or combination hereof, which is applied to food to reduce the most microorganisms of public health significance. Nowadays, alternatives to conventional thermal methods for the preservation of fruit juices include radiation treatments (UV light, high-intensity light pulses, γ-irradiation), electrical treatments (pulsed electric fields, radiofrequency, electric fields, ohmic heating), microwave heating, ultrasound, high-hydrostatic pressure, and inert gas treatments (supercritical carbon dioxide, ozonation) (Jiménez-Sánchez *et al.*, 2017).

Among these alternative technologies, exposure to radiation, whether ionizing or non-ionizing, is regarded as one of the non-thermal methods for food preservation with the best potential (Oms-Oliu *et al.*, 2012). Ionizing radiation includes X-rays, gamma-rays, and ionizing particles (beta-rays, alpha-rays, protons), whereas non-ionizing radiation includes ultraviolet and the adjacent visible spectral range (Koutchma, 2009).

1.2 Ultraviolet technology

1.2.1 Basic principles

UV light fills a wide band of wavelengths between 200 nm (X-rays) and 400 nm (visible light). The UV spectrum can be divided into three regions (Bintsis *et al.*, 2000):

1. Short-length UV light (UV-C) with wavelengths in the interval from 200 to 280 nm
2. Medium-length UV light (UV-B) with wavelengths in the interval from 280 to 320 nm.
3. Long-length UV light (UV-A) with wavelengths in the interval from 320 to 400 nm.

When UV light propagates, it interacts with the materials it encounters through absorption, reflection and scattering. Each of these phenomena is defined as follows (Koutchma, 2009):

Absorption. - The transformation of energy of light photons to other forms of energy as it travels through a substance.

Reflection. - The change in the direction of propagation experienced by light deflected by an interface.

Scattering. - The phenomenon that includes any process that deflects electromagnetic radiation from a straight path through an absorber when lights interact with a particle. Much of the scattered light is in the forward direction and is a significant portion of the transmitted light.

The absorption of radiation may lead to a chemical reaction. The magnitude of this photochemical change will depend on the intensity of the incident radiation as well on the ability of the reactants to absorb that radiation. The ability to absorb radiation is known as absorbance ($A(\lambda)$), which can be defined by the logarithm of the ratio between the incident ($P\lambda^0$) and the transmitted ($P\lambda$) spectral radiant power at wavelength λ. Taking into account the base of the logarithm, two definitions of absorbance are possible:

$$A_{10}(\lambda) = \log \frac{P_\lambda^0}{P_\lambda} \tag{1}$$

$$A_e(\lambda) = \ln \frac{P_\lambda^0}{P_\lambda} \tag{2}$$

Spectrophotometers usually measure the absorbance as $A_{10}(\lambda)$, while the model equations usually use $A_e(\lambda)$. Using this relation the complication is easily solved:

$$A_e(\lambda) = A_{10}(\lambda) \ln 10 \tag{3}$$

Lambert-Beer's law (Eq. 4) is the linear relationship between the absorbance at a fixed wavelength $A_e(\lambda)$ and the concentration of the absorber substance (C_A, mol·L^{-1}).

$$A_e(\lambda) = \varepsilon_\lambda \cdot C_A \cdot D_S \tag{4}$$

$\varepsilon\lambda$ is the molar extinction coefficient at the fixed wavelength which is a measure of the amount of light absorbed per unit concentration of the absorber substance. Its units are $L \cdot mol \cdot^{-1} \cdot cm^{-1}$. D_S is the length of the path of light through it.

The absorption coefficient (μ) is also used in calculations, being a function of the wavelength. It is defined as the absorbance divided by the path length (cm^{-1}):

$$\mu_\lambda = A_e / D_S \tag{5}$$

Or from Lambert-Beer's law as:

$$\mu_\lambda = \varepsilon_\lambda \cdot C_A \tag{6}$$

A plot of μ against wavelength is called the absorption spectrum of the substance. The principal use of this graph is to provide information about at which wavelength (λ_{max}) a compound has at its maximum value of the molar absorption coefficient (Wardle, 2009).

1.2.2 Sources of ultraviolet light

The selection of a UV source for a system is critical, since the efficacy and cost-efficiency of the process are closely related to the type of UV lamp used. Since light radiation must be absorbed to lead to a photochemical change, the most interesting type of light source to be used will be determined by the absorption spectrum of the reactants. In addition, the main characteristics that a radiation source must have in order to be of industrial utility are emission stability, long life, adequate physical dimensions, ease to use and low cost (Ibarz *et al.*, 2015a).

The sun is a source of the full spectrum of ultraviolet radiation (NASA Science Mission Directorate, 2010). The relative intensities of ultraviolet radiation reaching the earth's surface depend on attenuation by the atmosphere through absorption and scattering. UV-C is completely absorbed in the upper and middle atmospheres by ozone and molecular oxygen, whereas some UV-B does reach the surface and UV-A is barely affected (Bintsis *et al.*, 2000).

Lamps are artificial radiation sources of the greatest interest for use in photochemical reactions. The lamps that irradiate a large ultraviolet fraction are mercury vapour lamps, which consist of a tube filled with mercury in the gaseous state in which

an electric current flows. Concerning the gas pressure, these lamps are classified as low-, medium- and high-pressure lamps. The low-pressure lamps emit almost exclusively at 254 nm and as the pressure rises the emission spectrum becomes more complex (Fig. 4) (Ibarz *et al*., 2015a). Medium-pressure lamps emit polychromatic light with emission bands both in the ultraviolet and in the visible light regions (UV-Vis). Due to the higher pressures operated they are able to achieve a higher penetration depth (Koutchma, 2009).

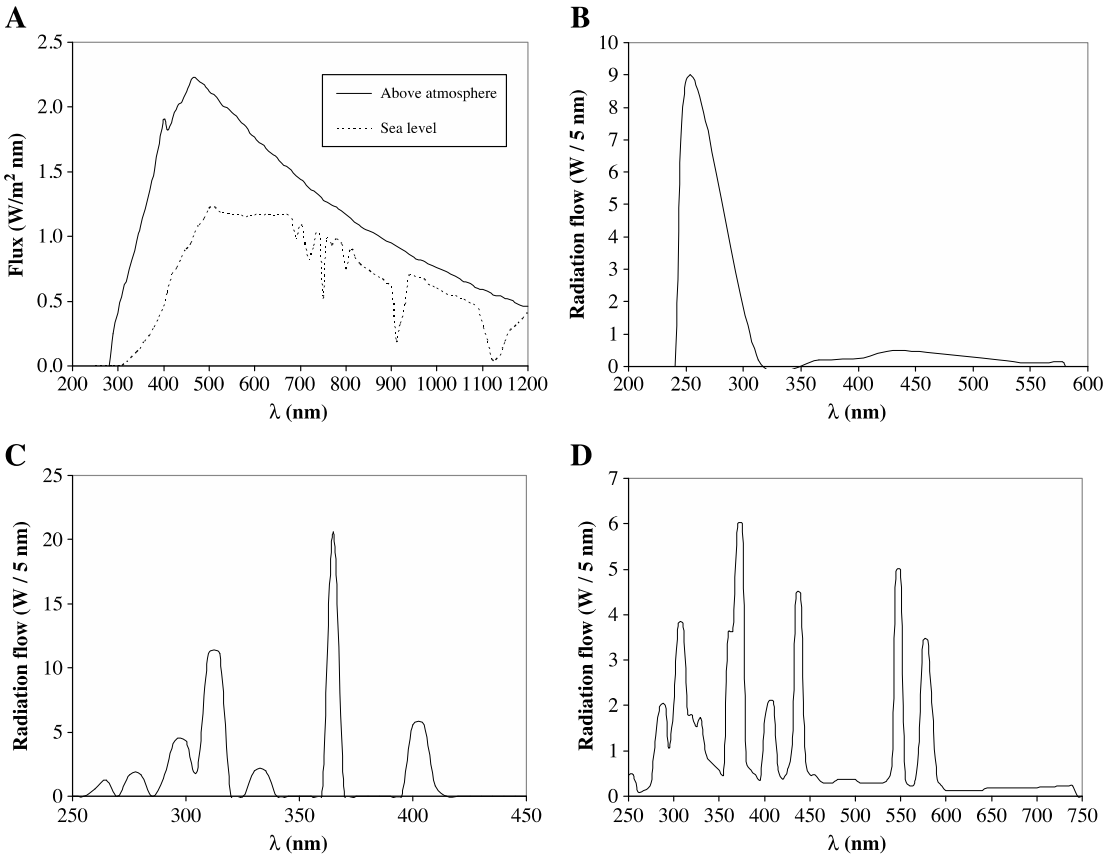

Figure 4. Emission spectra from different UV radiation sources. A: The sun. B: Low-pressure mercury lamp. C: Medium-pressure mercury lamp. D: High-pressure mercury lamp (from Falguera *et al*., 2011b).

1.2.3 Equipment

Critical decisions about the development of ultraviolet irradiation equipment include radiation sources, reactor geometry and reaction medium properties, and the relationship between all these parts will lead to the achievement of the desired effect on food systems and their components. There are many different reactors that are used in photochemical processes, but according to their mode of operation they can be classified as continuous and discontinuous. The former are used in reactions with large quantum yields, achieving a small irradiation time of the reactants. The latter are used to carry out

reactions with low quantum yield, which need high irradiation times or if the reactants have high viscosity (Falguera *et al.*, 2011b).

According to Koutchma *et al.* (2016) the reactors commonly used for UV processing of liquid foods such as juices are:

- Direct overhead exposure. This refers to an uncontained light source which is simply located above the sample. This approach is operated in batch and mostly used on lab-scale. An example of this system is the reactor described by Ibarz *et al*. (2005), which is schemed in Figure 5.

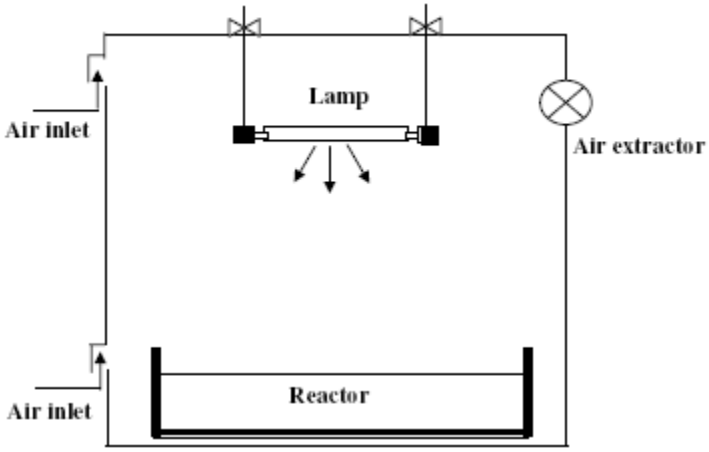

Figure 5. Direct overhead exposure photoreactor designed by Ibarz *et al.* (2005).

- Tubular annular (Fig. 6), which can be operated in laminar or turbulent flow. Consists of a cylinder with an annular section, with the lamp placed in this central annulus space (Ibarz *et al.*, 2015a).
- Coiled-tube, which is mainly composed of a coiled tube which is wound around a UV lamp (Müller *et al.*, 2014).
- Descendent film (Fig. 7), which consists of a tubular reactor in which the lamp is placed in the central axis and the reactant fluid flows in the form of a film down the inner face of the tube.

Other reactors used for photochemical processes are described by Ibarz *et al.* (2015a). To achieve high radiation doses, multi-lamp reactors are often used. They basically consist of a single reactor such as the ones described above with several lamps (Falguera *et al.*, 2011b).

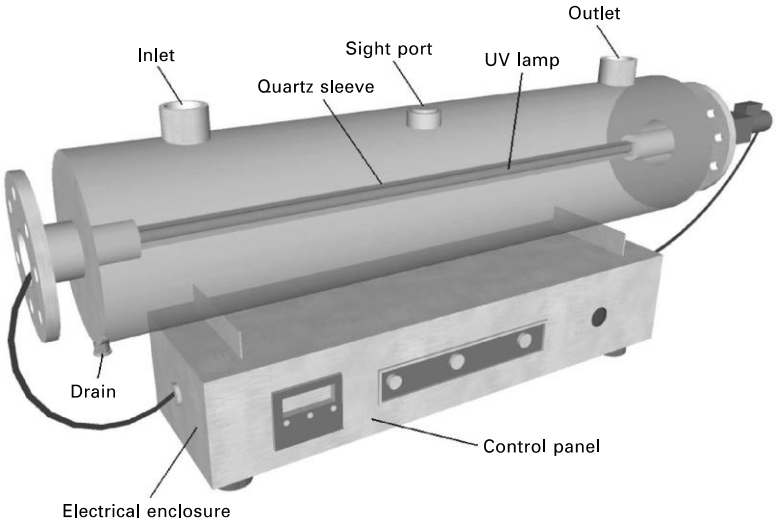

Figure 6. Illustration of a continuous tubular annular UV reactor.

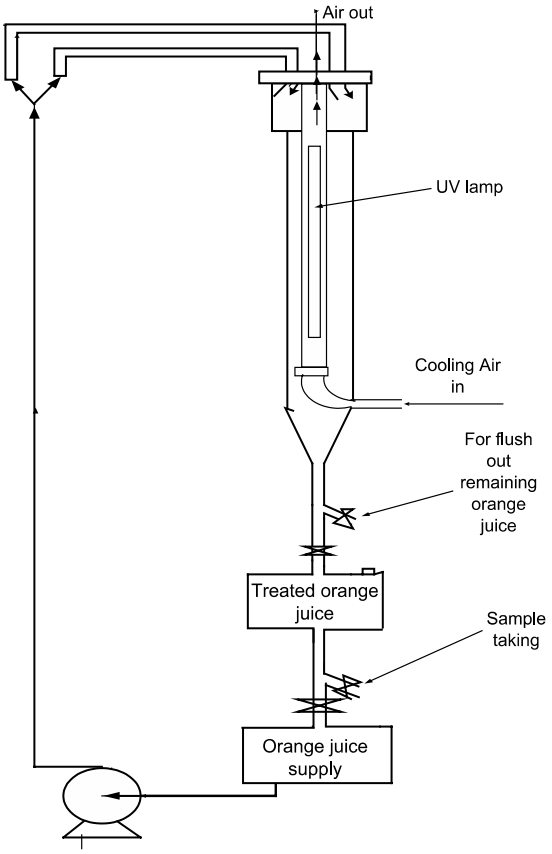

Figure 7. Descendent film photoreactor designed by Tran and Farid (2004).

1.2.4 Energy evaluation

The UV radiation dose is a critical process parameter that must be known in order to evaluate the effects of the UV irradiation on the material submitted to this physical

process. In general terms, the radiation dose can be known by the following relation (Bintsis *et al.*, 2000):

$$D_r = P(0) \cdot t \tag{7}$$

Where D_r is the UV dose expressed in J·cm^{-2}, $P(0)$ is the radiation flux or radiant power (in W·cm^{-2}), and t is the exposure time in seconds.

In batch systems, $P(0)$ corresponds to the incident radiant power at the surface of the product. This value depends on the configuration of the system and on the radiant power emitted by the lamp, but it is independent of the material being irradiated. Most studies calculate the radiation dose with the nominal power of the lamp given by the manufacturer. However, this value does not usually coincide with the real power emitted, because as time goes on the lamp power decreases. Moreover, not all the radiation emitted by the lamp reaches the material being irradiated.

The actual power emitted by the lamp (P_{emitt}) is usually measured by actinometrical reactions. An actinometrical reaction is a standard photochemical reaction with well-known absorption and kinetic characteristics, which easily allows changes to be measured in the concentration of some of the species involved in the reaction (Ibarz and Pagán, 1986). Another way to measure the real power from the lamp is the use of UV sensors that provide this magnitude in W·m^{-2} (Guerrero-Beltrán and Barbosa-Cánovas, 2004).

The UV light emitted (P_{emitt}) interacts with the UV reactor components such as the lamp, the lamp sleeve, the reactor walls, as well as the liquid substance being treated (Koutchma, 2009). Consequently, not all the radiation from the lamp will reach the material to be processed. This fraction will depend on the photoreactor design. In some discontinuous systems the radiation source is placed outside the reactor. Assuming a spherical emission from the lamp, some light rays will propagate towards a different direction where the reactor is placed. An accurate photochemical study must take into account the actual radiation power that reaches the product ($P(0)$). This value can be calculated from a radiation balance which takes into account the geometry of the system as well as the real lamp emission. A method for this calculation was developed by Garvín *et al*. (2015) and will be further described in the mathematical section.

In continuous systems, the fluid average residence time in the photoreactor is considered. With some arrangements, where the material flows around the lamp, the radiation absorbed by the lamp sleeve is depreciable and it may be assumed that most of the radiation emitted is in closed contact with the material being processed. Then, the nominal power can be used to calculate the UV dose using Equation 7. Sometimes, authors report the radiation dose in Joules per litre of liquid for continuous operation. In that case, the UV dose (D_{UV}) can be defined as (Koutchma *et al.*, 2016):

$$D_{UV} = \frac{P_{emitt}}{\overline{V}} \tag{8}$$

Where $\overline{V}$ is the volumetric flow rate of treated fluid (in $L \cdot s^{-1}$).

1.3 Ultraviolet processing for fruit juice preservation

For many years, UV-C processing has been used successfully for the disinfection of air, surfaces and drinking water (Bintsis *et al.*, 2000; Falguera *et al.*, 2011a; Keklik *et al.*, 2012). However, the low power of penetration of UV radiation has limited its application to disinfection of foods due to the complex composition and microstructure of these materials. Therefore, the use of this technology for fruit juice preservation has represented a challenge for food engineering. A brief account of the main advances reported in this topic is presented below.

1.3.1 Inactivation of microorganisms

Radiation in the range of 250-260 nm is lethal to most microorganisms, including bacteria, viruses, protozoa, mycelial fungi, yeasts and algae. This germicidal effect reaches a maximum value at 254 nm and falls to practically zero at 320 nm. Indeed, long-wave UV light has limited microbicidal properties. The damage inflicted by UV-C probably involves alterations of microbial DNA (deoxyribonucleic acid) through dimer formation. Once this molecule has been damaged, the microorganisms can no longer reproduce and the risk of disease arising from them is eliminated (Bintsis *et al.*, 2000).

UV light sensitivity of microorganisms varies significantly due to cell wall structure, thickness, and composition (Koutchma, 2009). For instance, larger microorganisms such as fungi are more resistant to UV-C light than bacteria (Tran and

Farid, 2004). Table 2 displays some examples of dose data for several types of microorganisms.

Table 2. UV-C light dosages (254 nm) needed to inhibit 100% of several types of microorganism (Guerrero-Beltrán and Barbosa-Cánovas, 2004).

Organism	Species	E (J·m^{-2})
Algae	*Clorella vulgaris*	220
	Blue green algae	4200
Bacteria (vegetative)	*Bacillus megatherium*	25
	Sarcina lutea	264
Bacteria (spores)	*Bacillus subtillis*	220
	Bacillus anthracis	462
Moulds	*Oospora lactis*	110
	Aspergillus niger	3300
Viruses	Adeno virus type III	45
	Tobacco mosaic	4400
Yeasts	Brewer's yeast	66
	Saccharomyces sp.	176

Low penetration of ultraviolet radiation inside liquid food systems has been stated to be one of the main limitations of this technology. The penetration effect of UV radiation depends on the characteristics of the liquid as well as on the photoreactor design. Because ultraviolet penetration is inversely proportional to the absorbance of the medium, the dose required to achieve a given microbial lethality treatment is affected by the presence of UV absorbing constituents. If multiple species that absorb light are present in a liquid sample, the total absorbance at a given wavelength is the sum due to all absorbers. Thus, dissolved solids (sugars, organic acids, pigments, vitamins, enzymes and others) are considered as hurdles that attenuate the irradiation flux. In addition, the presence of suspended solids attenuates the UV dose via light scattering, and also provides a site for the aggregation of bacteria to particle surfaces (Guerrero-Beltrán and Barbosa-Cánovas, 2004; Koutchma, 2009; Falguera *et al.*, 2011a,b; Tikekar *et al.*, 2011).

Koutchma (2009) compiled absorption coefficient data of fruit juices. For instance, this value in *e*-logarithmic base is 34.5 cm^{-1} for clear apple juice, 54.3 cm^{-1} for watermelon juice and 92 cm^{-1} for apple cider. Fruit juices that contain particulate and pulpy materials showed higher absorption coefficients, e.g., orange juice with pulp shows a value of 110.2 cm^{-1}. Garvín *et al.* (2015) modelled the absorption of UV light in function of the absorption coefficient and the depth in a plane photoreactor. Accordingly, for an absorption coefficient of 0.1 cm^{-1}, barely 30% of the incident radiation at the surface of the reactor is absorbed in the first 4 cm, while for a value of 100 cm^{-1}, 99% is absorbed in the first 0.05 cm.

For optimal disinfection, the ultraviolet light should reach all parts of the treated liquid food to ensure it has been treated thoroughly. With that purpose, descendent film reactors have been designed to reduce the radiation path length (Shama *et al.*, 1999; Tran and Farid, 2004). Another proposal consists of stirring the reaction medium, thus making sure that all the molecules of the reactant can reach the irradiated surface (Ibarz *et al.*, 2015a). Indeed, it has been shown that turbulent flow profiles increase the inactivation rates in continuous photoreactors (Koutchma *et al.*, 2004). To sum up, critical factors to achieve adequate microbial inactivation include the absorption coefficient of the product, the geometric configuration of the reactor, characteristics and physical arrangement of the UV source(s), the product flow profile, and the radiation path length (Sastry *et al.*, 2000).

In 2000, the US Food and Drug Administration (FDA) approved the use of UV-C light from low-pressure mercury lamps to reduce human pathogens in fruit juices when the system operates in turbulent flow (Reynolds' number > 2100). Initial approaches were tested for disinfection of fresh cider, which is defined as an unfiltered and unpasteurized apple juice (Wright *et al.*, 2000; Basaran *et al.*, 2004; Quintero-Ramos *et al.*, 2004; Unluturk *et al.*, 2004). Consequently, Health Canada (2003) issued no objections to the use of CiderSure 3500 UV (FPE Inc., Macedon, N.Y., U.S.A.) for apple juice/cider treatment to reduce the levels of microbial pathogens.

Since then, many studies have evaluated the effectiveness of UV technology as a method for disinfection of liquids foods and a considerable number of works have reported the efficacy of this method on reducing microbial counts in fruit juices (Tran and Farid, 2004; Keyser *et al.*, 2008, Guerrero-Beltrán *et al.*, 2009; Müller *et al.*, 2014; Kaya *et al.*, 2015; Unluturk and Atilgan, 2015). The 5-log reduction in pathogen microorganisms demanded by the FDA is only reported in some of these works,

Keyser *et al.* (2008) achieved a total elimination of mesophylls, yeasts and moulds in clear apple juice with a radiation dose of 230 $J \cdot L^{-1}$ (233.98 $mJ \cdot cm^{-2}$). The same dose was sufficient to reduce *E. coli* in the same product by 5 log cycles. However, smaller reductions were obtained under the same conditions in orange juice. This small efficiency was attributed to the great quantity of suspended matter, such as orange cells and fibre present in the product, which acts as a protective barrier for microorganisms against UV radiation. Further innovations in the engineering of reactors led to higher inactivation rates in turbid juices. For instance, Unluturk and Atilgan (2015) reached the 5-log goal in a freshly squeezed turbid grape juice using a multi-lamp continuous system which

provided a dose of 9.92 J·cm^{-2}. Similar successful results were reported for a melon-lemon juice blend processed under the same conditions (Kaya *et al.*, 2015).

1.3.2 Inactivation of enzymes

Since enzymatic reactions can lead to quality losses during storage, the inhibition of enzyme activity is almost as important as microbial inactivation to prevent spoilage reactions. While the inactivation of microorganisms in fruit juices is well investigated, little is known about the effect of UV treatments on enzymes in fruit juices. One of the earlier works that considered this technological issue was that by Tran and Farid (2004). They evaluated the effect of UV-C treatment (73.8 mJ·cm^{-2}) on the pectin methyl esterase (PME) activity of a fresh squeezed orange juice. Results showed that the dose applied was not sufficient to inactivate such an enzyme.

On the contrary, Manzocco *et al.* (2009) proved that exposure to ultraviolet and visible light is useful to inactivate polyphenol oxidase in model solutions and apple juice. They suggest that non-ionizing radiation promotes photo-oxidation processes that modify the native structure of the protein, leading to losses in its functional activity due to side-chain oxidation, backbone fragmentation and/or formation of cross-links and aggregates. The effectiveness of UV-C treatments at inactivating PPO was later corroborated by Müller *et al* (2014) for different juices (apple and grape). According to reviews (Guerrero-Beltrán and Barbosa-Cánovas, 2011; Koutchma *et al.*, 2016), the inactivation of juice enzymes is affected by the type of lamp, UV dose and as juice composition –involving amount and types of enzymes. For instance, PME has been shown to be the most UV-resistant enzyme tested.

The dose needed to inactivate enzymes like PPO is higher than that required for a substantial reduction in pathogenic microorganisms (Haddouche *et al.*, 2015). With the aim of improving the efficiency of ultraviolet pasteurization two approaches can be used. The first one consists of increasing the irradiation dose. In this way, the use of multi-wavelength lamps, which are more powerful than lamps that only generate UV, has shown successful results on inactivating PPO and POD in model solutions (Falguera *et al.*, 2012a and 2013b; Augusto *et al.*, 2015). Likewise, the use of this kind of lamps has been effective to inactivate PPO, POD and PME in apple juices (Falguera *et al.*, 2011d) as well as PPO and POD in grape and pear juices (Falguera *et al.*, 2013a and 2014, respectively). The second approach is based on combining the photochemical process with mild heating or other physical treatments. Some authors have proved that UV irradiations performed

at temperatures between 45 and 60 ºC improve the inactivation of enzymes (Gayán *et al.*, 2013; Sampedro and Fan, 2014).

1.3.3 Degradation of mycotoxins

The presence of mycotoxins represents a severe problem for food safety. In conventional thermal processes, mycotoxins are not affected. Thus, it becomes essential to find an alternative treatment to eliminate or at least reduce their content in food. It has been proved that UV technology can be useful to decompose some toxins that are not affected by thermal processing (Falguera *et al.*, 2011b). Ibarz *et al.* (2014 and 2015b) proved that patulin as well as ochratoxyn can be degraded in aqueous media by irradiation with a multi-wave emitting lamp.

1.3.4 Loss of vitamin C

Ascorbic acid absorbs radiations between 220 and 300 nm (Koutchma, 2009). Therefore, a number of studies have reported losses of ascorbic acid after UV irradiation of fruit juices (Tran and Farid, 2004; Falguera *et al.*, 2011d and 2014; Tikekar *et al.*, 2011; Unluturk and Atilgan, 2015). Such investigations have proved that ascorbic acid degradation is directly related to the UV dose applied.

Falguera *et al.* (2011d) observed losses of vitamin C between 4 and 70 % in apple juices irradiated for 120 min with a medium-pressure mercury lamp. This high difference between the results was attributed to variations in the juice pigmentation. Other components of fruits may influence the photo-degradation of ascorbic acid. For instance, the presence of fructose at levels found in apple juice increased the ascorbic acid degradation (Tikekar *et al.*, 2011). However, it must be taken into account that part of the degradation occurring during these treatments is due to the "regular" oxidation of the ascorbic acid and not to photochemical processes (Tran and Farid, 2004).

1.3.5 State of the art of UV technology for fruit juice processing

Due to the research into alternative technologies for food preservation instead of thermal treatments, during recent decades a number of studies have focused on the application of ultraviolet irradiation to reduce the food-borne microbial load in fresh foods. Since then, advances in science and engineering of UV irradiation and sufficient evidence have demonstrated that this technology is a viable alternative to the thermal pasteurization of liquid foods like fresh juices.

Different valuations are found in the literature about the application of UV technology for food processing. On the one hand, Koutchma (2009) affirms that the technology studied has a positive consumer image and is of interest to the food industry as low cost non-thermal method of preservation. On other hand, Oms-Oliu *et al.* (2012) argue that irradiation is not being widely used because of some misconceptions by consumers about its role causing cancer.

According to Guerrero-Beltrán and Barbosa-Cánovas (2004 and 2011), this technology has the advantage of not producing chemical residues, by-products or radiation. Besides, mycotoxyns and pesticide residues from fruit are decomposed (Falguera *et al.*, 2011c; Ibarz *et al.*, 2016b). Keklik *et al.* (2012) define UV pasteurization as a non-ionizing, non-chemical, and non-thermal technology, which is environmentally friendly, easy to handle, and cost-efficient.

Overall, UV-treated juices may have the added benefit of having a more fresh-like quality when compared to those processed by thermal pasteurization (Jiménez-Sánchez *et al.*, 2017). It has been observed that the colour of fruit juices is barely altered by UV light (Tran and Farid, 2004), whilst multi-wavelength radiations can counteract juice browning (Ibarz *et al.*, 2005). In addition, it has been proved that UV light processing does not have a significant impact on physicochemical characteristics such as pH, soluble solids content and turbidity (Falguera *et al.*, 2011d and 2013a; Santhirasegaram *et al.*, 2015).

Most of the scientific reports have evaluated the effects of UV pasteurization on fruits of high commercial value such as apple, orange and grape juices. Nontheless, scarce information was found about the application of ultraviolet radiation in peach and nectarine juices. These products have commercial potential. Peach juice is among the top five juice flavours preferred by consumers in the European Union (Fig. 3), whilst nectarine is an underutilized fruit for derivative products.

Besides, other quality issues should be considered for the application of UV pasteurization to fruit juices. The effect of this treatment on flavour and odour substances is still unknown. Knowledge of the degradation kinetics of vitamins, enzymes and bioactive compounds by UV light will allow optimization of this pasteurization method while losses of these health-related compounds are minimized. The formation or degradation of toxic compounds like HMF should also be considered.

Another concern is the high UV doses needed to inactivate enzymes present in juices. This is because an overexposure of juices to ultraviolet light may result in

significant losses of vitamins as well as changes in organoleptic characteristics. With the aim of improving the efficiency of UV treatments to inactivate microorganisms and enzymes, current research projects are focusing on combining this method with either mild thermal treatments – up to 60ºC - or other non-thermal technologies.

An interesting proposal is the combination of ultrasound and ultraviolet processing in a hurdle concept. Santhirasegaram *et al.* (2015) observed that the sensory attributes of mango juice were minimally affected after ultrasound-ultraviolet treatment. Ultrasound (US) is defined as sound waves with a frequency that exceeds the hearing limit of the human (>20 kHz). High-power US is disruptive when it propagates through a liquid medium (Awad *et al.*, 2012). Due to this property US processing or sonication has been shown to be effective at inactivating microorganisms (Piyasena *et al.*, 2003) and enzymes (Baltacioğlu *et al.*, 2017).

In this thesis, some gaps in the knowledge of UV technology were studied, as stated in the objectives presented bellow. In addition, the use of mild-thermal temperatures during irradiation was investigated. Finally, US technology was explored as a process to assist ultraviolet and mild-heat treatments used to inactivate microorganisms and enzymes in fruit juices.

CHAPTER 2. OBJECTIVES AND WORKING PLAN

2.1 Aims and objectives

Main aim:

Study the effect of ultraviolet-visible irradiation on the quality attributes (enzymatic activities, physicochemical properties, vitamin C and HMF) of clarified fruit juices.

Specific objectives:

a) Study the effect of UV-Vis processing on the content of 5-hydroxymethylfurfural in nectarine juices.
b) Study the photo-degradation of 5-hydroxymethylfurfural with UV irradiation under different temperature and pH conditions in order to propose a degradation mechanism and a mathematical model to describe the photo-degradation kinetics.
c) Model the photo-degradation kinetics of 5-hydroxymethylfurfural with UV irradiation in model solutions with different initial concentrations.
d) Determine the mechanism that controls the photo-degradation of HMF in aqueous solutions, applying kinetic and thermodynamic compensation.
e) Evaluate the effect of UV-Vis processing on the enzymatic activities and physicochemical properties (pH, acidity, soluble solids, colour, formol index, ascorbic acid, phenolics and sugars) of juices from different nectarine varieties.
f) Evaluate the effect of UV-Vis processing on the enzymatic activities and physicochemical properties (pH, acidity, soluble solids, colour, formol index, ascorbic acid, phenolics and sugars) of juices from different peach varieties.
g) Study the degradation of ascorbic acid in model solutions during the UV-Vis processing under different temperature and pH conditions in order to propose a degradation mechanism and a mathematical model to describe the kinetics of degradation.

Additional objective:

Study the effect of ultrasound processing - as a complementary technology for UV processing- on ascorbic acid content in model solutions and fruit juices.

2.2 Working plan

In pursuit of the abovementioned objectives, the general working plan was structured in the following stages:

1. Preliminary bibliographic review of the use of ultraviolet technology on liquid food products.
2. Identification of the main variables that determine the quality of fruit juices as well as the variables influencing UV processing efficiency.
3. Selection of commodities used to obtain the fruit juices for the experiments, considering availability and socioeconomic importance.
4. UV irradiation preliminary tests.
5. Optimization of the chromatographic method to determine the content of 5-hydroxymethylfurfural in aqueous media.
6. UV-Vis irradiation of model solutions of 5-hydroxymethylfurfural at different initial concentrations and temperature and pH conditions.
7. Modelling of the kinetics of photo-degradation of 5-hydroxymethylfurfural.
8. Determination of the rate-controlling mechanism in the photo-degradation of 5-hydroxymethylfurfural, applying kinetic and thermodynamic compensation.
9. Obtainment of fruit samples and processing into fruit juices.
10. UV-Vis irradiation of nectarine juices.
11. UV-Vis irradiation of peach juices.
12. Physicochemical analyses of irradiated fruit juice samples.
13. Actinometrical evaluation
14. UV-Vis irradiation of model solutions of L-ascorbic acid under different temperature and pH conditions.
15. Experiment to evaluate the effect of ultrasound processing on the ascorbic acid content of model solutions and real fruit juices.
16. Statistical analysis
17. Continuous bibliographic review.
18. Discussion of results, drafting of conclusions and communication of results in conferences and scientific papers.

CHAPTER 3. MATERIALS AND METHODS

The experiments developed for this thesis, except those that involved sonication, were performed at the Department of Food Technology of the University of Lleida (Lleida, Catalonia, Spain). The experiments with sonication were performed at the Department of Agri-food Industry, Food, and Nutrition (LAN) of the Luiz de Queiroz College of Agriculture of the University of São Paulo (Piracicaba, SP, Brazil). They were conducted under the supervision of Professor Pedro Esteves Duarte Augusto.

3.1 Materials

3.1.1 Reagents

The reagents used for the experiments are summarized in Table 3. Distilled water was used to prepare solutions and undertake regular analyses. Ultrapure water was used for the chromatographic analysis.

3.1.2 Buffer solutions

Buffer solutions with different pH values (3, 3.4, 4, 5 and 6) were prepared in order to establish the pH of the model solutions designed. With that purpose, adequate quantities of citric acid and sodium acid phosphate were dissolved in water as indicated in Table 4.

3.1.3 Model solutions

Aqueous solutions of 5-hydroxymethylfurfural with different pH values were prepared by dissolving this compound in buffer solutions. Likewise, aqueous solutions of L-(+)-ascorbic acid were prepared. All the model solutions used for the experiments are organized in Table 5.

For the experiment that evaluated the ascorbic acid content during sonication, degassed solutions were prepared as follows. Portions of 315 mL of buffer solutions were placed in 600-mL beakers and degassed by sonication for 20 min. After that, the beakers were heated or cooled to the working temperature. Meanwhile, a stock solution of ascorbic acid (2.5 $mg \cdot mL^{-1}$) was made and stored in darkness. Just before starting the treatments, after the desired temperature was reached, 35 mL of the corresponding stock solution were added to each beaker containing the buffer solution. The samples were carefully homogenized to avoid the incorporation of air to a concentration of 250 $mg \cdot L^{-1}$. This approach guaranteed the minimal presence of dissolved oxygen.

Table 3. Reagents used for the experiments.

Reagent	Supplier
2,6-Dichloroindophenol	Sigma-Aldrich, Steinheim, Germany
	Sigma-Aldrich, Rio de Janeiro, Brazil
4-Methylcatechol	Sigma-Aldrich, St. Louis, MO, USA
5-Hydroxymethyl-2-furfural (HMF)	Sigma-Aldrich, China
Acetic acid glacial	Labsynth, São Paulo, Brazil
	Panreac Química SLU, Barcelona, Spain
Acetonitrile (HPLC-gradient grade)	Panreac Química SLU, Barcelona, Spain
Citric acid anhydrous	Applichem, Darmstadt, Germany
	Labsynth, São Paulo, Brazil
Disodium hydrogen phosphate (Na_2HPO_4)	Applichem, Darmstadt, Germany
Folin-Ciocalteu reagent	Panreac Química SLU, Barcelona, Spain
Gallic acid	Merck KGaA, Darmstadt, Germany
L-(+)-ascorbic acid	Panreac Química SLU, Barcelona, Spain
	Labsynth, São Paulo, Brazil
Formaldehyde 35% v/v	Panreac Química SLU, Barcelona, Spain
Hydrogen peroxide 30% w/v	Foret, S.A., Barcelona, Spain
Metaphosphoric acid	VWR International, Leuven, Belgium
	Dinâmica, São Paulo, Brazil
Oxalic acid 2-hydrate	Panreac Química SLU, Barcelona, Spain
Pyrogallol	Fluka Analytical, St. Louis, MO, USA
Potassium permanganate ($KMnO_4$)	Panreac Química SLU, Barcelona, Spain
Sodium acid carbonate ($NaHCO_3$)	Panreac Química SA, Barcelona, Spain
Sodium carbonate (Na_2CO_3)	Prolabo, Fontenay sous Bois, France
Sodium hydroxide (NaOH) 1N	VWR International, Fontenay sous Bois, France
Uranyl nitrate crystallized	Panreac Química SLU, Barcelona, Spain

3.1.4 Fruit juices

Nectarines and peaches (*Prunus persica* L. Batsch) from different varieties were obtained from local producers in the region of Lleida (Catalonia, Spain). The varieties collected for the experiment are shown in Table 6.

Table 4. Volume of citric acid 0.1 M and Na_2HPO_4 0.2 M required to prepare 100 mL of buffer solution (McIlvaine, 1921).

pH	mL citric acid 0.1 M	mL Na_2HPO_4 0.2 M
3.0	79.45	20.55
3.4	71.50	28.50
4.0	61.45	38.55
5.0	48.50	51.50
6.0	36.85	63.15

Table 5. Model solutions used for the experiments.

Solute	Concentration ($mg \cdot L^{-1}$)	pH values
5-hydroxymethylfurfural	1	3, 4 and 5
	25	3, 4 and 5
	100	3, 3.4, 4 and 5
	10	4
L-(+)-ascorbic acid	250	3, 4, 5, and 6

Table 6. Raw materials used for juice production.

Fruit	Variety
Nectarine	Big Top
	Luciana
Peach	Baby Gold
	Calanda
Flat peach	Planet Top

The juice preparation process is schemed in Figure 8. The fruits were washed, cut in four, pitted, and squeezed with a household juicer. The resulting juice was centrifuged in an Avanti J-26XP centrifuge (Beckman Coulter, CA, USA), at 13000 rpm (26000g) for 25 min, following the method of Falguera *et al.* (2011d). This operation was undertaken at 4ºC to make separation of supernatant easier and reduce enzymatic activities. After centrifuging, the supernatant was recovered and the pellet was discarded. The juices from the Baby Gold peaches were further filtered with paper (pore size = 20 μm), because of the high content of insoluble polymers. Then, fractions of 800 mL of juice were stored in the freezer at -20 ºC.

For the experiment that evaluated the ascorbic acid content during sonication, commercial juices were used in order to avoid the presence of oxygen in the samples. Mandarin and orange juices (Tecpolpa Indústria e Comercio de Sucos Ltda, SP, Brazil) obtained by the UHT process and packaged in multi-layer packages (Tetra Pak®) were acquired in a local supermarket (Piracicaba, Brazil). These beverages do not contain other ingredients, additives or added water. The mandarin juice showed a pH = 3.72 ± 0.06 and 10.6 ± 0.1 ºBrix, and the orange juice showed a pH = 3.58 ± 0.10 and 10.8 ± 0.1 ºBrix.

3.2 Methods

3.2.1 UV installation

The samples were processed in a discontinuous plane photoreactor, used in previous theses (Falguera, 2012; Ibarz, 2016). The installation consists of a dark camera containing a single linear UV source and a reactor where the sample is placed (Fig. 9). Besides, the installation is coupled to an external refrigeration system to control the

temperature and has a magnetic stirrer used to guarantee that all the molecules of the reactant can reach the irradiated surface. The reactor was a methacrylate tank of parallelepiped shape. The UV source was a Philips HPM-12 mid-pressure mercury lamp of 460 W of nominal power that emits in a range between 250 and 740 nm (Philips, Eindhoven, Netherlands). The emission spectrum of the lamp, provided by the manufacturer, is shown in Figure 10.

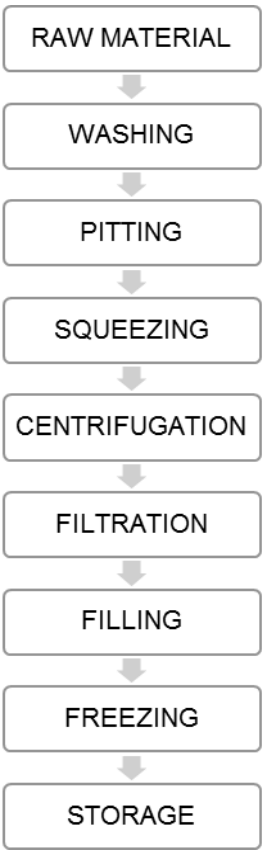

Figure 8. Diagram of processing of nectarine and peach juices.

3.2.2 Actinometry

The real power emitted by the lamp was determined by actinometry. The photo-decomposition of oxalic acid in the presence of uranyl cation was used. 800 mL of a solution of oxalic acid (0.05 M) and uranyl nitrate (0.001 M) were irradiated for 15 min, at 25ºC, in the installation described in the previous section. An aliquot was taken every minute and the oxalic acid content was quantified by titrating with $KMnO_4$ 0.05 M. The treatment and the analysis were carried out in duplicate. The oxalic acid conversion as a function of time was fitted to a straight line and the slope value was used to calculate the real power of the lamp according to Ibarz and Pagan (1986).

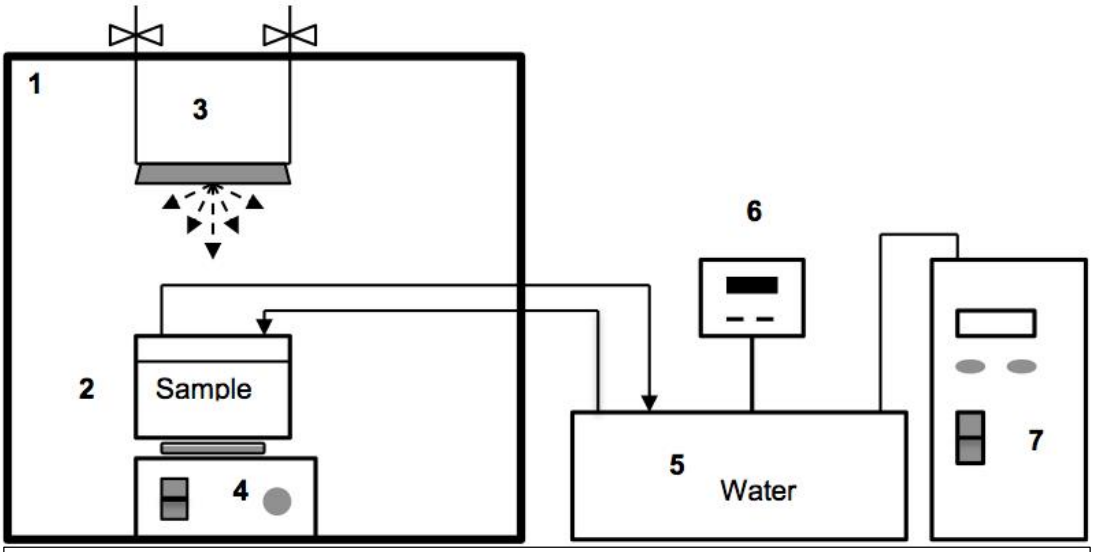

1. Dark camera 2. Reactor 3. Lamp with screen 4. Magnetic stirrer 5. Water bath 6. Heating system 7. Cooling system.

Figure 9. Scheme of the installation used for UV-Vis processing

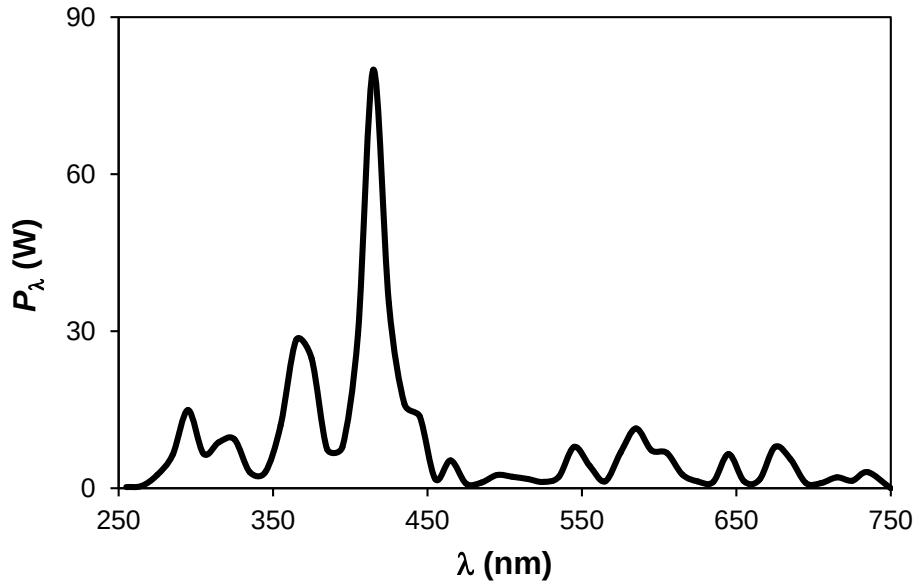

Figure 10. Emission spectrum of the lamp.

3.2.3 UV-Vis irradiations

Since the samples were processed under isothermal conditions, they were previously heated or cooled until the working temperature was reached. The frozen juice samples were unfrozen 24 h before processing at 8ºC. The HMF solutions were treated at 12, 25, 35 and 45 ºC. The AA solutions and fruit juices were treated at 25 and 45 ºC. Besides, HMF solutions at pH 3 were irradiated at 12 and 45 ºC without agitation. In the

case of the ascorbic acid degradation, the thermal effect was quantified by processing the samples in the same installation at the same temperatures but with the lamp off.

The lamp was turned on 10 min before putting the liquid in the chamber. Then, 800 mL of sample were processed in the reactor. The total irradiation time was 120 min for HMF solutions and fruit juices, and 60 min for AA solutions. Aliquots were taken at different processing times *t* for further analysis. The treatments were carried out in duplicate.

3.2.4 Ultrasound equipment and processing

For the experiment that evaluated the effect of US on ascorbic acid content, all the treatments were carried out inside an ultrasound bath (Q13/25 Ultronique, Brazil) with a nominal power of 700 W and a fix frequency of 25 kHz. The bath has its piezoelectric elements arranged below the tub, so that the mechanical waves are transmitted through the water and the product. The distribution of the ultrasonic waves in the water bath was determined by the aluminum foil method. The other good practices described by Vinatoru (2015) were also verified. The samples were placed in the parts where the waves had the highest and most homogeneous intensity. The actual volumetric power delivered to the samples was determined following the calorimetric method described by Tiwari *et al.* (2008), obtaining a value of 0.016 $W \cdot mL^{-1}$.

Glass beakers containing the samples were placed inside the ultrasonic bath. Six litres of distilled water were used as the transmission medium. In order to control the sample temperature (and also avoid overheating), a stainless steel heat exchanger coupled to an external water bath was placed inside the transmission medium. Once the temperature in the sample was reached, the AA was dissolved and the ultrasound was turned on. A scheme of the experiments performed in the US equipment is illustrated in Figure 11.

In a first experiment, 350-mL samples of different model solutions (pH 3, 4, 5 and 6) were placed in separate beakers and simultaneously processed for 60 min inside the ultrasonic bath. Four treatments were conducted: ultrasound processing at 25 ± 4 ºC (sonication), ultrasound processing at 55 ± 4 ºC (thermosonication), processing without ultrasound at 55 ± 4 ºC (thermal treatment), and processing without ultrasound at 25 ± 4 ºC (control treatment). Once the temperature inside the sample had been set, the ultrasonic input was turned on (for sonication and thermosonication) or kept off (for thermal and control treatments). All the treatments were performed in triplicate. Aliquots were taken

out for analysis at the start (t = 0) and every 5 min. They were quickly cooled in an ice/water bath before the quantification of the ascorbic acid.

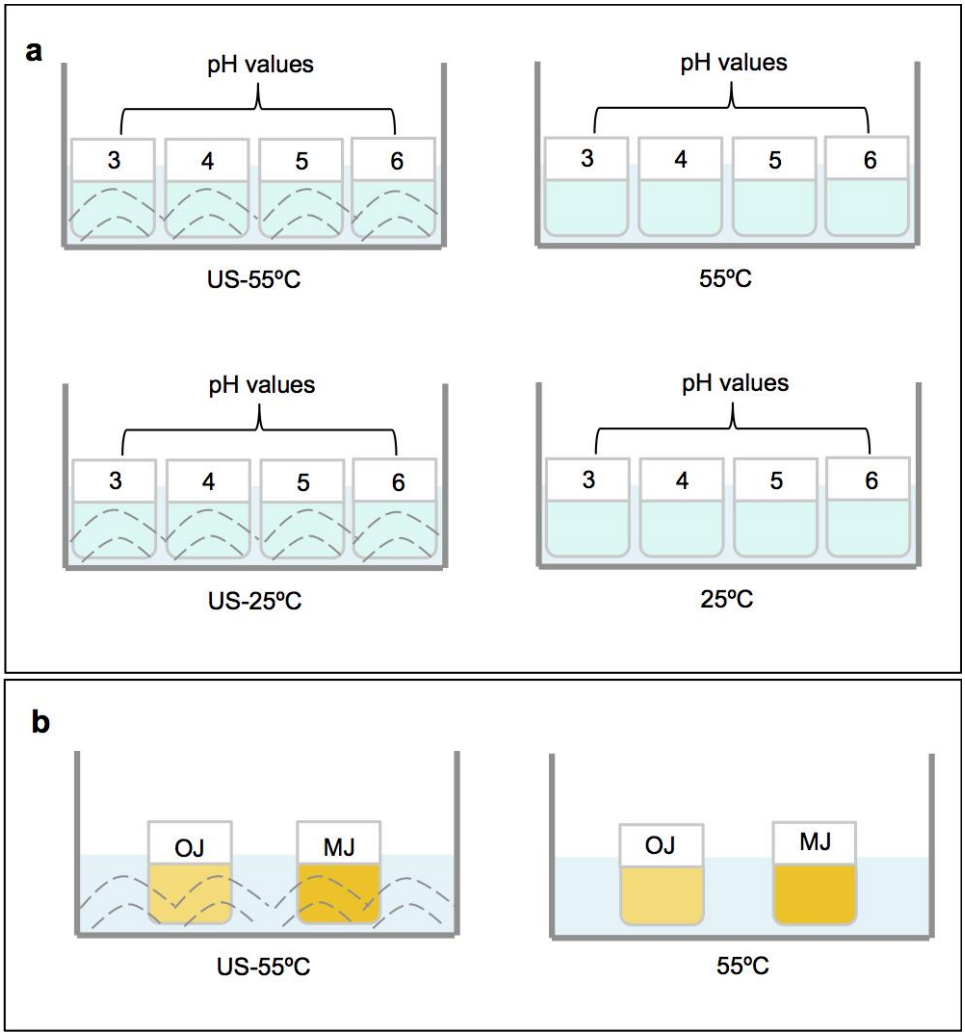

Figure 11. Treatments applied in degasified (a) model solutions and (b) fruit juices.

A second experiment consisted of sonicating deaerated juice samples exclusively at 55ºC in order to evaluate the ascorbic acid stability under the most severe conditions of the first experiment. As control treatments, samples of each juice were submitted to thermal processing (55ºC without sonication) (Fig. 11b). The procedure was similar to the first experiment. The temperature of 55ºC was chosen to emulate the conditions used in previous studies to accomplish significant reductions in pathogens whilst preserving quality attributes (Walking-Ribero *et al.*, 2009; Martínez-Flores *et al.*, 2015).

3.2.5 Sample analyses

The fruit juice samples were filtered with paper (pore size = 20 μm).

3.2.5.1 Absorption spectrum

The absorption spectrum was obtained by measuring the absorbance at different wavelengths between 200 and 750 nm. The measurements were performed with a Helios Omega (Thermo Fisher Scientific, Madison, U.S.A) spectrophotometer, using a 1-cm width quartz cell.

3.2.5.2 Determination of 5-hydroxymethylfurfural

The HMF content was determined by high performance liquid chromatography (Lee *et al*., 2014). 1260 Infinity HPLC equipment was used for this analysis. The stationary phase was a ZORBAX Eclipse Plus C18 -4.6 x 100 mm, 3.5 μm- column (Agilent Technologies, U.S.A.). The mobile phase consisted of 1 $mL \cdot min^{-1}$ of water and acetonitrile mix at a ratio of 99/1. A 10-μL sample was injected after being filtered with a 0.45 μm Chromafil GF/PET-45/25 filter (Macherey-Nagel, Düren, Germany). The quantification was performed with a diode-arrayed-detector –DAD- (Agilent Technologies, Germany) by means of the signal detected at 276 nm.

3.2.5.3 Determination of ascorbic acid

The ascorbic acid content in the samples was determined following the Official Method (AOAC, 2007), which consists of titration with 2,6-dichloroindophenol. The relative concentration C_{AA}/C_{AA}^{0} was calculated for model solutions, C_{AA} being the ascorbic acid concentration at the processing time t and C_{AA}^{0} the initial ascorbic acid concentration.

3.2.5.4 Physicochemical analyses

The pH was determined using a Crison micropH 2000 pH meter (Crison Instruments, S. A., Alella, Spain). The soluble solids content was measured using an Atago RX-1000 Digital Refractometer (Atago Co. Ltd. Japan). The juice colour was monitored using a Chroma Meter CR-400 tristimulus colorimeter (Konica Minolta Sensing, Inc., Japan). The total phenolic content was determined as described by Shaghaghi *et al.* (2008), using the spectrophotometric method and the Folin-Ciocalteu reagent. Titratable acidity was assayed following the official method of the International

Federation of Fruit Juice Producers (IFU, 1996a). The content of amino acids was evaluated by means of the formol index, determined by potentiometric titration (IFU, 1984).

The sugar and sorbitol contents were determined by HPLC (IFU, 1996b). The 1260 Infinity HPLC chromatograph equipped with a RID detector (Agilent Technologies, Germany) was used. The separation was performed in a Hi-Plex Ca 300 x 7.7 mm x 8 μm column (Agilent Technologies, GB) at 80ºC. The mobile phase consisted of 0.5 $mL \cdot min^{-1}$ of ultrapure water.

3.2.5.5 Enzymatic activities

The enzymatic activity of PPO was determined for each sample by measuring the increase in absorbance at 420 nm when the 4-methylcatechol substrate reacted with the enzyme in the juice (Yerlitürk *et al.*, 2008). In each assay, 1.0 mL of the juice sample and 2.5 mL of 4-methylcatechol (Sigma-Aldrich Co, India) 0.01 M in buffer solution at pH 4.0 (citric acid and Na_2HPO_4, Panreac, Spain) were mixed in a 1-cm quartz cuvette. The absorbance at 420 nm was measured every 5s for 3 min using a Helios Omega spectrophotometer (Thermo Fisher Scientific Inc., USA).

The enzymatic activity of POD was determined for each sample by measuring the increase in the absorbance at 420 nm when the substrate pyrogallol reacted with the POD enzyme present in the juice (Kwak *et al.*, 1995). In each assay, 160 μL of the juice sample, 2.25 mL of buffer solution at pH 6.0 (citric acid and Na_2HPO_4, Panreac, Spain) and 320 μL of 5% (w/v) pyrogallol (Sigma-Aldrich, China) solution were mixed in a 1-cm quartz cuvette. Finally, 160 μL of 0.147 M H_2O_2 solution (Foret, Spain) were added to start the reaction.

3.2.6 Statistical analysis

Average and standard deviations were calculated from the experimental results. The variables monitored during processing were graphed in function of time. Different mathematical models were used to fit the HMF degradation as well as the enzymatic inactivation data. Those fittings were conducted using Microsoft Office Excel (Microsoft, Co., USA, v. 2003) or StatPlus:mac (AnalystSoft, Inc., USA, v. 5) data processing software. The fittings of the AA content in function of time were performed with the STATGRAPHICS statistical software package.

The physicochemical characteristics of fruit juices were compared by means of a factorial analysis of variance (ANOVA) and a Tukey test, in order to find significant differences. This analysis was performed with the STATISTICA v.8 (Statsoft, Inc., USA) statistical software package.

The content of ascorbic in aqueous solutions at different processing times was compared in the samples treated with and without ultraviolet radiations. With that purpose a comparison of means was performed.

With the aim of knowing the effect of the ultrasound processing on the AA concentration, a one-way ANOVA (C_{AA}/C_{AA}^{0} vs t or C_{AA} vs t) was performed for each treatment. These analyses were run with the statistical software STATISTICA v.7 (Statsoft, Inc., USA).

A 95% significance level was considered in all the statistical tests.

CHAPTER 4. MATHEMATICAL MODELS

In order to quantify and predict chemical changes produced by ultraviolet radiation in a food system, a concrete modelling is required in each case.

4.1 Radiation balance

When a photochemical process occurs it is necessary to perform a radiation balance since the amount of absorbed radiation has a definitive effect on the reaction rate. This radiation balance is posed by adopting a model that is able to provide information about light rays, taking certain considerations about the kind of emission and the geometry of the system (Falguera *et al.*, 2011b).

The experiments for this thesis were carried out using a discontinuous plane photoreactor. The system consists essentially of a device with a parallelepiped shape with an external lamp without reflectors (Fig. 12). Consequently, there is only a direct radiation flow between the lamp and the reactor.

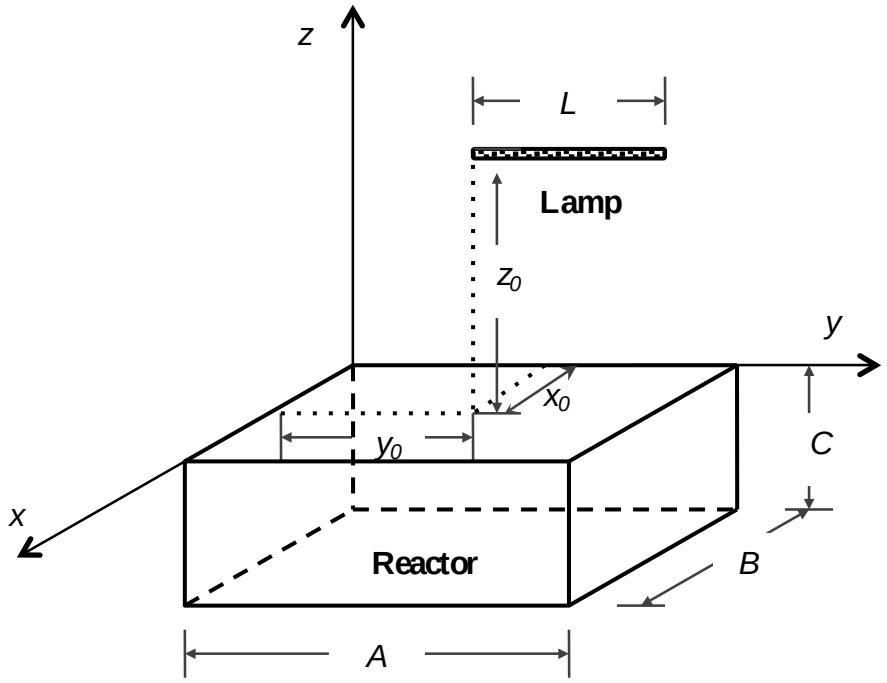

Figure 12. Scheme of a plane photoreactor.

Falguera *et al.* (2011b) mention three light emission models (radial, spherical or specular and diffuse) as well as three models for the emission source, depending on wether the lamp is considered as a line, a cylindrical surface or a volumetric region with cylindrical shape. In this work, the spherical linear model was used, which assumes the

lamp is a line that emits spherically. Extended descriptions of this model can be found in the literature (Jacob and Dranoff, 1970; Esplugas and Vicente, 1991).

4.1.1 Incident radiation at the reactor surface

Considering a plane photoreactor, the e-base absorbance, the Lambert-Beer law, the linear spherical emission model, and the spectral radiant power emitted by the lamp, Garvín *et al.* (2015) developed the following equation to obtain the incident spectral radiant power reaching a specific point inside the solution $P(x, y, z)$ at each wavelength:

$$P(x,y,z) = \sum_{\lambda} P_{\lambda}(x,y,z) = \sum_{\lambda} \frac{P_{emitt,\lambda} / L}{4\pi D^2} \int_{y_L=y_0}^{y_L=y_0+L} \exp\left(-\mu_{\lambda} \frac{z}{\sin\beta}\right) dy_L \tag{9}$$

In this equation (x, y, z) are the coordinates of a specific point inside the reactor, whereas (x_0, y_L, z_0) are the coordinates for each specific point of the lamp (Fig. 13); $P_{emitt,\lambda}$ is the real power emitted by the lamp at wavelength λ; D is the radius of the sphere defined by both the emitting lamp point and the solution point considered; β is the angle defined by D and the reactor surface. D and β can be obtained from the following expressions:

$$D^2 = (x - x_0)^2 + (y - y_L)^2 + (z + z_0)^2 \tag{10}$$

$$\sin\beta = \frac{z_0 + z}{D} \tag{11}$$

The incident spectral radiant power for a specific depth (z) of the reactor is obtained by integrating Eq. 9 for all the x and y values for the specific z value (Garvín *et al.*, 2015):

$$P(z) = \int_{x=0}^{x=A} \int_{y=0}^{y=B} P(x,y,z)\,dx\,dy = \sum_{\lambda} \frac{P_{emit,\lambda}}{4\pi} \int_{x=0}^{x=A} \int_{y=0}^{y=B} \int_{y_L=y_0}^{y_L=y_0+L} \frac{e^{-\mu_{\lambda}\frac{z}{\sin\beta}}}{D^2} dy_L\,dy\,dx \tag{12}$$

The values of $P(z)$ for z=0 and z=C are the incident radiation power on the surface ($P(0)$) and the bottom of the reactor ($P(C)$), respectively. The incident radiation power on the

reactor surface ($P(0)$) represents the intensity of UV irradiation, also called irradiance or radiation flux (in $W \cdot m^{-2}$).

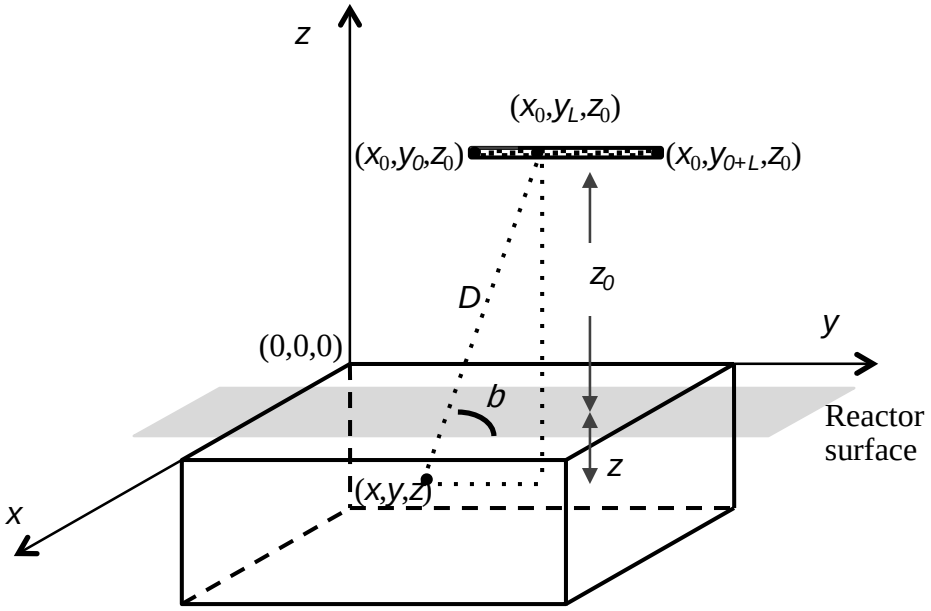

Figure 13. Localization of points in the photoreactor using a three-dimensional system of coordinates.

4.1.2 Radiant power absorbed by the solution (P_{abs})

Although the total radiation power absorbed by the solution depends on the incident radiation power at the reactor surface, only a fraction of this incident radiation power is absorbed. In fact, not even the incident radiation dose on the surface could be absorbed. In the case of diluted solutions, where the values of $\mu\lambda$ are low, Ibarz *et al.* (2014) developed a simplified equation to calculate the spectral radiant power that is absorbed by the whole solution contained in the reactor from the whole lamp:

$$P_{abs} = \frac{1}{V}\sum_{\lambda}\int_{x=0}^{x=A}\int_{y=0}^{y=B}\int_{z=0}^{z=C}\int_{y_L=y_0}^{y_L=y_0+L}\frac{P_{emit,\lambda}/L}{4\pi D^2}\,e^{-\mu_\lambda\frac{z}{\sin\beta}}\,\mu_\lambda\frac{dz}{\sin\beta}\,dy_L\,dx\,dy\,dz \qquad (13)$$

Nevertheless, Garvín *et al.* (2015) demonstrated that Eq. 13 is not applicable for high concentrations of the absorber in the solution. With the aim of solving that problem, they proposed dividing the reactor into layers (Fig. 14) leading to an equation suitable for any concentration value:

$$P_{abs} = \frac{1}{V}\sum_{\lambda}\sum_{i(z)=1}^{i(z)=n}\int_{x=0}^{x=A}\int_{y=0}^{y=B}\int_{y_L=y_0}^{y_L=y_0+L}\frac{P_{emit,\lambda}/L}{4\pi D^2}dy_L\left[e^{-\mu_\lambda D_{i-1}} - e^{-\mu_\lambda (D-D_0)}\right]dxdy \qquad (14)$$

Where *i* refers to each layer and *n* to the total number of layers.

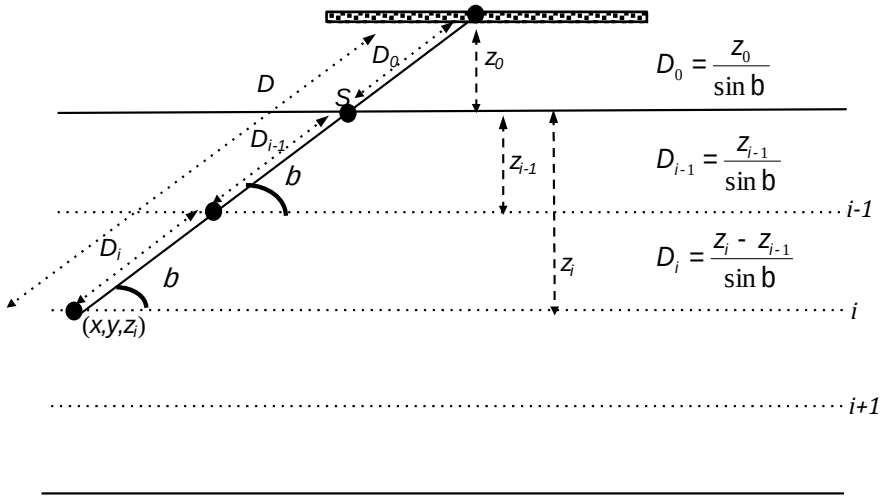

Figure 14. Frontal sight of a plane photoreactor divided into layers (Garvín *et al.*, 2015).

Equations 12, 13 and 14, need to be calculated for each concentration value by using the Simpson numerical method.

4.1.3 Quantum yield

When molecules absorb radiation, their energy states are quantized. The lowest energy state in which a molecule or atom can exist is called fundamental or normal state. In general, these states have paired electrons where the total spin is zero (singlet state). If an electron in one of these states goes to a higher energy level, it may remain unpaired, resulting in a state of non-zero total spin. If the molecule is excited, its natural tendency is to move towards a minimum energy state, deactivating itself.

For a given photochemical reaction consisting of a multi-stage reaction mechanism, Falguera *et al.* (2011b) defined the *quantum yield* (φ) as follows:

For each mechanism:

$$\varphi_i = \frac{\text{Number of excited molecules deactivated by the } i \text{ mechanism}}{\text{Total number of excited molecules}} \qquad (15)$$

If the final product of each process is P_j:

$$\varphi_i = \frac{\text{Total number of } P_j \text{ molecules produced}}{\text{Total number of photons absorbed}} \quad (16)$$

If the expression refers to the reactants and the global process:

$$\varphi_i = \frac{\text{Total number of deactivated molecules}}{\text{Total number of photons absorbed}} \quad (17)$$

or also:

$$\varphi_i = \frac{\text{Reactant disappearance molar rate}}{\text{Absorbed photons flow}} \quad (18)$$

4.2 Photo-degradation of 5-hydroxymethylfurfural

The kinetic equation depends on the reaction mechanism, which depends on the energy absorbed by the reactants. A simple case of a photochemical reaction mechanism is the assumption that there are three stages, as shown in the following scheme (Ibarz *et al.*, 2014 and 2015b):

$$\text{HMF} \xrightarrow{P_{abs}} \text{HMF*}$$
$$\text{HMF*} \xrightarrow{k_D} \text{HMF}$$
$$\text{HMF*} \xrightarrow{k} \text{Photoproducts}$$

Following that mechanism, in a first stage the HMF in its fundamental state absorbs radiation and goes into an excited state HMF*. From this state, it can return to its fundamental state or be decomposed into photoproducts. P_{abs} is the total spectral radiant power absorbed by the whole solution inside the reactor. Its units have to be Einsteins (mole of photons) per volume unit and per time unit, and can be calculated according to section 4.1.2. Considering that the irradiation is performed in a perfectly stirred reactor

working on batch process, the variation of each of the species that take part in the reaction mechanism can be expressed as:

$$r_{HMF} = \frac{dC_{HMF}}{dt} = k_D C_{HMF*} - P_{abs} \quad (19)$$

$$r_{HMF*} = \frac{dC_{HMF*}}{dt} = P_{abs} - k_D C_{HMF*} - kC_{HMF*} \quad (20)$$

where r_{HMF} and r_{HMF*} are the intensive reaction rates for HMF and HMF*, respectively. Assuming a pseudo-steady state for the excited intermediate HMF*, its net intensive reaction becomes zero:

$$P_{abs} - k_D C_{HMF*} - kC_{HMF*} = 0 \quad (21)$$

Isolating the concentration of the excited intermediate:

$$C_{HMF*} = \frac{1}{k_D + k} P_{abs} \quad (22)$$

Adding Eq. 22 to Eq. 19:

$$r_{HMF} = \frac{k_D}{k_D + k} P_{abs} - P_{abs} \quad (23)$$

Grouping and rearranging Eq. 23, this leads to:

$$r_{HMF} = \frac{dC_{HMF}}{dt} = \frac{-k}{k_D + k} P_{abs} \quad (24)$$

The term $\frac{k}{k_D + k}$ may be substituted by a global constant

$$K_{HMF} = \frac{k}{k_D + k} \tag{25}$$

Consequently,

$$\frac{dC_{HMF}}{dt} = -K_{HMF} P_{abs} \tag{26}$$

The K_{HMF} constant represents the quantum yield of overall photo-degradation as degraded moles per absorbed photon mole (Einstein).

With the aim of developing an accurate mathematical model to describe the photo-degradation of 5-hydroxymethylfurfural in aqueous media, it is necessary to solve Eq. 26. With that purpose, the relation between P_{abs} and the absorber concentration (C_{HMF}) must be defined.

As set forth above, both parameters are related according to Equation 14. Then, by means of a spreadsheet it is possible to calculate different values of spectral radiant power corresponding to different concentrations of the absorber substance. Garvín *et al.* (2015) obtained a curve of P_{abs} vs concentration for aqueous solutions of patulin (Fig. 15). That curve showed that P_{abs} increases with the concentration of patulin (C_P) in a non-linear way, tending to an asymptote for high concentrations. Interestingly, this asymptote coincides with the incident spectral radiant power at the surface of the reactor.

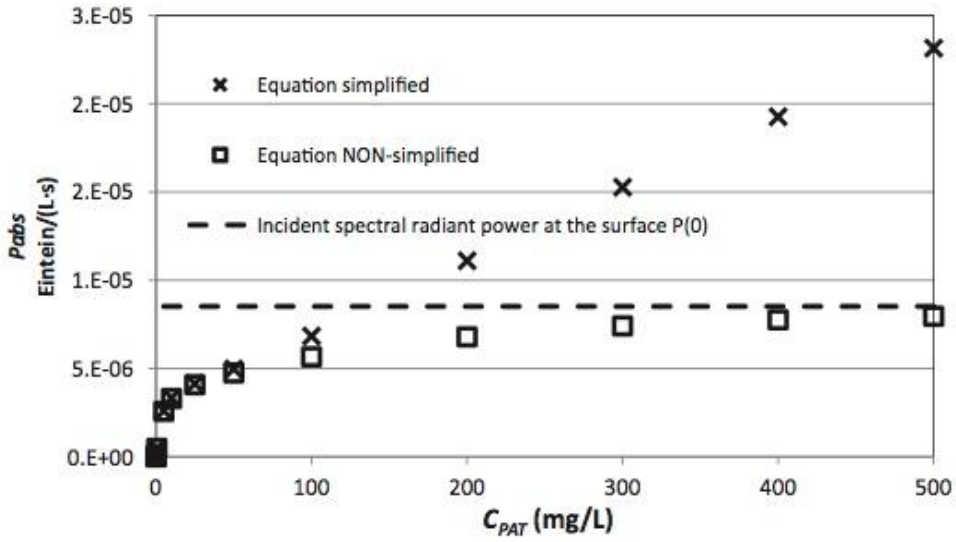

Figure 15. Spectral radiant power absorbed as a function of the absorber concentration (C_{PAT}) in aqueous patulin solutions. Results obtained using Eqs. 12, 13, and 14 (From Garvín *et al.*, 2015).

Considering narrow intervals of concentrations, it is possible to define P_{abs} as a function of the absorber concentration with simple mathematical models. For instance, Ibarz *et al.* (2014 and 2015b) proposed a linear equation -with origin ordinate equal to zero. Applying this relation for HMF:

$$P_{abs} = k_R C_{HMF} \tag{27}$$

This linear relationship is followed when the solution has low values of concentration of the absorber substance. This behaviour is due to the fact that, as not all the radiation that enters the solution is absorbed, an increase in the concentration of the absorbing substance will cause a proportional increase in the absorbed energy. In this case, integrating Eq. 27, a first-order kinetic is obtained:

$$C_{HMF} = C_{HMF}^{0} \cdot \exp(-m_{HMF} \cdot t)\,;\; m_{HMF} = K_{HMF} \cdot k_R \tag{28}$$

If P_{abs} does not depend on the absorber substance, it becomes constant

$$P_{abs} = k_R \tag{29}$$

Then, a zero-order kinetic is obtained:

$$C_{HMF} = C_{HMF}^{0} - m_{HMF} \cdot t\,;\; m_{HMF} = K_{HMF} \cdot k_R \tag{30}$$

This constant behaviour can be expected for high concentration values and hence, high absorption coefficients. It is assumed that this phenomenon occurs when all the radiation that reaches the surface of the reactor is totally absorbed. In this case, P_{abs} coincides with the incident radiant power on the surface of the reactor ($P(0)$).

For concentration ranges between the limits considered above, a curve relationship is expected. For narrow ranges, the curve could be approximated to a straight line with a non-zero origin ordinate, leading to a pseudo first-order kinetic.

$$P_{abs} = a + b \cdot C_{HMF} \tag{31}$$

$$\ln\left(\frac{a + b \cdot C_{HMF}}{a + b \cdot C_{HMF}^{0}}\right) = b \cdot K_{HMF} \cdot t\,;\; C_{HMF} = -\frac{a}{b} + \left(\frac{a}{b} + C_{HMF}^{0}\right)\exp(-b \cdot K_{HMF} \cdot t) \tag{32}$$

For these intermediate concentrations, if the origin ordinate *a* is much higher than the slope *b*, P_{abs} will be almost constant and a zero-order kinetic could also show good regression coefficients.

All values of k_R in Equations 27 and 29 are constant within each range of concentrations studied.

4.2.1 Thermodynamic compensation theory

The determination of control mechanisms in some physical, biological, and chemical processes can be described in terms of enthalpy-entropy compensation (Starikov and Nordén, 2012). For instance, some authors have suggested the existence of a linear relationship between enthalpy and entropy in water sorption in some foods (Beristain *et al.*, 1996; Azuara and Beristain, 2006), while others have proposed this relationship for air-drying (García *et al*., 2008). The interactions between water and other molecules have also been explained in terms of entropic and/or enthalpic mechanisms (Lum *et al.*, 1999; Chandler, 2002; Wilfong *et al.*, 2011; Ryde, 2014).

Initial studies, where the enthalpy-entropy compensation theory was developed, did not consider the practical relevance of this theory. However, over the last few years, this phenomenon has attracted attention because of possible applications in food science and technology. Thus, some works have related the enthalpy-entropy compensation to food microstructure (Azuara and Beristain, 2006; Chodera and Mobley, 2013) and stability (Azuara and Beristain, 2007; Pascual-Pineda *et al.*, 2014). Flores-Andrade *et al.* (2009) used this thermodynamic theory to develop low-temperature drying processes.

Williams *et al.* (2001) explain enthalpy-entropy compensation as a competition between dynamics and bonding, where it is the change in dynamics between two states (measured by the entropy change) that is primarily correlated with the reduction in bonding between the two states (measured by the enthalpy change).

It is known that when a reaction takes place different factors interact (e.g. pH, presence of metallic ions, water activity, etc.). Therefore, the frequency factor (K_0), the

activation energy (E_a), the enthalpy (ΔH), and the entropy (ΔS) can be obtained for each factor. For instance, for a family of pH values, a study of kinetic and/or thermodynamic compensation can help to know the reaction and its mechanism better (Leffler, 1955; Barnes *et al*, 1969; Zsako, 1976; Sun and Wicker, 1999). If the frequency factor is related linearly with the activation energy and the enthalpy of activation is also related linearly with the entropy of activation, the existence of the isokinetic temperature (T_B) can be concluded (Barnes *et al.*, 1969; Pysiak and Sabalki, 1979). T_B is defined as the temperature at which all the kinetic constants have the same value.

The isokinetic temperature can be estimated from an Arrhenius-type equation:

$$k = K_0 e^{-(E_a / RT)} \tag{33}$$

Where k is the reaction kinetic constant (in mole·L^{-1}·s^{-1}), K_0 the frequency factor (in mole·L^{-1}·s^{-1}), E_a the activation energy (in J·mol^{-1}), R the universal gas constant (in J·mol^{-1}·K^{-1}), and T the absolute temperature (in K).

In the case of HMF photo-degradation, the Arrhenius equation can be used to calculate the activation energy from the kinetic constants obtained from the experimental results at constant pH value and four temperatures.

$$m_{\mathrm{HMF}} = K_0 e^{-(E_a / RT)} \tag{34}$$

Once E_a and K_0 have been calculated at each pH value, the isokinetic temperature can be estimated with the linearized form of Eq. 34, feeding into it the ln K_0 vs E_a data and obtaining the slope.

$$K_0 = k_{eq} e^{\frac{E_a}{RT_B}} \tag{35}$$

$$\ln K_0 = \ln k_{eq} + \frac{E_a}{RT_B} \tag{36}$$

k_{eq} being the equilibrium kinetic constant predicted for all pH values when the HMF photo-degradation is carried out at the isokinetic temperature (T_B).

Another way to compute the isokinetic temperature is from a thermodynamic equation based on the transition state theory (Missen *et al.*, 1999). In the case of HMF photo-degradation, that equation would be expressed as:

$$\ln\left(\frac{k_{HMF}}{C^{0}_{HMF}}\right) - \ln\left(\frac{K_B T}{h}\right) = \frac{\Delta S}{R} - \frac{\Delta H}{RT} \tag{37}$$

K_B is the Boltzmann constant (in $J \cdot K^{-1}$) and h is the Planck's constant (in J·s.)

The enthalpy-entropy compensation can be established through the following equation, from which the isokinetic temperature is calculated (Beristain *et al.*, 1996):

$$\Delta H = T_B \Delta S + \Delta G_B \tag{38}$$

ΔG_B represents the change in Gibbs free energy at the isoequilibrium point (in $J \cdot mol^{-1}$) and can be obtained with the following equation:

$$\Delta G_B = \Delta H - T\Delta S \tag{39}$$

The method to confirm the existence of compensation is by comparing T_B with the harmonic mean temperature (T_{hm}). The harmonic mean temperature is defined as:

$$T_{hm} = \frac{N}{\sum_1^N \left(1/T\right)} \tag{40}$$

N being the total number of treatments. According to the test of Krug *et al.* (1976), if T_{hm} falls within the T_B interval, the data distribution observed (ΔH) – (ΔS) is due to the propagation of the experimental error and not to chemical or biological factors. In addition, Leffler's criterion (1955) is used to determine which mechanism controls the process. This criterion establishes that if $T_B > T_{hm}$, the process is enthalpy controlled and, contrarily, if $T_B < T_{hm}$, the process is entropy controlled.

4.3 Enzymatic inactivation

Both polyphenol oxidase and peroxidase enzymes catalyze reactions whose

products absorb radiation at 420 nm while the reactants do not. As a consequence, the increase in the absorbance at 420 nm can be fitted to an increasing exponential curve with an asymptotic limit described by the following equation:

$$A(t_{an}) = A^{\infty} - (A^{\infty} - A^{0}) \cdot \exp(-k_{an} \cdot t_{an}) \quad (41)$$

where $A(t_{an})$ is the absorbance at 420 nm of the sample at any analysis time t_{an}, A^0 is the initial absorbance, A^{∞} is the asymptotic absorbance and k_{an} is the kinetic constant of this analytical reaction used to determine the enzymatic activity.

Considering the Lambert-Beer equation, the absorbance of the solution during analysis follows the equation bellow:

$$A(t_{an}) - A^{0} = \varepsilon_P L C_P \quad (42)$$

ε_P being the extinction molar coefficient of the product of the enzymatic reaction, L the optical path of the beam used to check the absorbance (1cm of the quartz cell) and C_P the concentration of the product of the analytical enzymatic reaction. For both analytical enzymatic reactions, the reactant concentration used (C_R) is known to be much lower than the M kinetic value of the Michaelis-Menten kinetic equation. Thus, the kinetic equation behaves like a first-order kinetic.

$$r_R = -\frac{k_{cat} C_E C_R}{M + C_R} \approx -\frac{k_{cat} C_E}{M} C_R \quad (43)$$

$$r_R = \frac{dC_R}{dt} = -\frac{k_{cat} C_E}{M} C_R \quad (44)$$

C_E being the initial concentration of the enzyme and k_{cat} the kinetic constant for the product formation reaction from the complex enzyme-substrate.

Considering the cell where the absorbance is checked as a stirred tank and 1:1 being the stoichiometric ratio between reactant (R) and product (P), the evolution of both the reactant and reaction product (C_P) follows exponential equations:

$$C_R = C_R^0 \exp\left(-\frac{k_{cat} C_E}{M} t_{an}\right) \quad (45)$$

$$C_P = C_R^0 \left(1 - \exp\left(-\frac{k_{cat} C_E}{M} t_{an}\right)\right) \quad (46)$$

Adding Equation 46 to Equation 42:

$$A(t_{an}) - A^0 = \varepsilon_P L C_R^0 \left(1 - \exp\left(-\frac{k_{cat} C_E}{M}\right) t_{an}\right) \quad (47)$$

From the absorbance evolution, the enzymatic activity (*EA*) for any sample (after t_{UV} irradiation time) is defined as the initial analytical reaction rate that corresponds to the maximum reaction rate:

$$EA(t_{UV}) = \left(\frac{dA(t_{an})}{dt_{an}}\right)_{t_{an}=0} \quad (48)$$

From Equation 41, the enzymatic activity becomes:

$$EA(t_{UV}) = (A^{\infty} - A^0) \cdot k_{an} \quad (49)$$

And from Equation 47:

$$EA(t_{UV}) = \varepsilon_P L C_R^0 \frac{k_{cat} C_E}{M} \quad (50)$$

From Equation 50, it can be seen that the enzymatic activity is proportional to the concentration of the enzyme present in the solution being analyzed.

The relative enzymatic activity at a specific inactivation time t_{UV} ($REA(t_{UV})$) is defined by the ratio between the enzymatic activity at this specific inactivation time t_{UV} ($EA(t_{UV})$) and the initial enzymatic activity of the solution prior to being irradiated ($EA(t_{UV}=0)$). This parameter can be used to know the enzymatic inactivation kinetic:

$$REA(t_{UV}) = \frac{EA(t_{UV})}{EA(t_{UV} = 0)} = \frac{C_E(t_{UV})}{C_E^0} \tag{51}$$

Sometimes, the inactivation of the enzyme during irradiation (t_{UV}) follows a first-order kinetic equation (e.g. Falguera *et al.*, 2012), E_N being the native form of the enzyme and E_D the denatured form.

$$E_N \xrightarrow{k} E_D \tag{52}$$

$$C_E(t_{UV}) = C_E^0 \exp(-kt_{UV}) \tag{53}$$

$$REA(t_{UV}) = \frac{EA(t_{UV})}{EA(t_{UV} = 0)} = \exp(-kt_{UV}) \tag{54}$$

where k is the first-order kinetic constant of the enzymatic inactivation, whose value can be obtained by fitting the experimental data of the evolution of the relative enzymatic activity.

Some other times, the denaturation process of the enzyme follows a serial first-order reaction through an intermediate form (I) that also has enzymatic activity, and this activity can even be higher than the one for the native form (Giner-Seguí *et al.*, 2006).

$$E_N \xrightarrow{k_1} E_I \xrightarrow{k_2} E_D \tag{55}$$

For this case, the evolution of the concentration of each enzyme form in a stirred tank is:

$$C_{E_N}(t_{UV}) = C_{E_N}^0 \exp(-k_1 t_{UV}) \tag{56}$$

$$CE_I(t_{UV}) = \frac{C_{E_N}^0 k_1}{k_2 - k_1}\left[\exp(-k_1 t_{UV}) - \exp(-k_2 t_{UV})\right] \tag{57}$$

In this case, the analytical determination of the enzymatic activity includes the activity of both the native and the intermediate forms.

$$A(t_{an}) - A^0 = \varepsilon_R L C_R^0 \left(\left(1 - \exp\left(- \frac{k_N C_{E_N}(t_{UV})}{M} \right) \right) + \left(1 - \exp\left(- \frac{k_I C_{E_I}(t_{UV})}{M} \right) \right) \right) \quad (58)$$

$$EA(t_{UV}) = \varepsilon_R L C_R^0 \left(\frac{k_N C_{E_N}(t_{UV})}{M_N} + \frac{k_I C_{E_I}(t_{UV})}{M_I} \right) \quad (59)$$

$$EA(t_{UV} = 0) = \varepsilon_R L C_R^0 \left(\frac{k_N C_{E_N}^0}{M_N} \right) \quad (60)$$

$$REA(t_{UV}) = \frac{C_{E_N}(t_{UV})}{C_{E_N}^0} + \frac{k_I}{k_N} \frac{M_N}{M_I} \frac{C_{E_I}(t_{UV})}{C_{E_N}^0} \quad (61)$$

$$REA(t_{UV}) = \exp(-k_1 t_{UV}) + \frac{k_I / M_I}{k_N / M_N} \frac{k_1}{k_2 - k_1} \left[\exp(-k_1 t_{UV}) - \exp(-k_2 t_{UV}) \right] \quad (62)$$

Defining Λ as:

$$\Lambda = \frac{k_I / M_I}{k_N / M_N} \quad (63)$$

$$REA(t_{UV}) = \exp(-k_1 t_{UV}) + \frac{\Lambda k_1}{k_2 - k_1} \left[\exp(-k_1 t_{UV}) - \exp(-k_2 t_{UV}) \right] \quad (64)$$

Λ is the ratio between the kinetic constants of the intermediate and native enzyme forms for the analytical enzymatic reaction. The value of this parameter shows which enzyme form is more active in the presence of the reagent used in the analytical method (faster analytical enzymatic reaction). If this parameter is greater than 1, it means that the intermediate enzyme form has more activity than the native form. k_1 and k_2 are the first-order kinetic constants of the serial inactivation UV process of the native enzyme form through the intermediate enzyme form (Eq. 55).

4.4 Ascorbic acid oxidation

The oxidation of ascorbic acid (AA) occurs in two steps. The first step involves the formation of dehydroascorbic acid (DHAA), which is very unstable to hydrolysis. Such hydrolysis is irreversible, forming 2,3-diketogulonic acid (DKGA) (Vieira, 2000;

Gregory, 2008). A kinetic model based on this mechanism was properly developed by Serpen and Gökmen (2007). However, under specific conditions, e.g. in the absence of reducing agents like cysteine, simpler models fitted the oxidation of ascorbic acid well.

To date, several authors have studied the ascorbic acid degradation kinetics in fruit derivatives under pasteurization and storage conditions (Burdurlu *et al.*, 2006; Wibowo *et al.*, 2015). Those authors stated that the reaction follows a first order reaction mode

$$\frac{C_{AA}}{C_{AA}^{0}} = e^{-k_O \cdot t} \tag{65}$$

Where C_{AA} is the concentration of ascorbic acid (AA) at time *t*, C_{AA}^{0} the initial AA concentration and k_O the rate constant. Other researchers (Vieira *et al.*, 2000) concluded that the thermal degradation reaction of ascorbic acid deviates from simple first-order and proposed a fractional conversion kinetic model:

$$\frac{C_{AA} - C_{AA}^{\infty}}{C_{AA}^{0} - C_{AA}^{\infty}} = e^{-k_O t} \tag{66}$$

Where C_{AA}^{∞} is the relative AA concentration at time ∞.

4.5 Photo-degradation of ascorbic acid

In this work, a mechanism of photochemical degradation for the ascorbic acid it is proposed which is analogous to that developed by Ibarz *et al.* (1996) for the photo-degradation of benomyl. A four stage mechanism is supposed to occur. In an initial stage, the molecule of AA absorbs the incident radiation from a ground state into an excited one (AA*). The excited molecule can decline to its fundamental state (Stage 2) or degrade to form photoproducts (Stage 3). A fourth stage is added, which represents the oxidation of the ascorbic acid (See section 4.4):

Stage 1: $AA \xrightarrow{P_{abs}} AA^{*}$

Stage 2: $AA^{*} \xrightarrow{k_D} AA$

Stage 3: $AA^{*} \xrightarrow{k} \text{Photoproducts}$

Stage 4: $AA \xrightarrow{k_O} DKGA$

P_{abs} was defined in previous sections, being calculated with Eq. 14. Assuming a pseudo-steady state for the excited intermediate AA*, the intensive reaction rate for AA can be expressed as:

$$r_{AA} = -K_{AA} P_{abs} - k_O C_{AA} \tag{67}$$

Where K_{AA} is a dimensionless constant which depends on k and k_D:

$$K_{AA} = 1 - \frac{k_D}{k + k_D} = \frac{1}{1 + \frac{k_D}{k}} \tag{68}$$

According to the proposed mechanism, the K_{AA} constant represents the quantum yield of overall photo-degradation as degraded moles per absorbed photon mol (Einstein).

As the irradiation processes were performed in a perfectly stirred reactor of volume V, working on a batch process, the next equation is obtained from a mass balance:

$$\frac{dC_{AA}}{dt} = -K_{AA} P_{abs} - k_O C_{AA} \tag{69}$$

For low values of the concentration of the absorber substance, P_{abs} can be fitted to a linear equation with origin ordinate. If applicable, the next relation is defined:

$$k_R = \frac{P_{abs}}{C_{AA}} \tag{70}$$

Adding Equation 70 to Equation 69, the following is obtained:

$$\frac{dC_{AA}}{dt} = -(K_{AA} k_R + k_O) C_{AA} \tag{71}$$

If k_R does not vary considerably during the irradiation process, an average value can be considered approximately constant. Thus, Equation 69 can be integrated to obtain:

$$C_{AA} = C_{AA}^{0} \exp(-m_{AA} t) \; ; \; m_{AA} = K_{AA} k_R + k_O \tag{72}$$

As can be observed in Equation 70, from the proposed mechanism, the photo-degradation of ascorbic acid can be fitted to a first-order kinetic model, with a global photo-degradation constant m_{AA}.

CHAPTER 5. RESULTS AND DISCUSSION

5.1 Actinometry

The actinometrical evaluation concluded that the lamp emitted a real power of approximately $1.38 \cdot 10^{-3}$ Einstein$\cdot s^{-1}$.

5.2 Effect of the ultraviolet-visible irradiation on the HMF content

5.2.1 Irradiation of clarified nectarine juice

No HMF content was observed in clarified nectarine juice for irradiation treatments between 0 and 120 min, confirming that UV irradiation is an alternative method to thermal treatment because it does not produce HMF.

5.2.2 Absorption spectrum

In order to study the effect of the radiation on a substance, the specific absorption spectrum at different wavelengths needs to be known. This absorption spectrum usually presents maximum absorbance peaks, which determine the optimum range of working wavelengths (Ibarz *et al.*, 2015a). Figure 16 shows the evolution of the absorption spectrum in an irradiated HMF solution at pH 4, showing an absorption band between 250 and 330 nm. Checking the emission spectrum of the lamp used (Fig. 10), it is expected that HMF molecules absorb a fraction of the energy emitted from the lamp in this wavelength range, initiating the mechanism of photo-chemical degradation.

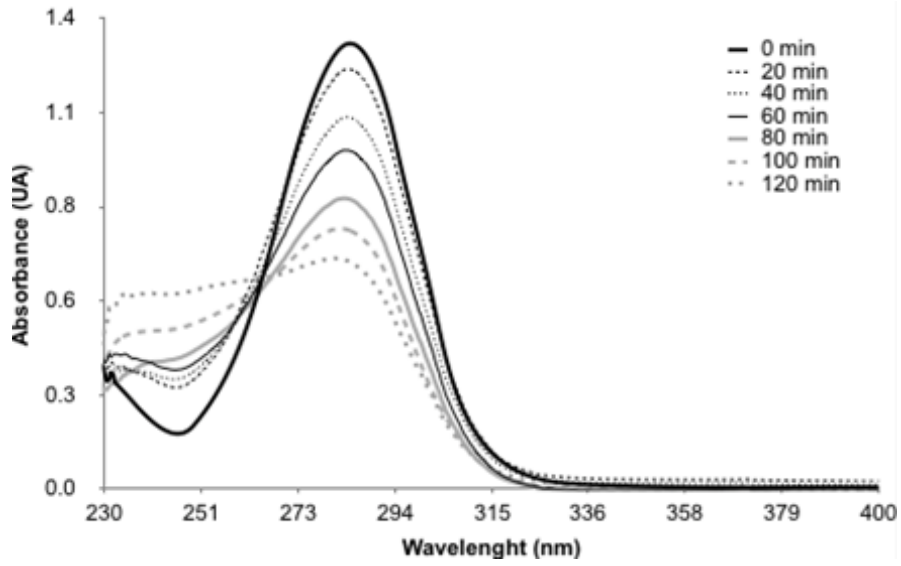

Figure 16. Absorption spectrum of a 10-mg$\cdot L^{-1}$ HMF solution at pH=4 during UV irradiation at 12 ºC.

The absorption spectra for the 10-mg·L^{-1} HMF solution at pH 3 and 5 were also obtained, fully matching with the curve in Figure 16, which was obtained at pH 4. It can thus be concluded that the UV absorption by HMF does not depend on the pH value within the pH range between 3 and 5. This range of pH values was chosen according to the pH range found in most fruit juices (Falguera *et al.*, 2012b, Koutchma, 2009).

Figure 16 also shows a gradual decrease in the absorption at 280 nm as the irradiation time lengthens. Taking into account Lambert-Beer's law, the disappearance of peak absorption suggests a reduction in HMF content during the ultraviolet processing. At 45ºC, a new peak near 250 nm appears and increases during irradiation, suggesting the formation of an unknown compound (Fig. 17). This does not occur at 12 ºC.

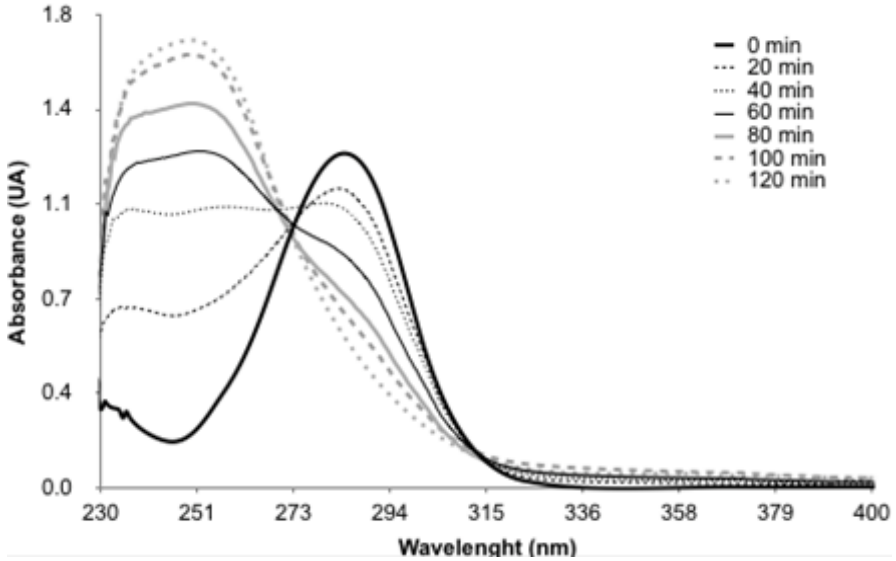

Figure 17. Absorption spectrum of a 10-mg·L^{-1} HMF solution at pH=4 during UV irradiation at 45 ºC.

5.2.3 Incident radiation

Table 7 displays the molar extinction coefficients ($\varepsilon\lambda$) calculated from the absorption spectrum obtained for the 25 mg·L^{-1}-HMF solution at pH 4, applying the Lambert-Beer equation (Eq. 4). This table also shows the absorption coefficients ($\mu\lambda$) for the HMF solutions of 1 and 100 mg·L^{-1}.

The absorption coefficients obtained were used to calculate the incident radiant power reaching the surface of the reactor ($P(0)$) and its bottom ($P(C)$), depending on the other coordinates (x and y). This calculation was performed for two reactors of different dimensions (22x15x10 cm and 12.5x10.5x10 cm) and considering a 100-mg·L^{-1} HMF solution. The results for the big and small reactor are shown in Figures 18 and 19,

respectively. As expected, in both cases the energy that reaches the surface of the reactor is greater than the energy that reaches the bottom, suggesting that a portion of the irradiation that enters the reactor is absorbed by the solution.

Table 7. 5-hydroxymethylfurfural molar extinction coefficients at different wavelengths. Absorption coefficients for solutions of different concentrations.

λ (nm)	ε_λ ($L \cdot mol^{-1} \cdot cm^{-1}$)	μ_λ (C=1 $mg \cdot L^{-1}$) (cm^{-1})	μ_λ (C=100 $mg \cdot L^{-1}$) (cm^{-1})
235	17	0.0001	0.01
240	1643	0.0130	1.30
245	2171	0.0172	1.72
250	3636	0.0288	2.88
255	6116	0.0485	4.85
260	10042	0.0796	7.96
265	14898	0.1181	11.81
270	20235	0.1605	16.05
275	24755	0.1963	19.63
280	27502	0.2181	21.81
285	28224	0.2238	22.38
290	26184	0.2076	20.76
295	20910	0.1658	16.58
300	14704	0.1166	11.66
305	8424	0.0668	6.68
310	4305	0.0341	3.41
315	1928	0.0153	1.53
320	795	0.0063	0.63
325	525	0.0042	0.42
330	326	0.0026	0.26
335	236	0.0019	0.19

Both the total incident radiation at the reactor surface (P(0) and the total incident radiation at the reactor bottom (P(C) were calculated from Equation 12, considering the wavelength interval between 235 and 335 nm and a 100-$mg \cdot L^{-1}$ HMF solution inside the reactor. The results for both reactors are shown in Table 8. It can be said that only 20.2% of the radiation at the surface reaches the bottom of the 22x15x10 cm reactor whereas in the small reactor only 8.2% of the incident radiation at the surface reaches the bottom. This indicates that the rest of the radiation is absorbed by the solution, making the degradation reaction possible. However, a small part would correspond to radiation that exits the reactor by the lateral surfaces without reaching the reactor bottom.

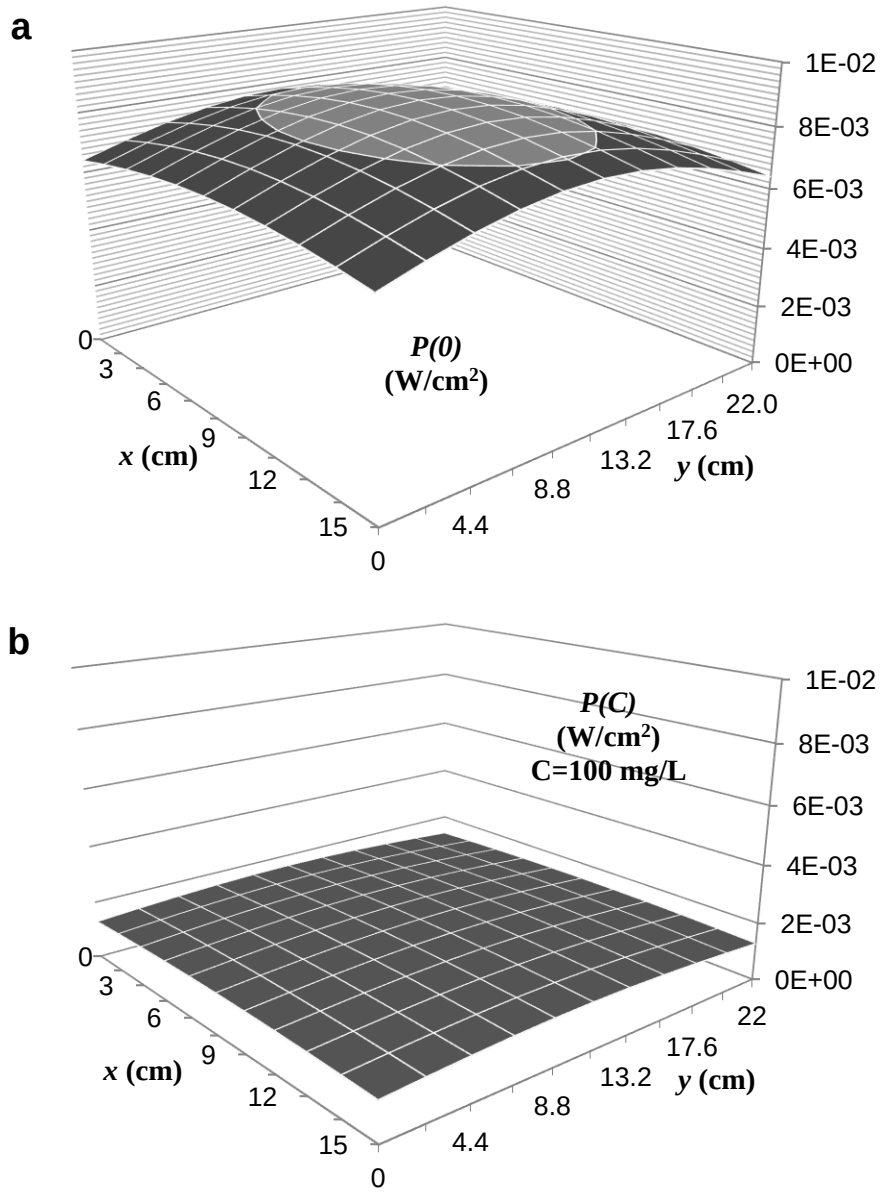

Figure 18. Incident spectral radiant power (235-335 nm) on the 22 x 15 x 10 cm reactor (z_0 = 22.5 cm) (a) on the surface ($P(0)$) (b) at the bottom ($P(C)$), considering a 100-mg·L^{-1} HMF solution.

5.2.4 Absorbed radiation power

The spectral radiant power absorbed by the whole solution (P_{abs}) inside each of the used reactors used was also calculated. In the case of the 22x15x10 cm reactor, Figure 20 depicts the results from the simplified (Eq. 13) and the non-simplified (Eq. 14) equations. As can be seen, the results from both equations match for HMF concentrations below 20 mg·L^{-1}, diverging above this value. In the case of the 12.5x10.5x10 cm reactor, the results from Eq. 13 and 14 coincide for HMF concentrations below 10 mg·L^{-1} and diverge above this value (Fig. 21). As HMF solutions of concentrations higher than 10

mg·L^{-1} were irradiated, all the values of P_{abs} hereafter were computed using the non-simplified equation (Eq. 14).

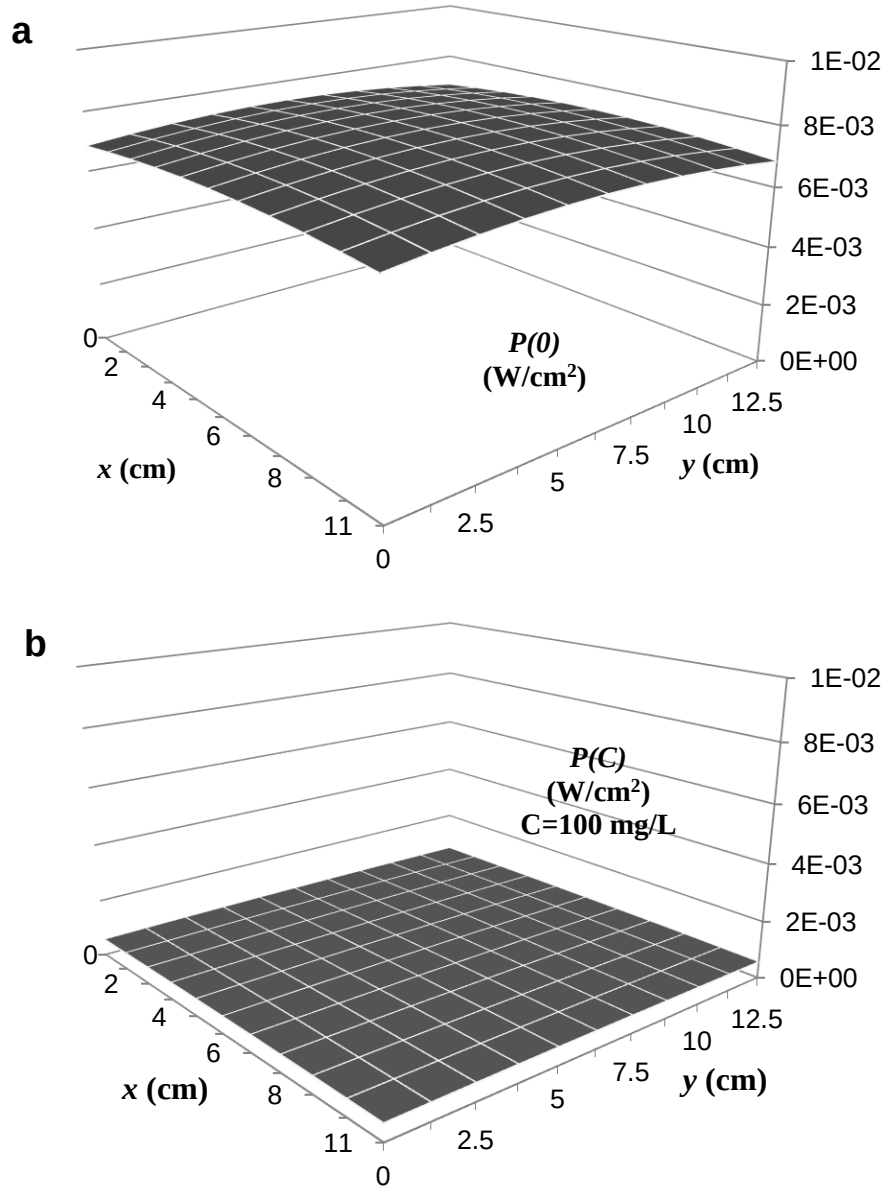

Figure 19. Incident spectral radiant power (255-355 nm) on the 12.5 x 10.5 x 10 cm reactor (z_0 = 23.9 cm) (a) on the surface ($P(0)$) (b) at the bottom ($P(C)$), considering a 100-mg·L^{-1} HMF solution.

Table 8. Total incident radiation on the reactor surface and at the reactor bottom considering a 100-mg·L^{-1} HMF solution inside the reactor.

Reactor dimensions (cm)	z_0 (cm)	$P(0)$ (W)	$P(0)$ (W·cm^{-2})	$P(C)$ (W)	$P(C)$ (W·cm^{-2})
22 x 15 x 10	22.5	2.56	$7.75 \cdot 10^{-3}$	0.52	$1.57 \cdot 10^{-3}$
12.5 x 10.5 x 10	23.9	0.97	$7.35 \cdot 10^{-3}$	0.08	$6.03 \cdot 10^{-4}$

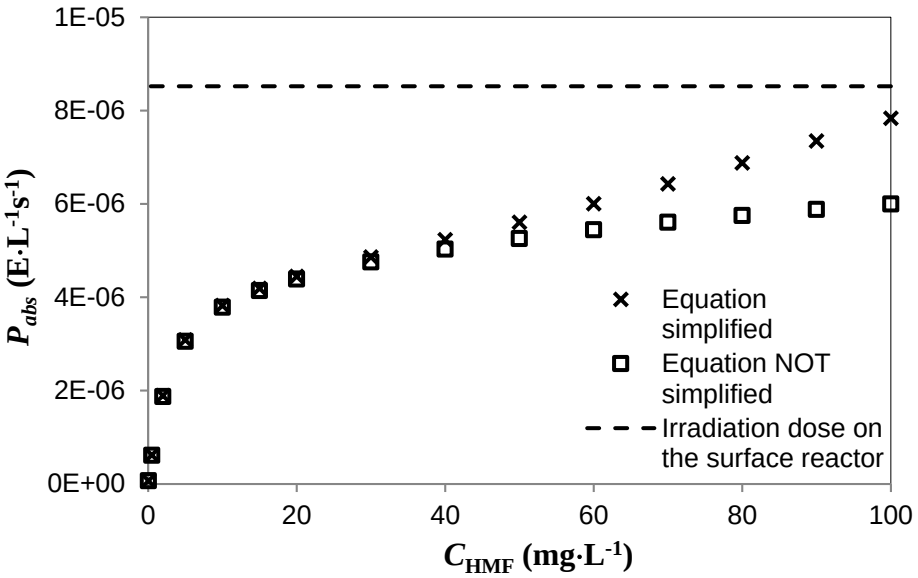

Figure 20. Spectral radiant power absorbed as a function of HMF concentration (22x15x10 cm tank, z_0 = 22.5 cm).

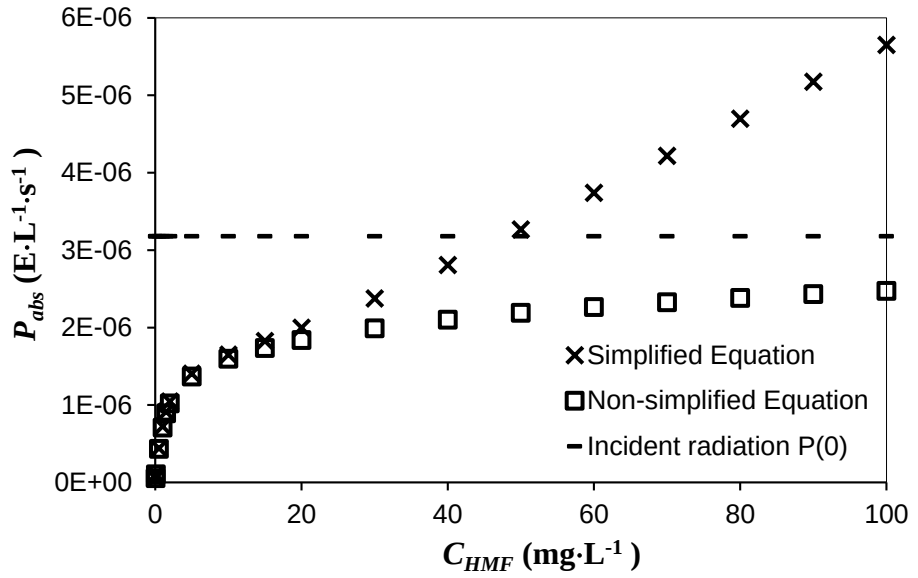

Figure 21. Spectral radiant power absorbed as a function of HMF concentration (12.5x10.5x10 cm tank, z_0 = 23.9 cm).

Figures 20 and 21 also illustrate how the absorbed radiation tends asymptotically to the incident radiation on the reactor surface as previously reported by Garvín *et al.* (2015). Considering a 100-mg·L^{-1} HMF solution, P_{abs} resulted in 1.86 W ($5.64 \cdot 10^{-3}$ W·cm^{-2}) and 0.766 W ($5.83 \cdot 10^{-3}$ W·cm^{-2}) for the big and the small reactors, respectively. The total radiation absorbed by the HMF solution was lower in the small reactor due to the fact that the surface was also lower. Nevertheless, the absorbed radiation per surface unit

remains practically constant, due to the slightly bigger distance between the lamp and the surface of the 12.5x10.5x10 cm vessel.

Figure 22 shows how the ratio between the calculated absorbed radiation (P_{abs} from Eq. 14) and the calculated incident radiation on the liquid surface ($P(0)$) from Equation 12) varies with the reactor depth for three different HMF concentrations. In all cases, this ratio increases asymptotically when the depth of the reactor is increased. Obviously, the greater the HMF concentration, the less depth is needed to absorb all the radiation that can be absorbed.

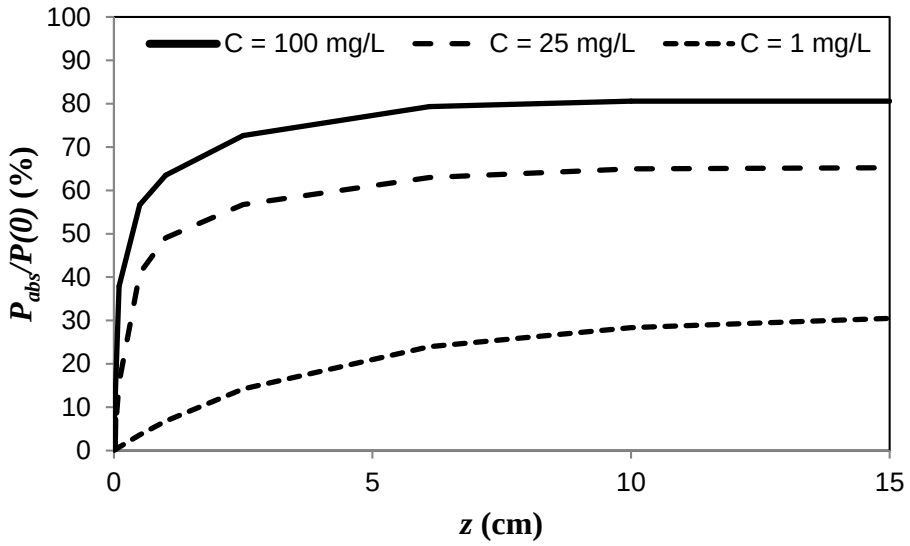

Figure 22. Dependence of the ratio absorbed/incident radiation on the HMF concentration and depth (z) (reactor dimensions 12.5 x 10.5 x 10 cm).

Table 9 displays the depth needed to absorb 50% of the incident radiation on the reactor surface. The absorbed radiation would never reach values over 30% for HMF concentration of 1 $mg \cdot L^{-1}$, regardless of the depth of the reactor. The vessel depth needed to absorb 50% of the incident radiation at the reactor surface is around 10 and 0.4 cm for HMF concentrations of 25 and 100 $mg \cdot L^{-1}$, respectively. These values contradict the established preconception that the radiation only reaches the surface. Obviously, the penetration depth depends on the absorption coefficient, which depends on the absorber concentration. In any case, whatever the absorber concentration, the radiation can reach any absorber molecule inside the solution either when the solution is stirred or if the reactor is designed so that the light beams only pass through a thin layer of the solution.

For example, Shama *et al.* (1996) used a tube shaper reactor, placing the lamp in the central axis and the solution flowing as a film down the inner face of the tube.

Table 9. Asymptote values and depth needed to achieve an absorbed radiation of 50% of the incident radiation at the reactor surface for different HMF concentrations.

C_{HMF} ($mg \cdot L^{-1}$)	Asymptote (%)	$z_{50\%}$ (cm)
1	31	--
25	65	10
100	80	0.4

From Figure 22, the fact that the asymptotic value of the curve depends on the HMF concentration is also worth remarking: the greater the HMF concentration the higher the asymptotic value. This asymptotic value represents the maximum fraction of the incident radiation that can be absorbed if the reactor is deep enough, this value depending on the concentration of 5-hydroxymethylfurfural (absorption coefficient). If the reactor is deep enough for a specific concentration, a further increase in its depth will not lead to any increase in the absorbed radiation. The beams that follow paths exiting by the upper area of the lateral vessel surfaces will only be totally absorbed if the solute concentration is high enough. The greater the HMF concentration the fewer the beams that exit the tank without being totally absorbed. Therefore, the maximum ratio that can be absorbed (asymptote) increases with the HMF concentration (absorption coefficient). Obviously, for very high concentrations, this limit would be almost 100%. The asymptotic value is only about 31% for a HMF concentration of 1 $mg \cdot L^{-1}$, but around 65 and 80% for concentrations of 25 and 100 $mg \cdot L^{-1}$, respectively.

5.2.5 Photo-degradation modelling - effect of temperature and pH -

With the aim of studying the photo-degradation of HMF in aqueous solution and proposing an adequate model to describe this photo-chemical process, an experiment was conducted irradiating solutions of HMF with a multi-wavelength emitting lamp. The effect of temperature and pH was also evaluated. In this experiment, the irradiation treatments were performed using the reactor whose dimensions are 22 x 15 x 10 cm. The mechanism proposed in this thesis to describe the photo-chemical degradation of 5-hydroxymethylfurfural is based on the quantity of radiation absorbed by the reactant. As concentration values between 40 and 100 $mg \cdot L^{-1}$ were found in the samples analyzed

during the irradiation treatments, P_{abs} as a function of the HMF concentration was graphed exclusively at that interval of concentrations (Fig. 23).

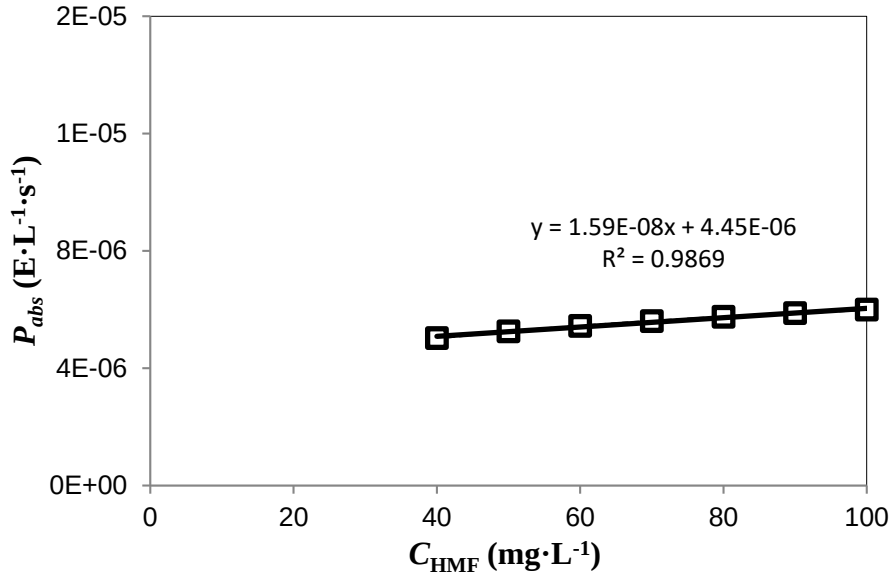

Figure 23. Total spectral radiant power absorbed by HMF solutions of concentrations between 40 and 100 mg·L^{-1}. Fitted equation and correlation coefficient. Reactor dimensions: 22 x 15 x 10 cm, z_0 = 22.5 cm.

In Figure 23, it can be seen that the absorbed radiant power could be considered a constant value for the interval between 40 and 100 mg·L^{-1} and, hence, Eq. 29 can be used. Indeed, P_{abs} just varies from 5.03·10^{-6} to 5.99·10^{-6} E·L^{-1}·s^{-1}, the average being 5.57·10^{-6} E·L^{-1}·s^{-1}. This value was considered as k_R in Eq. 29. In Figure 22, it is also demonstrated that for the same range of HMF concentrations, P_{abs} can be fitted to Eq. 31. The fitted values for *a* and *b* were, respectively, 4.45·10^{-6} E·L^{-1}·s^{-1}and 1.59·10^{-8} E·mg^{-1}·s^{-1}, with a determination coefficient of 0.9869.

The evolution of the HMF content when an aqueous solution of 100 mg·L^{-1} is irradiated is illustrated in Figures 24 and 25. In all cases, HMF is degraded during the irradiation of the solutions, showing a linear trend, which seems to match a zero-order kinetic model.

Figure 24 shows the effect of the temperature for solutions at pH=5. While at temperatures of 12, 25 and 35 ºC, the HMF concentration decreased about 30% after 120 min of irradiation, at 45ºC, the degradation reached 60%. Therefore, the photo-degradation of the compound studied was faster at a slightly higher temperature of 45ºC. Akillioglu *et al.* (2011) achieved similar results after a treatment time of 100 min with

yeast fermentation. Although fermentation shows a similar effect on the HMF degradation, that treatment is only applicable when the associated changes are desired.

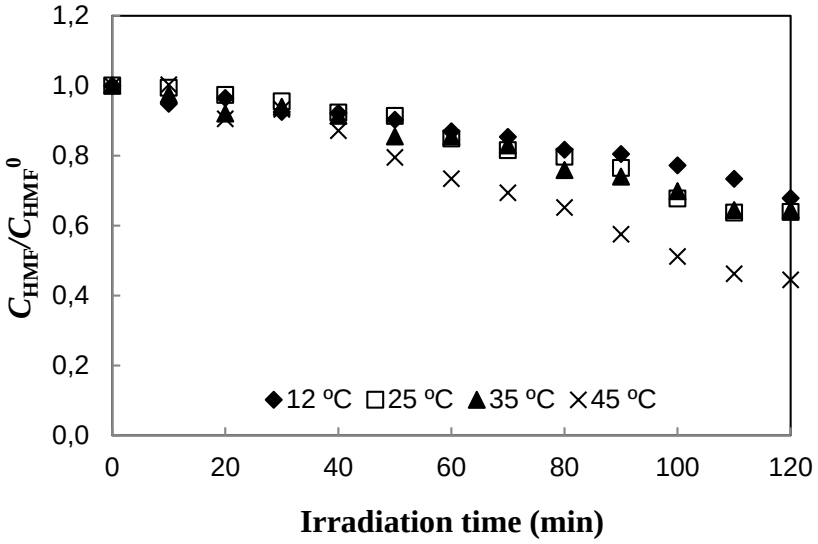

Figure 24. Evolution of HMF content during the irradiation of aqueous solutions at initial concentration of 100 mg·L^{-1}, pH=5 and different temperatures.

Figure 25 shows the effect of pH. It can be seen that the higher the pH value the faster the HMF degradation. This behaviour could be due to the fact that 5-hydroxymethylfufural seems to be more stable in acidic media (Lee *et al.*, 2014). Tables 10 and 11 summarize the parameters fitting both the zero-order (Eq. 30) and pseudo-first order (Eq. 32) kinetic models and the k_D/k ratio obtained from K_{HMF} (Eq. 25).

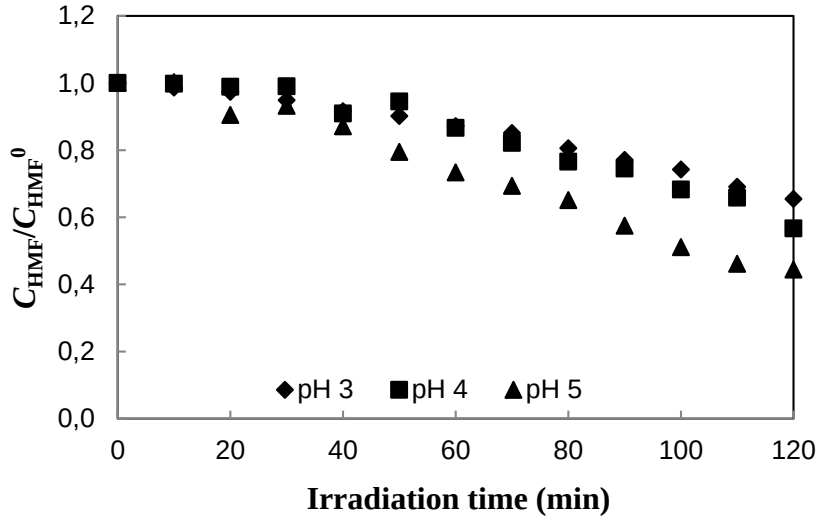

Figure 25. Evolution of HMF content during the irradiation of aqueous solutions at initial concentration of 100 mg·L^{-1}, 45ºC and different pH values.

Table 10. Fitting parameters for the zero-order kinetic to model the photo-degradation of HMF in aqueous solutions (C_{HMF}^0 = 100 mg·L^{-1}). Reactor dimensions: 22 x 15 x 10 cm.

$C_{HMF} = C_{HMF}^0 - m_{HMF} \cdot t$; $m_{HMF} = K_{HMF} \cdot k_R$

pH	T (ºC)	$m_{HMF}\cdot 10^8$ (mole·L^{-1}·s^{-1})	$K_{HMF}\cdot 10^3$ (mole·E^{-1})	k_D/k	R^2
3	12	2.67 ± 0.13	4.80 ± 0.24	207 ± 10	0.9756
3	25	3.32 ± 0.23	5.97 ± 0.41	167 ± 11	0.9681
3	35	3.59 ± 0.16	6.45 ± 0.29	154 ± 7	0.9802
3	45	3.91 ± 0.16	7.03 ± 0.28	141 ± 6	0.9841
4	12	2.89 ± 0.11	5.19 ± 0.20	194 ± 8	0.9848
4	25	3.32 ± 0.27	5.96 ± 0.48	169 ± 15	0.9393
4	35	4.67 ± 0.28	8.39 ± 0.50	120 ± 8	0.9685
4	45	5.83 ± 0.11	10.47 ± 0.20	96 ± 2	0.9964
5	12	3.17 ± 0.21	5.70 ± 0.39	175 ± 11	0.9555
5	25	4.21 ± 0.19	7.55 ± 0.34	131 ± 6	0.9844
5	35	4.41 ± 0.24	7.91 ± 0.44	125 ± 7	0.9791
5	45	7.24 ± 0.26	13.01 ± 0.46	76 ± 3	0.9876

Table 11. Fitting parameters for the pseudo-first-order kinetic to model the photo-degradation of HMF in aqueous solutions (C_{HMF}^0 = 100 mg·L^{-1}). Reactor dimensions: 22 x 15 x 10 cm.

$$\ln\left(\frac{a + bC_{HMF}^0}{a + bC_{HMF}}\right) = b \cdot K_{HMF} \cdot t$$

pH	T (ºC)	$K_{HMF}\cdot 10^3$ (mole·E^{-1})	k_D/k	R^2
3	12	5.05 ± 0.26	197 ± 10	0.9931
3	25	6.50 ± 0.45	153 ± 10	0.9852
3	35	6.95 ± 0.33	143 ± 6	0.9870
3	45	7.56 ± 0.34	131 ± 6	0.9473
4	12	5.46 ± 0.23	182 ± 7	0.9897
4	25	6.33 ± 0.52	157 ± 12	0.9864
4	35	9.04 ± 0.55	110 ± 6	0.9808
4	45	10.85 ± 0.26	91 ± 2	0.9473
5	12	5.96 ± 0.43	167 ± 11	0.9869
5	25	7.92 ± 0.38	125 ± 6	0.9713
5	35	8.50 ± 0.49	117 ± 6	0.9852
5	45	13.96 ± 0.51	72 ± 3	0.9877

Comparing the values of R^2, both kinetic models fit really well, leading to similar values of K_{HMF}. Thus, according to the greater simplicity of the zero-order kinetic model, this seems to be more appropriate for describing the photo-degradation of HMF in aqueous solutions in concentrations ranging from 40 to 100 mg·L^{-1}. The m_{HMF} and K_{HMF} values show the same trend that in Figure 24, confirming that the optimal conditions for degrading HMF in the range studied are 45 ºC and pH=5. It is convenient to point out that this temperature is much lower than the one used in thermal treatments. However, Figure 18 indicates that a by-product could be generated at this condition.

All the values of the k_D/k ratio calculated in Tables 10 and 11 are greater than 1. As this parameter is the ratio of the rates between the declining stage to the fundamental state and the stage of forming photoproducts, this means that, in all the cases, the declining step was faster than the photoproduct formation. It can also be observed that the ratio decreases when the temperature is increased, confirming that the efficiency of the photo-degradation increases with temperature.

5.2.6 Effect of the initial concentration on the photo-degradation kinetic model

With the aim of studying the effect of the initial concentration on the photo-degradation kinetics of 5-hydroxymethylfufural, aqueous solutions of different concentrations were irradiated. The reactor used in this experiment has dimensions of 12.5 x 15 x 10 cm and the lamp was placed 23.9 cm from the liquid reactor surface. The absorbed radiant power as a function of the HMF concentration in this photo-reactor is shown in Figure 21. The values for P_{abs} resulted in 0.766 W ($5.83 \cdot 10^{-3}$ W·cm^{-2}), 0.068 W ($4.63 \cdot 10^{-3}$ W·cm^{-2}) and 0.231 W ($1.76 \cdot 10^{-3}$ W·cm^{-2}) for HMF concentrations of 100, 25 and 1 mg·L^{-1}, respectively.

Although Figure 21 clearly shows that the relation between P_{abs} and HMF concentration is a curve that rises asymptotically towards the incident radiation at the reactor surface, a straight line can be fitted for narrow ranges of concentration. Thereby, the curve can be subdivided in three different sections (Fig. 26):

a) from 0 to 2 mg·L^{-1} a linear relationship with origin ordinate can be fitted, obtaining R^2 value of 0.9287. As Equation 27 describes this case, a first-order kinetic model would be expected.
b) from 2 to 20 mg·L^{-1} a linear relationship can also be fitted, but in this case a non-zero origin ordinate is obtained with an R^2 value of 0.8984. In this case, Equation 31 describes the relationship and therefore a pseudo-first-order kinetic model would be expected.

It is worth remarking that the origin ordinate value obtained is much higher than the slope value (Fig 25b). Consequently, P_{abs} only varies from $1.02 \cdot 10^{-6}$ to $1.84 \cdot 10^{-6}$ E·L^{-1}·s^{-1}, for 2 and 20 mg·L^{-1}, respectively. Therefore, the absorbed radiation could be considered constant for this range of HMF concentrations, the arithmetic mean value being $1.59 \cdot 10^{-6}$ E·L^{-1}·s^{-1}. Taking into account this almost constant value, P_{abs} follows

Equation 29 and a zero-order kinetic model should also fit the experimental data well. The constant value to be considered should be the arithmetic mean of P_{abs} within this range.

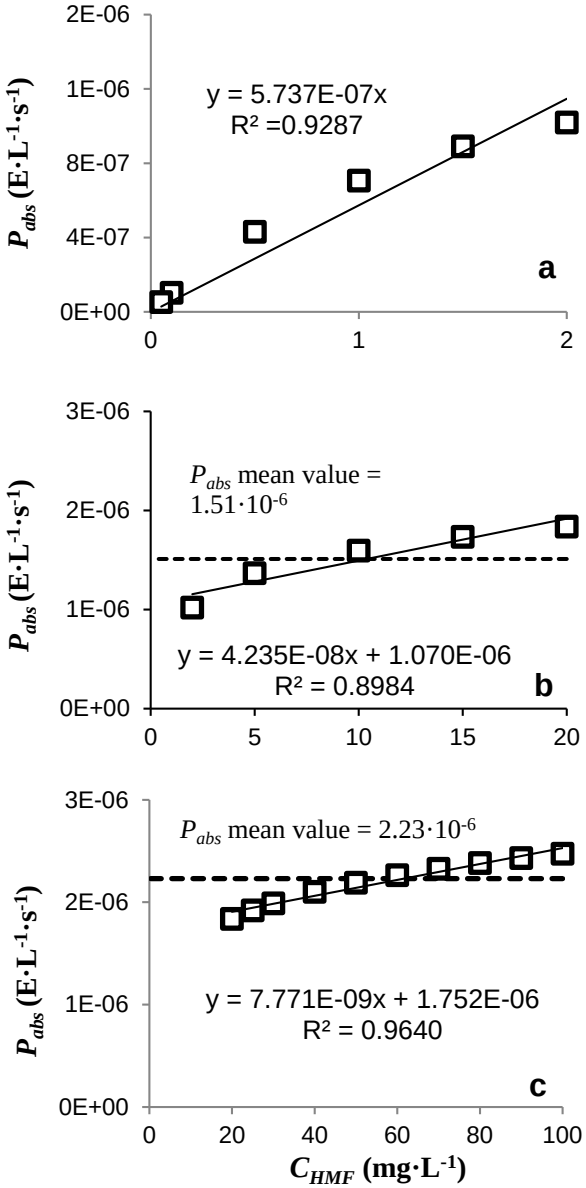

Figure 26. Total spectral radiant power absorbed by the solution (P_{abs}) as a function of the HMF concentration (reactor dimensions: 12.5 x 10.5 x 10 cm) considering diferent intervals of concentrations.

c) From 20 to 100 mg·L^{-1} a linear relationship with non-zero origin ordinate can also be fitted, obtaining an R^2 value of 0.9640. Consequently, the experimental data would also be expected to fit a pseudo-first-order kinetic model well.

In this case, the origin ordinate value obtained is also much higher than the slope value, the difference being even higher than in the previous case. Thus, P_{abs} only varies

from $1.92 \cdot 10^{-6}$ to $2.47 \cdot 10^{-6}$ $E \cdot L^{-1} \cdot s^{-1}$ for HMF concentrations of 20 and 100 $mg \cdot L^{-1}$, respectively. Therefore, the absorbed radiant power could be considered constant for this range of HMF concentrations, the arithmetic mean value being $2.23 \cdot 10^{-6}$ $E \cdot L^{-1} \cdot s^{-1}$. Consequently, P_{abs} almost follows Equation 29 and a zero-order kinetic model should also fit the experimental data well.

Table 12 summarizes the equations and fitted parameters for each range of HMF concentrations.

Table 12. Fitted parameters for the relation between P_{abs} and HMF concentration at different ranges of concentrations.

C_{HMF} Range ($mg \cdot L^{-1}$)	Equation	Kinetic model	Parameters	R^2
0 – 2	$P_{abs} = k_R C_{HMF}$	First-order	$k_R = 5.47 \cdot 10^{-7}$ $E \cdot mg^{-1} \cdot s^{-1}$	0.9287
2-20	$P_{abs} = a + bC_{HMF}$	Pseudo-first-order	$a = 1.07 \cdot 10^{-6}$ $E \cdot L^{-1} \cdot s^{-1}$ $b = 4.23 \cdot 10^{-8}$ $E \cdot mg^{-1} s^{-1}$	0.8984
	$P_{abs} = k_R$	Zero-order	$k_R = 1.51 \cdot 10^{-6}$ $E \cdot L^{-1} \cdot s^{-1}$	—
20-100	$P_{abs} = a + bC_{HMF}$	Pseudo-first-order	$a = 1.75 \cdot 10^{-6}$ $E \cdot L^{-1} \cdot s^{-1}$ $b = 7.77 \cdot 10^{-9}$ $E \cdot mg^{-1} \cdot s^{-1}$	0.9640
	$P_{abs} = k_R$	Zero-order	$k_R = 2.23 \cdot 10^{-6}$ $E \cdot L^{-1} \cdot s^{-1}$	—

Figure 27 shows the evolution of the relative concentration of 5-hydroxymethylfurfural for the three different initial concentrations considered. It can be seen that for the highest concentration, 100 $mg \cdot L^{-1}$, the decrease follows a straight line quite closely, matching a zero-order model, as expected given that P_{abs} can be considered constant within the concentration range (Fig. 27a). On the other hand, when the initial concentration is low enough, in this case 1 $mg \cdot L^{-1}$, the relative concentration decreases exponentially (Fig. 27c), as also expected given that, in this case, the absorbed radiation can be considered to depend linearly on the HMF concentration with the origin ordinate equal to zero. In fact, for an initial concentration of 25 $mg \cdot L^{-1}$ (Fig. 26b), when conversions of around 90% are achieved, a slight change is seen from linear behaviour (zero-order kinetics) corresponding to high HMF concentrations, to an exponential case (first-order kinetics), corresponding to low concentrations.

Figure 27 also shows that the higher the initial HMF concentration the lower the conversion achieved. This is because when zero-order kinetics are followed, the slope of the relative concentration evolution is the kinetic constant divided by the initial

concentration. In this way, after 120 min of UV irradiation, a conversion of almost 90% was achieved for 25 mg·L^{-1} but only 50% for 100 mg·L^{-1}, both at pH 4 and 45 ºC.

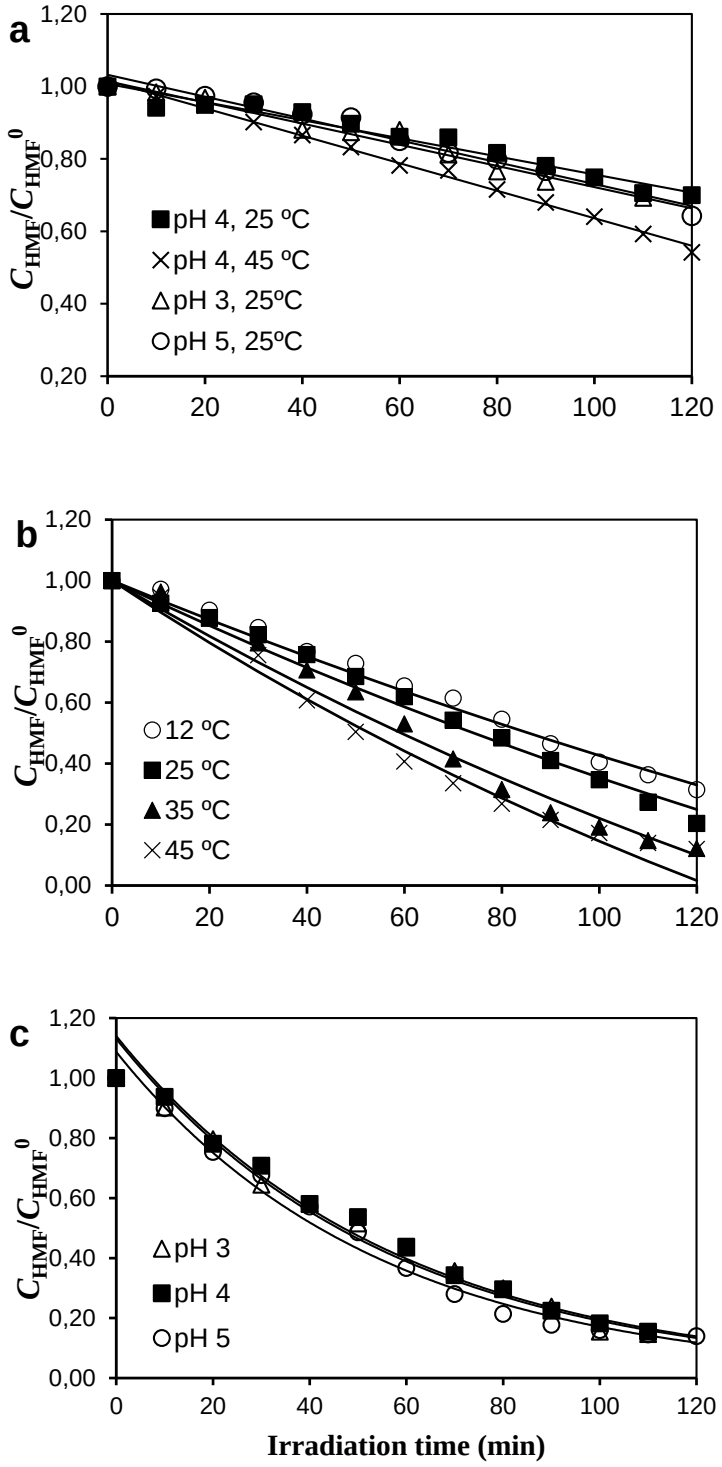

Figure 27. Evolution of HMF content with irradiation time for solutions at different initial concentrations. (a) 100 mg·L^{-1}. Lines represent zero-order kinetic model. (b) 25 mg·L^{-1} and pH=4. Lines represent pseudo-first-order kinetic model. (c) 1 mg·L^{-1}. Lines represent first-order kinetic model.

Table 13 shows the resulting parameters when the experimental data for the low initial concentration of 1 mg·L^{-1} were fitted to a first-order kinetic model. According to the determination coefficients, it can be said that the kinetics fit the first-order model well. Other toxic substances have also been reported to follow an exponential decay (El-Moseley, 2009; Ibarz *et al.*, 2014 and 2015b).

Table 13. Fitting parameters for the zero-order kinetic to model the photo-degradation of HMF in aqueous solutions at an initial concentration of 1 mg·L^{-1} (reactor dimensions: 12.5 x 10.5 x 10 cm).

$C_{HMF} = C^0_{HMF} \cdot \exp(-m_{HMF} \cdot t)$; $m_{HMF} = K_{HMF} \cdot k_R$

pH	T (ºC)	$m_{HMF} \cdot 10^4$ (s^{-1})	$K_{HMF} \cdot 10^3$ (mole·E^{-1})	k_D/k	R^2
3	25	2.63 ± 0.11	3.63 ± 0.12	274 ± 15	0.9857
4	25	2.64 ± 0.08	3.64 ± 0.09	273 ± 11	0.9908
5	25	2.91 ± 0.08	4.02 ± 0.09	248 ± 10	0.9928

Tables 14 and 15 show the parameters obtained when the experimental data for the high initial concentrations of 25 mg·L^{-1} were fitted to zero-order and pseudo-first-order kinetic models, respectively. According to Garvín *et al.* (2015), this behaviour is always expected for high concentrations. In order to be able to compare both behaviours, Tables 14 and 15 also show the values for 100 mg·L^{-1} that were previously calculated for section 5.2.4. Although the determination coefficients are slightly bigger when a pseudo-first-order kinetic model is used, the fact that the zero-order model is clearly simpler would justify its selection. K_{HMF} fitted values in Tables 14-15 prove that the photo-degradation does not depend on pH for the range 3-4, but it increases slightly for pH 5. This trend was also found in the previous section, exclusively for the initial HMF concentration of 100 mg·L^{-1}.

Table 14. Fitting parameters for the zero-order kinetic to model the photo-degradation of HMF in aqueous solutions at different initial concentrations.

$C_{HMF} = C^0_{HMF} - m_{HMF} \cdot t$; $m_{HMF} = K_{HMF} \cdot k_R$

Initial concentration (mg·L^{-1})	pH	T (ºC)	$m_{HMF} \cdot 10^8$ (mole·L^{-1}·s^{-1})	$K_{HMF} \cdot 10^3$ (mole·E^{-1})	k_D/k	R^2
25	4	12	1.49 ± 0.02	9.87 ± 0.13	100 ± 1	0.9976
25	4	25	1.84 ± 0.02	12.19 ± 0.13	81 ± 2	0.9987
25	4	35	2.06 ± 0.08	13.60 ± 0.53	73 ± 3	0.9847
25	4	45	2.27 ± 0.13	15.03 ± 0.86	66 ± 4	0.9743
100	3	25	3.32 ± 0.23	14.89 ± 1.00	66 ± 5	0.9681
100	4	12	2.89 ± 0.11	12.96 ± 0.48	76 ± 2	0.9848
100	4	25	3.32 ± 0.27	14.89 ± 1.16	66 ± 5	0.9393
100	4	35	4.67 ± 0.28	20.94 ± 1.21	47 ± 2	0.9685
100	4	45	5.83 ± 0.11	26.14 ± 0.48	37 ± 1	0.9964
100	5	25	4.21 ± 0.19	18.88 ± 0.82	52 ± 2	0.9844

Tables 14-15 also display the calculated ratio k_D/k. In all cases, this value was greater than 1. As this ratio consists of the relation between the rates of the declining-to-the-fundamental stage and the forming-photoproducts stage, the declining step was faster than the photo-product formation. As the ratio decreased with the increase in temperature, the photo-degradation step of the proposed mechanism was enhanced by the temperature increase as concluded in section 5.2.5.

Table 15. Fitting parameters for the pseudo-first-order kinetic to model the photo-degradation of HMF in aqueous solutions at different initial concentrations.

$$\ln\left(\frac{a+bC_{HMF}^{0}}{a+bC_{HMF}}\right) = b \cdot K_{HMF} \cdot t$$

Initial concentration mg·L^{-1}	pH	T (ºC)	$K_{HMF} \cdot 10^3$ (mole·E^{-1})	k_D/k	R^2
25	4	12	8.69 ± 0.15	114 ± 2	0.9966
25	4	25	10.80 ± 0.21	92 ± 2	0.9958
25	4	35	12.70 ± 0.30	78 ± 2	0.9940
25	4	45	14.26 ± 0.32	69 ± 2	0.9954
100	3	25	10.34 ± 0.49	96 ± 3	0.9889
100	4	12	8.54 ± 0.31	116 ± 3	0.9911
100	4	25	10.41 ± 0.53	95 ± 3	0.9822
100	4	35	13.45 ± 0.73	73 ± 2	0.9817
100	4	45	17.51 ± 0.41	56 ± 1	0.9963
100	5	25	11.10 ± 0.78	89 ± 4	0.9731

5.2.7 Rate controlling mechanism

In order to extend the study of HMF photo-degradation so as to find the mechanism that controls this reaction, the kinetic constants obtained in section 5.2.4 for 100-mg·L^{-1} HMF solutions were used. Additionally, first-order kinetic constants of photo-degradation were obtained for 100-mg·L^{-1} HMF solutions at pH=3.4. With the aim of evaluating the effect of the agitation on the chemical process studied, 100-mg·L^{-1} HMF solutions at pH=3 were also irradiated, this time without agitation, exclusively at 12 and 45 ºC. The kinetic constants for the zero-order kinetic model were also calculated. Table 16 compares all the kinetic constants obtained for the photo-degradation of 5-hydroxymethylfurfural in aqueous solutions of 100-mg·L^{-1}. The linear regression coefficients are high in all cases, 0.9393 being the lowest value.

In order to study the kinetic compensation, E_a and K_0 were calculated at each pH value by means of an Arrhenius' type equation (Eq. 33), taking the kinetic constants shown in Table 16. Kinetic compensation takes place when the graph of ln K_0 vs E_a

follows a straight line. Figure 28 shows the graph of ln K_0 vs E_a for HMF photo-degradation with agitation at different pH values. Each point in Figure 27 corresponds to the same reaction but taking place in a medium where only the pH has been modified. As this graph follows a straight line, it means that the change caused in the activation energy by a change in the pH value is compensated by the change in the frequency factor (K_0). In this way, the derivative of the graphed function (d lnK_0/ d E_a) is constant. This derivative corresponds to the slope of the straight line, being equal to $1/T_B$ (Eq. 36). T_B is the isokinetic temperature, being 278.0 K. This value defines the kinetic compensation and helps to know the isoequilibrium point of this reaction family.

Table 16. Fitting parameters for the zero-order kinetic model for HMF aqueous solutions irradiated with and without agitation.

$C_{HMF} = C^0_{HMF} - m_{HMF} \cdot t\ ;\ m_{HMF} = K_{HMF} \cdot k_R$

pH	T (ºC)	$m_{HMF}\cdot 10^8$ (mole·L^{-1}·s^{-1}) Agitated reaction vessel	R^2	$m_{HMF}\cdot 10^8$ (mole·L^{-1}·s^{-1}) Non-Agitated reaction vessel	R^2
3	12	2.67 ± 0.13	0.9756	2.24 ± 0.06	0.9472
3	25	3.32 ± 0.23	0.9681		
3	35	3.59 ± 0.16	0.9802		
3	45	3.91 ± 0.16	0.9841	2.90 ± 0.05	0.9793
3.4	12	2.56 ± 0.05	0.9864		
3.4	25	2.98 ± 0.10	0.9734		
3.4	35	3.65 ± 0.23	0.9788		
3.4	45	4.19 ± 0.18	0.9947		
4	12	2.89 ± 0.11	0.9848		
4	25	3.32 ± 0.27	0.9393		
4	35	4.67 ± 0.28	0.9685		
4	45	5.83 ± 0.11	0.9964		
5	12	3.17 ± 0.21	0.9555		
5	25	4.21 ± 0.19	0.9844		
5	35	4.41 ± 0.24	0.9791		
5	45	7.24 ± 0.26	0.9876		

It also helps to know which kinetic parameter, whether E_a or K_0, is controlling the reaction rate. The activation energy is related to the activation enthalpy in a liquid medium through the approximated Equation 36 whereas the frequency factor (K_0) is an entropic factor that represents the number of collisions that the reactant molecules suffer. Therefore, when a reaction is controlled by the enthalpy, the changes in the activation energy are proportionally bigger than the changes in the frequency factor. In the same way, when the entropy controls a reaction, it means that the changes in the frequency factor are bigger than the changes in the activation energy and the reaction rate would benefit from a change that would cause a larger number of collisions of the reactant molecules.

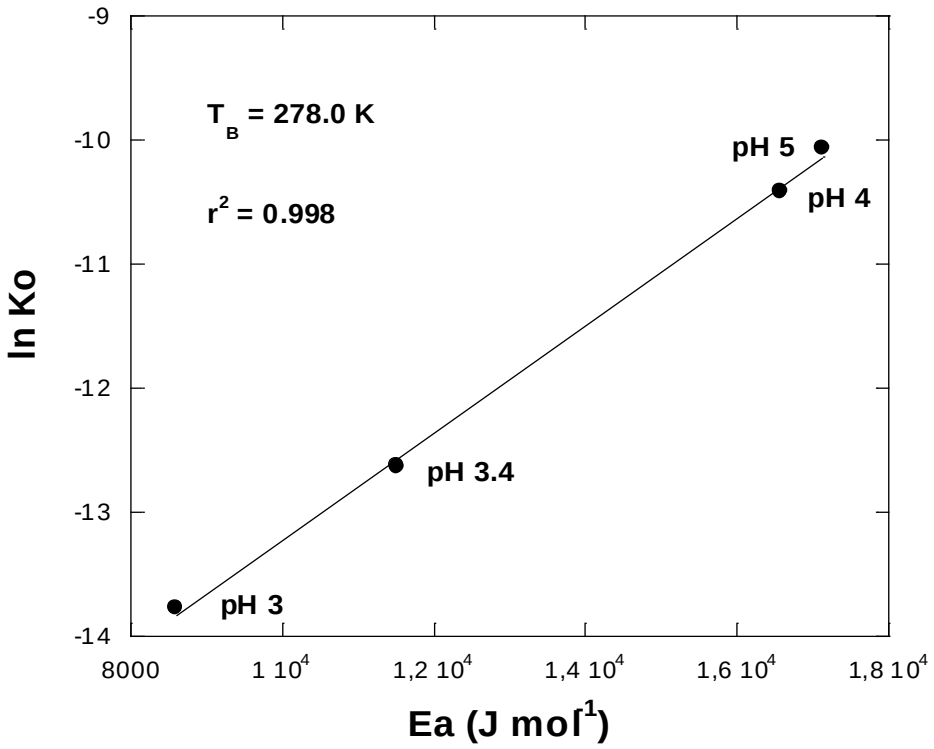

Figure 28. Kinetic compensation for HMF photo-degradation – with agitation - at different pH values.

From Figure 28, it can be concluded that for all the pH values considered, the mechanism controlling HMF photo-degradation is entropic, because the isokinetic temperature (T_B = 278.0 K) is lower than the mean harmonic temperature (T_{hm} = 301.9 K) –calculated from Equation 40. An entropic control implies that the kinetic parameter that influences the most in the value of the kinetic constant is the frequency factor instead of the activation energy.

Table 17 displays the activation energy and frequency factor values at each pH value. It is worth remarking that an increase in the pH value, from 3 to 5, causes new activation energy two times bigger, while the new frequency factor value is 41 times the previous one. This means that the increase in the kinetic constant by increasing the pH value is mainly due to a high increase in the number of collisions between molecules rather than the slight change in the activation energy. Obviously, for each pH value, an increase in the temperature would cause an increase in the kinetic constant. However, the kinetic compensation allows an increase to be predicted in the kinetic constant by changing only the pH value.

Table 17. Arrhenius' equation fitting parameters for HMF photo-degradation in aqueous solutions at an initial concentration of 100 mg·L^{-1} and different pH conditions.

pH	E_a (J·mol^{-1})	$K_0 \cdot 10^6$ (mole·L^{-1}·s^{-1})	R^2
3	8609.98	1.03	0.9862
3.4	11525.70	3.24	0.9922
3	16592.25	29.86	0.9727
5	17150.95	42.33	0.9359
3	5902.19	0.27	0.9999
Non-agitated reaction vessel			

The rate-controlling mechanism can also be evaluated studying thermodynamic compensation. Figure 29 shows the enthalpy-entropy compensation for the HMF photo-degradation by UV irradiation. It can be seen that the isokinetic temperature from Equation 38 (T_B = 277.8 K) is lower than the mean harmonic temperature (T_{hm} = 301.9 K). Consequently, the reaction kinetic is controlled by the changes in the entropy caused by the collision of molecules. The isokinetic temperature obtained using thermodynamic compensation is only 0.2 K lower than the value obtained using kinetic compensation, confirming the existence of these compensation processes for HMF photo-degradation. Beristain *et al.* (2011) reported that thermodynamics and kinetics are closely interrelated, as the equilibrium state of a system greatly depends on the kinetics followed to reach it. Both kinetic and thermodynamic compensation show paths to reach isoequilibrium.

The temperature of isoequilibrium called isokinetic temperature (T_B) for the whole family of reactions studied is defined as the temperature value at which the kinetic constant would be the same (k_{eq}) for any pH value. Figure 30 shows how the kinetic constant varies with temperature for each pH studied. For all the pH values studied, the lines go towards the isoequilibrium point (T_B, k_{eq}), meaning that kinetic constant tend to the same value ($k_{eq} = 2.37 \cdot 10^{-8}$ mole·L^{-1}·s^{-1}) when the reaction takes place at the isokinetic temperature (T_B = 278.0 K). It is worth noting that the isoequilibrium point found by isokinetic compensation is a real point and that, if some experiments were performed at this isokinetic temperature, the kinetic constant obtained for different pH values would be the same (Flores-Andrade *et al.*, 2009).

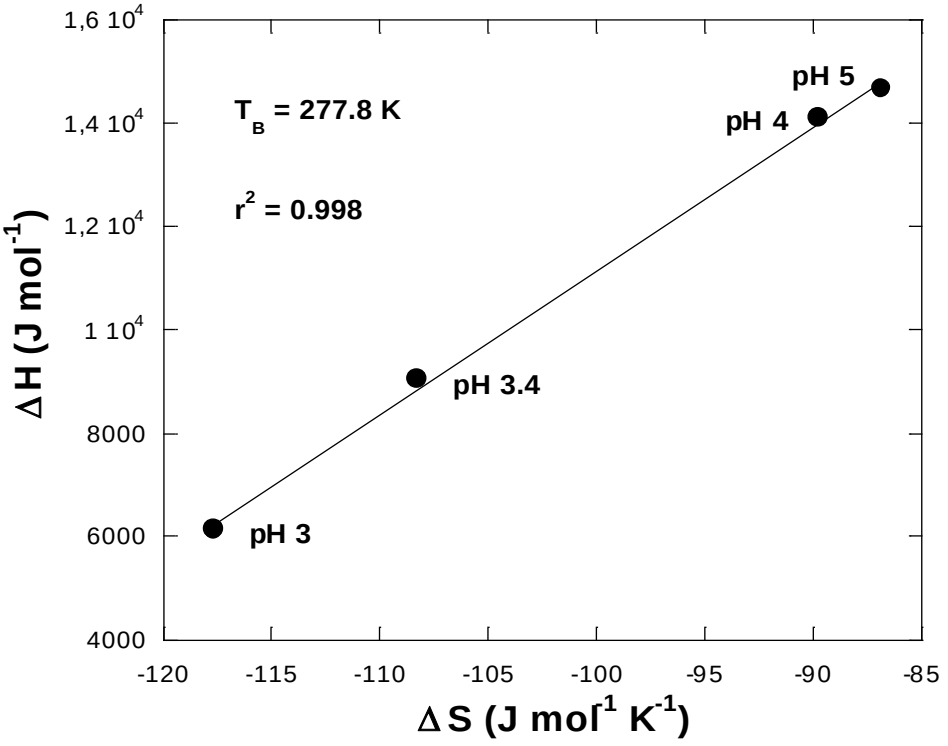

Figure 29. Thermodynamic compensation for HMF photo-degradation – with agitation - at different pH values.

Thermodynamic compensation also concludes the existence of the isokinetic temperature (T_B) for the whole family of reactions studied, defined by different pH values. Thus, the isokinetic temperature is the value at which the reaction takes place with the same value of free energy of activation (ΔG_B). Figure 31 shows how the free energy of activation (ΔG) varies with temperature for each pH value considered. The lines show the trend toward the isoequilibrium point (T_B, ΔG_B). As mentioned above, the isokinetic temperature found by kinetic compensation is almost the same as the value obtained from thermodynamic compensation, confirming the close relation between both compensation processes. The value obtained for the free energy of activation at the isoequilibrium point is ΔG_B=39807 J·mol^{-1}, being the isokinetic temperature (T_B = 277.8 K). This isoequilibrium point means that if the reaction took place at the isokinetic temperature and any pH value, the free energy of activation would be the same regardless of the pH value.

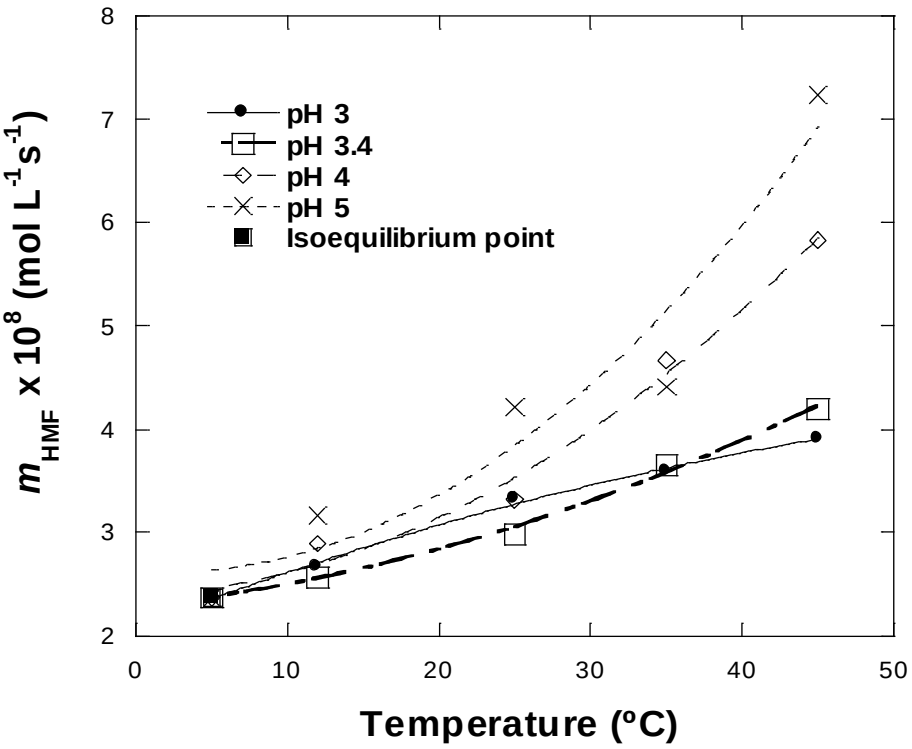

Figure 30. Variation of the kinetic constant as a function of temperature and pH for HMF photo-degradation.

As both, the kinetic and thermodynamic compensation processes, conclude an entropic control of the reaction, it is supposed that the kinetic constant can be increased at constant temperature by using a non-thermal energy. In order to verify this fact, two new experiments were carried out at pH=3 but without agitation: one at 12ºC and the other at 45ºC. Comparing the two experiments at pH=3 from Table 17, it can be said that the agitation enhanced the frequency by 3.8 times while the activation energy only increased by 1.5 times. According to Arrhenius' equation (Eq. 33), if the temperature is constant, the kinetic constant augments proportionally with the frequency factor while decreasing exponentially with the activation energy.

Figure 32 illustrates clearly the effect of the agitation at the same temperature. The improvement in the kinetic constant by adding agitation is greater than the enhancement by increasing the temperature from 12 to 45 ºC. For both temperatures, 12 and 45 ºC, the kinetic constant is always larger when the solution is stirred. The results found agree with the fact that the reaction is controlled by entropy (physical barriers).

Hence, an increase in the process temperature is not the only way to enhance the rate. In this thesis, it is suggested that it is possible to enhance an entropy-controlled process by modifying the barriers of the system with non-thermal treatments, such as agitation. The usefulness of enthalpy-entropy compensation to develop low-temperature processes for industry has been already suggested (Flores-Andrade *et al.*, 2009).

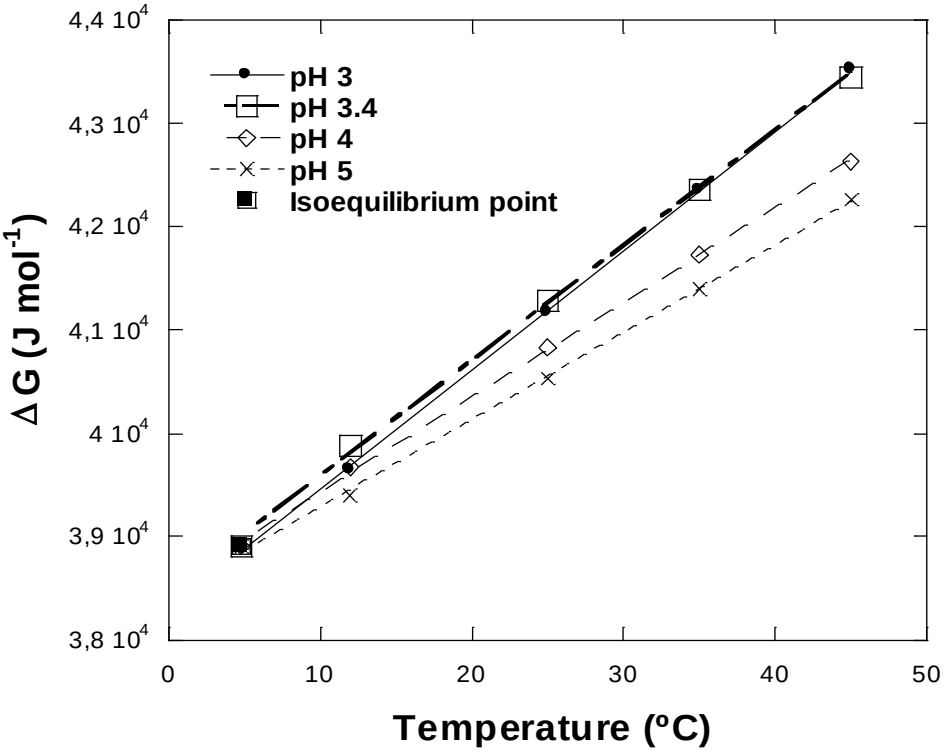

Figure 31. Gibbs free energy changes as a function of temperature and pH value for HMF photo-degradation.

Once it is known that the photo-degradation of HMF is controlled by entropic mechanisms, it is important to explain the effect of the pH of the media on the degradation rate. Solvation can be defined as the process used by a solvent surrounding the solute molecules, allowing the solute to dissolve inside the solvent. Hydrophobic molecules in water generally tend to aggregate, therefore minimizing their surface contact and associated surface energy with water (Mikheev *et al.*, 2007). Consequently, hydrophobic hydration is accompanied by a negative entropy change produced by the increased order in the surrounding water (Imai and Hirata, 2005). In the same way, pH changes in the

aqueous solution can diminish the hydrophobic hydration and the entropy becomes less negative, due to the greater mobility of the molecules.

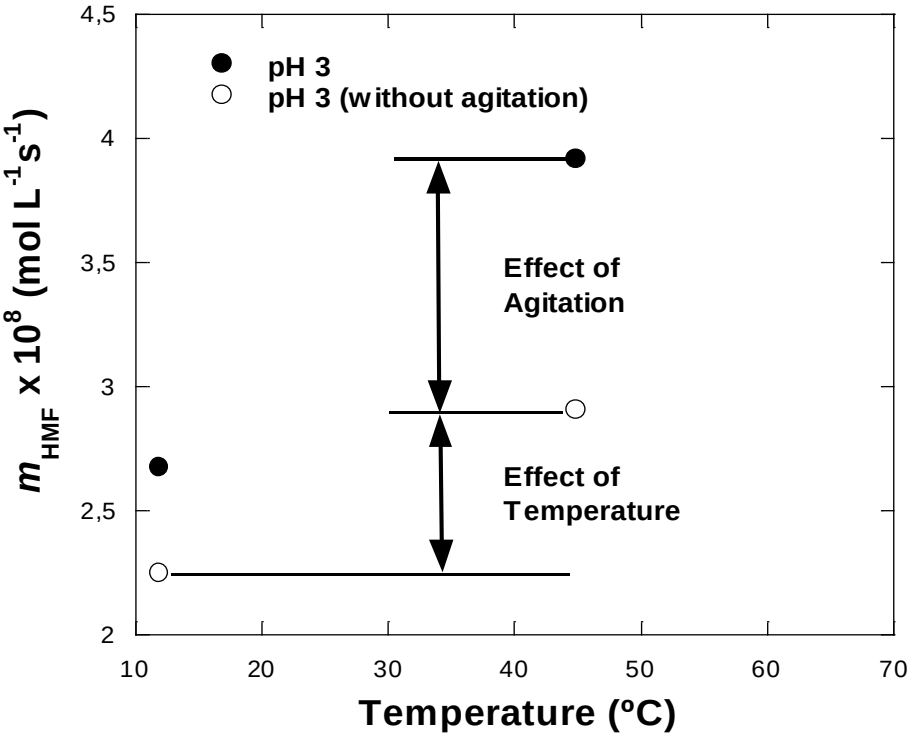

Figure 32. Effect of agitation on the kinetic constant for the photo-degradation of HMF.

The changes in the activation enthalpy and entropy at different pH values are plotted in Figure 33. When the pH varies from 3 to 5, the entropy augments from -117.6 to -86.8 $J \cdot mol^{-1} \cdot K^{-1}$, as expected according to the increase in HMF solubility. The augmentation in the entropy of the reaction system is due to the greater mobility of the molecules, favouring collisions, which matches the values for K_0 in Table 17. The enthalpy also rises from 6109.7 to 14651.0 $J \cdot mol^{-1}$. This enhancement is associated with an increase in the activation energy, and is probably a consequence of the fact that the high mobility of the molecules also causes stronger interactions between HMF and water molecules, forming stronger bonds that need more energy to be broken. Figure 33 also shows the data obtained without agitation. It can be seen that both enthalpy and entropy are lower when the reaction takes place in a non-agitated aqueous medium.

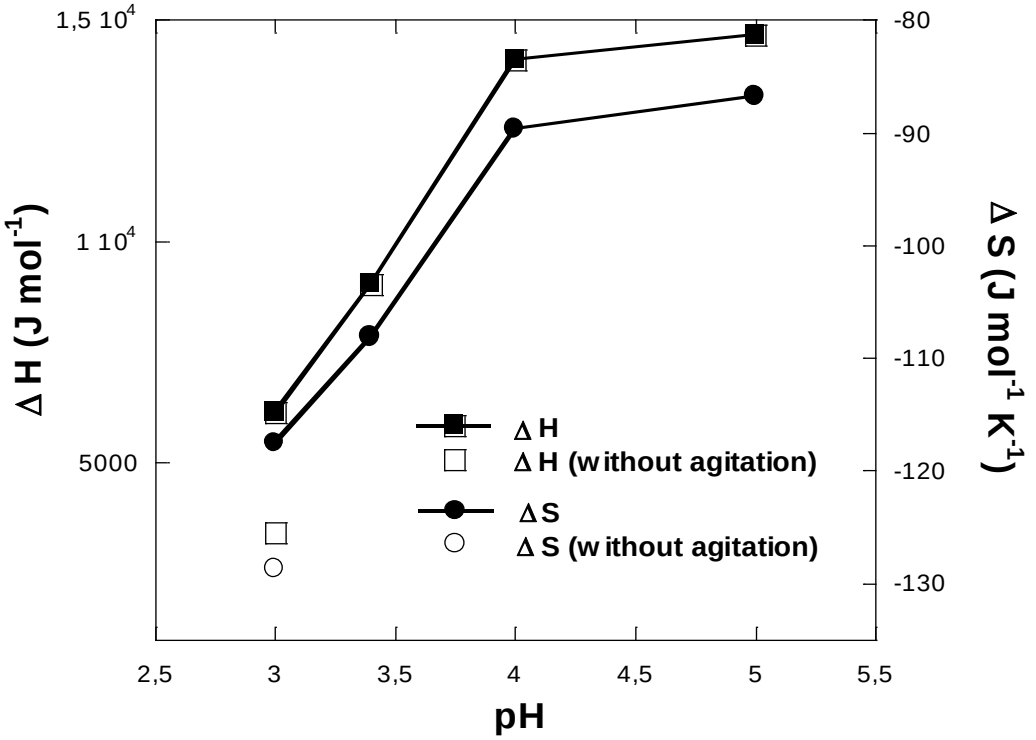

Figure 33. Variation of enthalpy and entropy as a function of the pH value for HMF photo-degradation.

5.3 UV-Vis processing of peach and nectarine juices

5.3.1 Irradiation dose

Figure 33 shows the irradiation profile on the liquid surface of the reactor for both 255 nm and 255-740 nm. Furthermore, the incident spectral power on the liquid surface of the reactor was calculated using Equation 12. For all the lamp emitting wavelengths (from 250 to 750 nm), a value of $4.49 \cdot 10^{-2}$ W·cm^{-2} was obtained. Considering exclusively the 255 nm wavelength, widely known for its germicidal effect, $P(0)$ was $2.40 \cdot 10^{-5}$ W·cm^{-2}. As Guerrero-Beltrán and Barbosa-Cánovas (2004) reported, $46.2 \cdot 10^{-3}$ J·cm^{-2} are required to eliminate the most resistant microorganisms. Therefore, with the lamp used in the present work, UV-treatment times of 32.1 min are needed to inactivate the most resistant microorganisms that could be found in the fruit juice. In another study, Keyser *et al.* (2008) achieved a complete reduction of mesophylls, yeasts and moulds in a clear apple juice with a UV-dose of 230 J·L^{-1} ($233.98 \cdot 10^{-3}$ J·cm^{-2}). Considering the whole germicidal interval of the lamp used in this work (250-300 nm), the incident radiation on

the reactor surface was $2.8 \cdot 10^{-3}$ W·cm^{-2}. Therefore, only 1.39 min would be needed to inactivate the microbial load of a fresh clear juice.

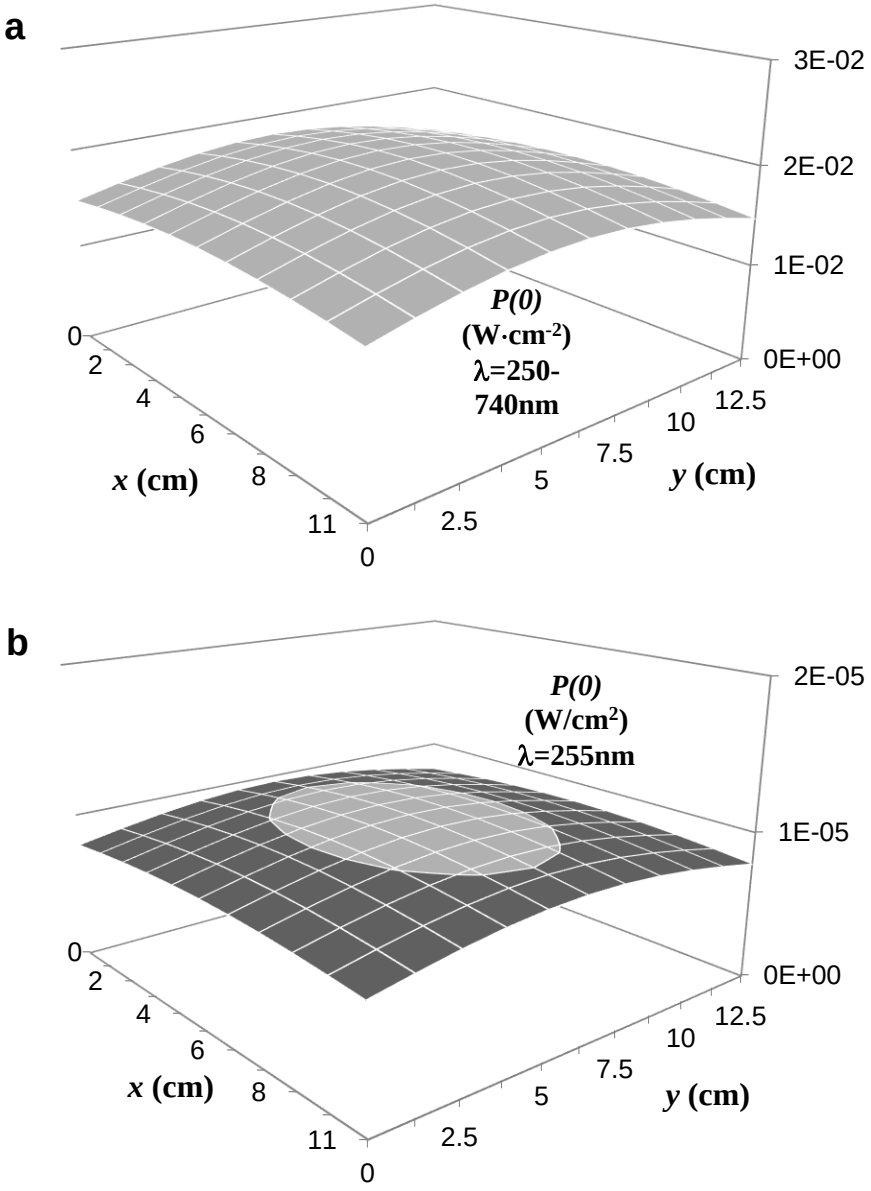

Figure 34. Incident spectral radiant power on the liquid surface of the reactor ($P(0)$) (a) for 255 nm (b) for 250-740 nm.

5.3.2 Effect on the physicochemical properties of nectarine juices

The data obtained from the physicochemical analyses performed on nectarine samples from the two varieties studied, before and after 2h of irradiation, at 25 and 45 ºC, are presented in Table 18.

Table 18. Change of physicochemical parameters of nectarine juices with UV-Vis processing.

Nectarine variety	T (ºC)	t_{UV} (min)	pH	TA	SS	TP	FI	AA	TS
Big Top	25	0	4.23 ± 0.00^{ab}	4.4 ± 0.0^{b}	9.6 ± 0.0^{a}	45.5 ± 2.6^{a}	17.0 ± 0.0^{a}	4.8 ± 0.0^{c}	93.7 ± 0.1^{d}
		120	4.22 ± 0.01^{ab}	4.4 ± 0.0^{b}	9.5 ± 0.0^{a}	38.6 ± 2.6^{a}	18.5 ± 0.7^{a}	4.8 ± 0.0^{c}	90.0 ± 0.0^{c}
	45	0	4.00 ± 0.12^{b}	4.6 ± 0.0^{bc}	9.7 ± 0.1^{ab}	64.3 ± 16.2^{a}	14.4 ± 1.1^{a}	1.8 ± 0.6^{ab}	86.2 ± 0.9^{b}
		120	4.12 ± 0.00^{ab}	4.8 ± 0.2^{c}	10.0 ± 0.1^{b}	53.2 ± 6.8^{a}	13.6 ± 1.1^{a}	1.2 ± 0.0^{b}	84.3 ± 0.0^{b}
Luciana	25	0	4.25 ± 0.00^{a}	3.7 ± 0.0^{a}	9.6 ± 0.1^{a}	118.1 ± 5.1^{b}	18.5 ± 4.9^{a}	2.5 ± 0.0^{a}	103.5 ± 0.4^{e}
		120	4.25 ± 0.00^{a}	3.5 ± 0.0^{a}	9.5 ± 0.1^{a}	115.6 ± 6.0^{b}	17.5 ± 9.2^{a}	2.5 ± 0.0^{a}	102.5 ± 0.4^{e}
	45	0	4.25 ± 0.00^{a}	3.7 ± 0.0^{a}	9.6 ± 0.1^{a}	72.0 ± 6.8^{a}	18.6 ± 2.5^{a}	2.5 ± 0.0^{a}	93.5 ± 0.3^{d}
		120	4.25 ± 0.00^{a}	3.5 ± 0.0^{a}	9.5 ± 0.1^{a}	77.1 ± 1.7^{ab}	19.4 ± 4.2^{a}	2.5 ± 0.0^{a}	69.6 ± 0.3^{a}

			CIELab colorimetric parameters		
Nectarine variety	T (ºC)	t_{UV} (min)	L^*	a^*	b^*
Big Top	25	0	25.11 ± 0.41^{c}	5.23 ± 0.27^{de}	10.64 ± 0.78^{c}
		120	24.05 ± 0.32^{bc}	4.45 ± 0.59^{bcde}	9.81 ± 0.14^{bc}
	45	0	23.48 ± 0.64^{bc}	5.54 ± 0.13^{e}	8.02 ± 0.35^{abc}
		120	22.41 ± 0.07^{ab}	4.16 ± 0.07^{abcd}	6.93 ± 0.02^{ab}
Luciana	25	0	22.63 ± 0.25^{ab}	3.27 ± 0.18^{a}	5.54 ± 0.45^{a}
		120	23.42 ± 0.59^{bc}	4.01 ± 0.08^{abc}	7.54 ± 0.81^{abc}
	45	0	21.45 ± 0.70^{a}	5.10 ± 0.10^{cde}	7.00 ± 1.90^{ab}
		120	24.60 ± 0.01^{c}	3.55 ± 0.34^{ab}	8.67 ± 0.08^{abc}

Mean value ± standard deviation. Different superscript letters (for each parameter) indicate significant differences from Tukey Test. TA = Titratable acidity expressed as $g \cdot L^{-1}$ malic acid, SS = soluble solids (ºBrix), TP = total phenols expressed as $mg \cdot L^{-1}$ gallic acid, FI = formol index expressed as mL NaOH 0.1N/100 mL, AA = ascorbic acid content ($mg \cdot L^{-1}$), TS = total sugar content ($g \cdot L^{-1}$).

From Table 18, it is worth highlighting the fact that the pH, acidity, soluble solids, total phenols, formol index and ascorbic acid values were almost the same when the juices were irradiated at 25ºC. Low values of vitamin C are attributed to the loss during the juice preparation.

At 45ºC some slight variations were manifested. For instance, in the Big Top nectarine, the soluble solids content and the acidity were increased probably due to partial water evaporation from the sample as a consequence of the energy entrance as heat. Falguera *et al.* (2014) reported similar behaviour in some pear juices. Additionally, there was a loss in ascorbic-acid content for the Big Top variety, as expected knowing the sensitivity of this compound to temperature (Ling *et al.*, 2015). This effect was not detected in the Luciana variety, probably due to its low initial content of the vitamin.

Radiation processing at 45ºC also resulted in a decreased in the total sugar content. Figure 35 shows that the treatment induced changes in the sugar composition, e.g. a decrease in the sucrose content which indicates hydrolysis of this molecule to fructose and glucose. Ibarz *et al.* (1989) reported degradation of sucrose in thermal treatments of pear juices and found that a further degradation occurs when the hexoses participate in Maillard reactions, caramelization, and formation of HMF. Therefore, the reduction in the total sugar content of nectarine juices (Table 18) may be caused by those reactions. Although 45ºC is a lower temperature than that used in traditional thermal treatments, it seems high enough to produce slight changes.

Regarding the juice colour, Figure 36 shows the evolution of colorimetric parameters during a 120-min UV process. Even when only small variations are observed in the three colorimetric parameters, it is noticeable that the evolution of colour depends on the nectarine variety as well as on the temperature in the sample. Looking at Table 18, it can be said that no significant variations were found in the colorimetric parameters after treatments at 25ºC. However, the processing at 45ºC induced slight changes.

For the Big Top variety, the L^* value for the juice irradiated at 45 ºC was lower than the value for fresh juice (T = 25ºC, t_{UV} = 0 min). According to Ibarz *et al.* (2005), brightness (L^*) decreases with the soluble solids content. This decrease in brightness may be related to the increase in the soluble solid content during the process. For the Luciana variety, a slight increase in brightness (L^*) and a decrease in redness (a^*) were produced during the UV-Vis treatment at 45 ºC (Table 18). Both the rise in L^* and the decrease in a^* can be attributed to the destruction of pigments, either initially present in the fruit juice or formed by the rapid actions of PPO (melanins) as well as the Maillard reaction between

sugars and amino acids (melanoidins), as found by Ibarz *et al.* (2005) and Falguera *et al.* (2011 and 2014) in apple, peach, lemon and pear juices.

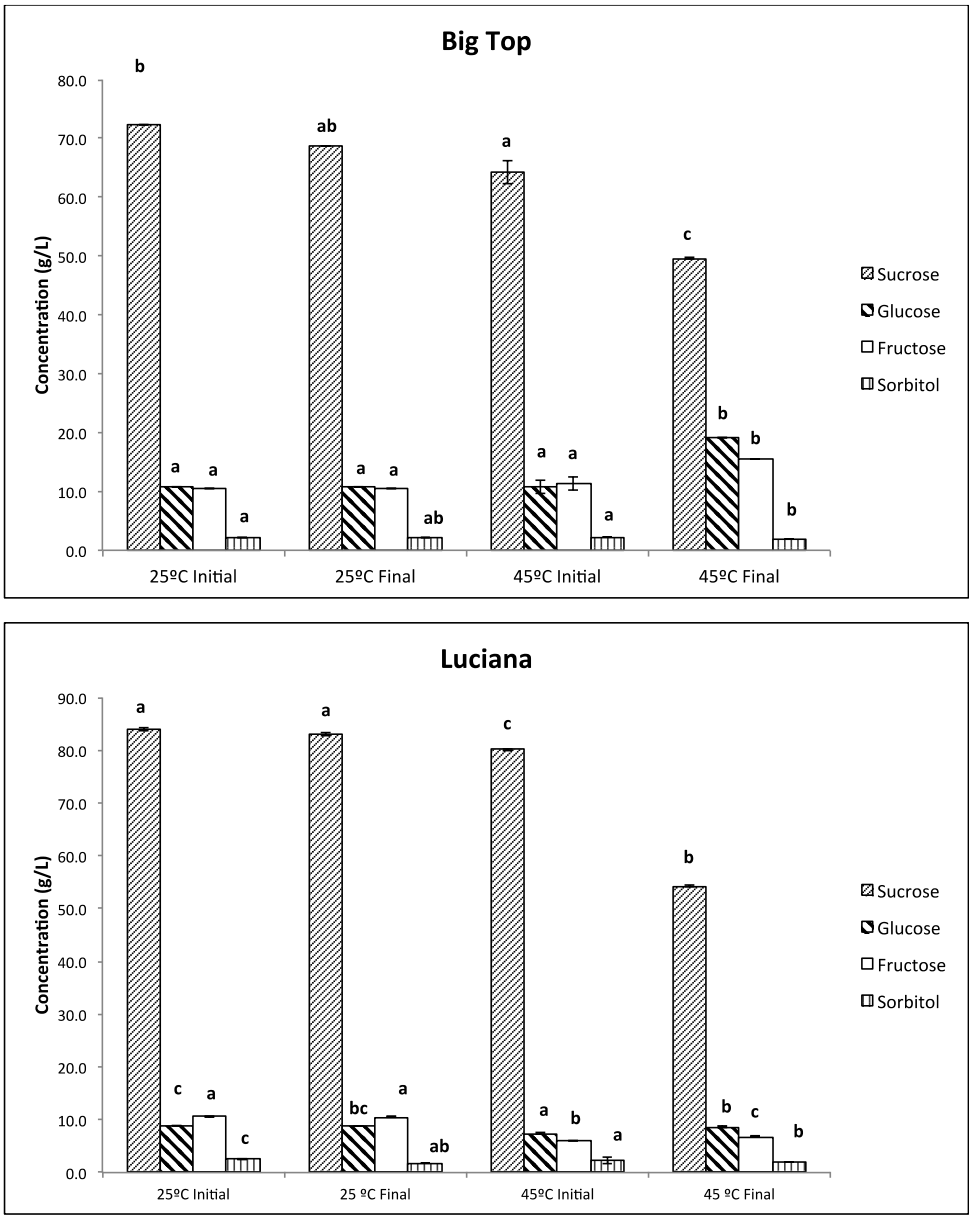

Figure 35. Sugar profile in nectarine juices from Big Top and Luciana varieties before and after UV-Vis processing at 25 ºC and 45 ºC. Mean values and error bars.

Another way to visualize the changes occurring in the colorimetric parameters is by representing *b** (blue-yellow) versus *a** (green-red) (Fig. 37). From this graph, a slight decrease in both parameters during irradiation of Big Top nectarine juices is clear, mainly at 45ºC. According to Ibarz *et al.* (2005), this trend is contrary to the one that takes place in the browning process and indicates destruction of the coloured polymeric compounds during irradiation.

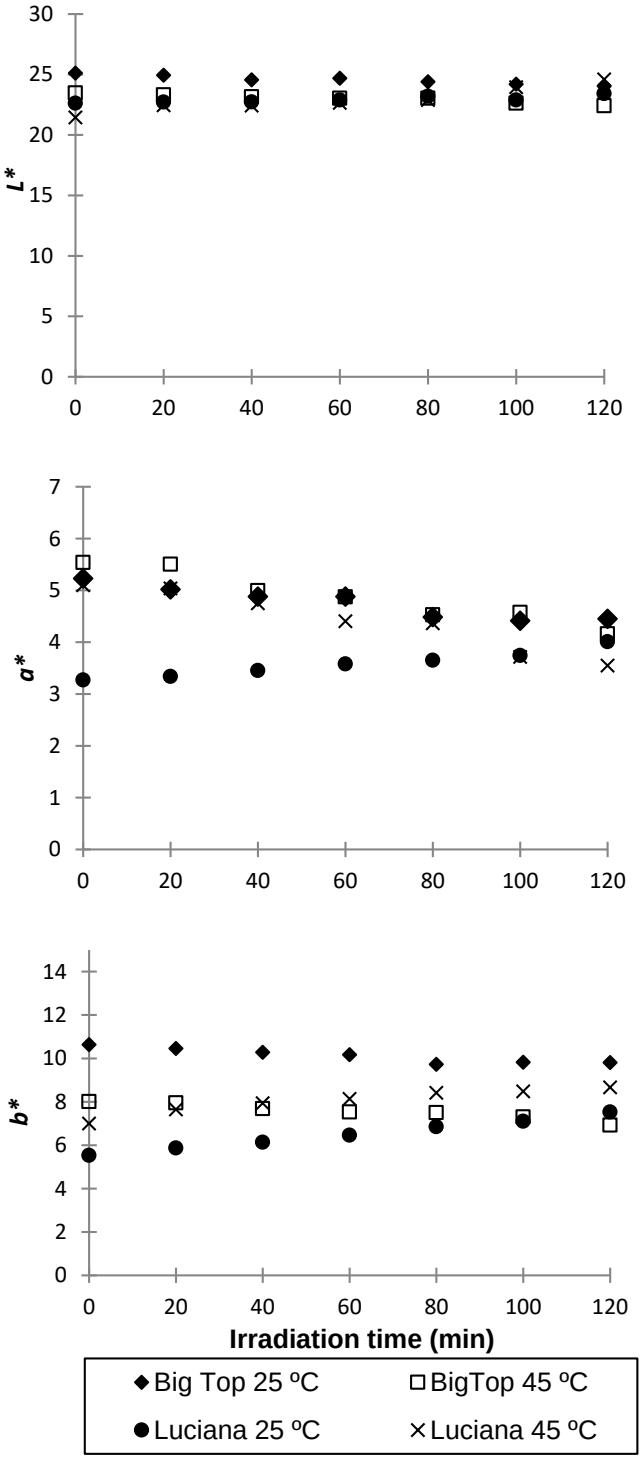

Figure 36. Evolution of the CIELab parameters in nectarine juices with the irradiation time.

Contrary to the Big Top variety, a slight but not significant increase in the *b** parameter was observed in the Luciana variety (Fig. 37). Falguera *et al.* (2011 and 2014) also found opposite trends in the evolution of yellowness during the UV-Vis treatment of different varieties of apple and pear juices.

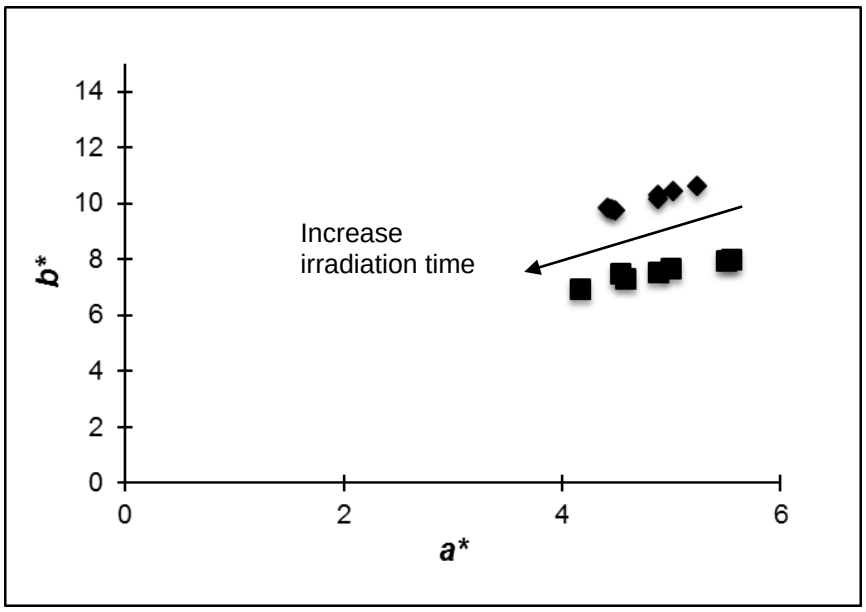

Figure 37. Evolution of a*-b* parameters for Big Top nectarine juices UV-Vis processed at 25ºC(♦) and 45ºC(■).

The information about the evolution of colour during the UV-Vis treatment in nectarine juices was complemented by comparing the absorption spectra before and after irradiation of the juices (Fig. 38).

For the Big Top variety (Fig 38a), only a minimal difference was observed in the absorption at the region near 420 nm, matching the maximum band in the emission spectrum of the lamp (Fig. 10). The *A*(420) value is related to the non-enzymatic browning and the presence of melanoidins (Ibarz *et al.*, 2005). Thus, the slight decrease in *A*(420) coincides with the previous results that showed an evolution in colour contrary to the browning process.

For the Luciana variety, the spectra show interesting information (Fig 38b). First, when the juice is heated at 45ºC before irradiation, the absorbance increases at every wavelength, probably due to a browning process. It is possible that this nectarine variety be particularly susceptible to browning reactions due to its high content of sugars and phenols (Table 18). After the irradiation at 45ºC the absorbance values decrease, confirming the photo-degradation of coloured compounds.

In any case, at the end of the UV-Vis treatment, the absorption spectra for treated and fresh juices were very similar. These results are contrary to those reported by Manzocco *et al.* (2009) and Müller *et al.* (2014), who observed a browning process after UV-C irradiation. Thus, the use of a medium-pressure mercury lamp is an advantage in the processing of fruit derivatives.

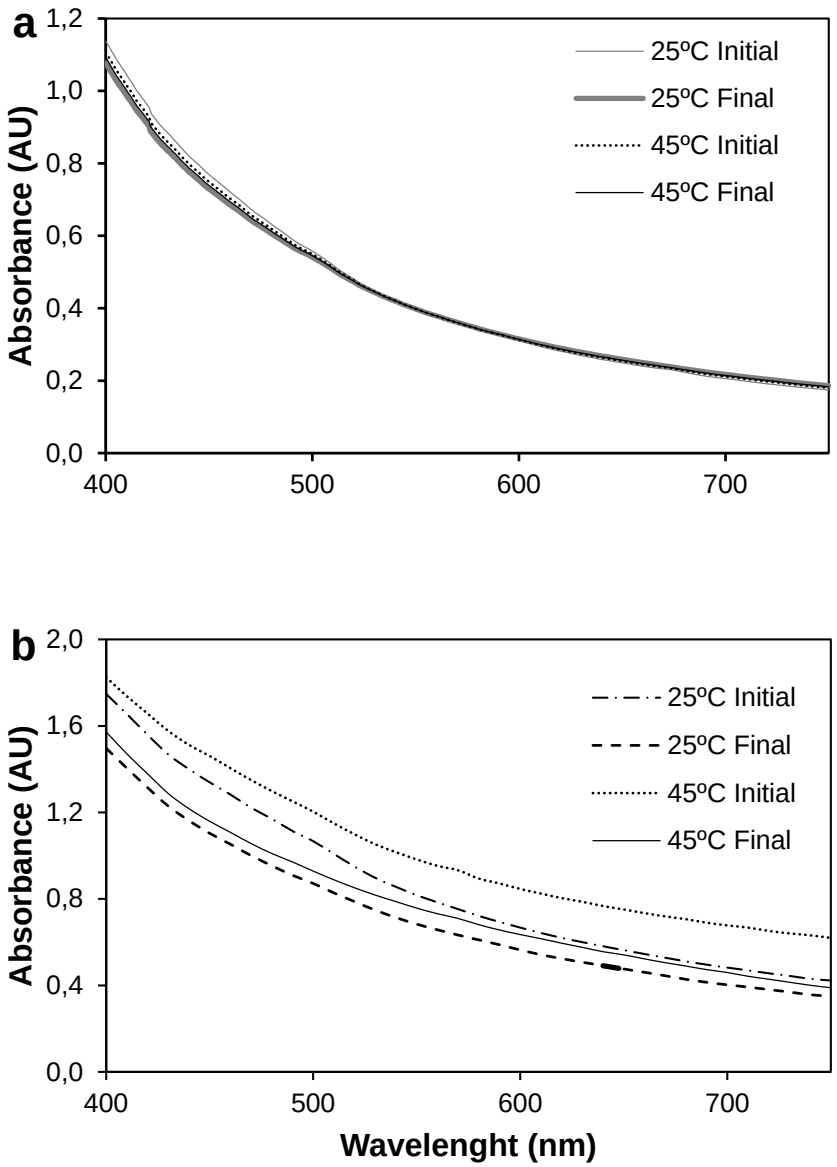

Figure 38. Absorbance spectra for nectarine juices irradiated at 25 and 45ºC. (a) Big Top variety (b) Luciana variety.

5.3.3 Effect on the physicochemical properties of peach juices

The results from the physical and chemical determinations in peach juices are summarized in Table 19. It can be seen that no significant changes were observed in the pH value, acidity, or vitamin C content after UV-Vis radiation processing, regardless of the variety.

Table 19. Change of physicochemical parameters of peach juices with UV-Vis processing.

Peach variety	Treatment	pH	TA	SS	TP	FI	AA	TS
Baby Gold	Control	4.54 ± 0.08^{a}	2.15 ± 0.07^{a}	7.0 ± 0.6^{a}	46.7 ± 3.8^{ab}	19.8 ± 3.2^{a}	2.8 ± 0.4^{a}	52.9 ± 3.6^{a}
	UV25	4.43 ± 0.22^{a}	2.25 ± 0.10^{a}	7.5 ± 0.1^{a}	39.4 ± 1.1^{a}	23.5 ± 0.7^{a}	2.3 ± 0.4^{a}	54.7 ± 2.7^{a}
	UV45	4.68 ± 0.18^{a}	2.35 ± 0.07^{a}	7.5 ± 0.7^{a}	54.8 ± 3.3^{b}	24.0 ± 4.2^{a}	2.3 ± 0.4^{a}	58.3 ± 2.7^{a}
Calanda	Control	4.05 ± 0.02^{a}	8.65 ± 0.35^{a}	10.4 ± 1.4^{a}	294.4 ± 27.7^{ab}	27.5 ± 0.7^{b}	9.3 ± 0.4^{a}	92.2 ± 6.9^{a}
	UV25	4.13 ± 0.25^{a}	9.20 ± 0.10^{a}	10.8 ± 0.6^{a}	339.0 ± 23.4^{b}	22.0 ± 0.1^{a}	10.5 ± 0.7^{a}	90.5 ± 3.9^{a}
	UV45	3.99 ± 0.01^{a}	9.11 ± 0.57^{a}	10.6 ± 0.8^{a}	217.9 ± 14.1^{a}	21.5 ± 0.7^{a}	11.8 ± 1.1^{a}	88.6 ± 0.7^{a}
Planet Top	Control	4.47 ± 0.22^{a}	2.05 ± 0.07^{a}	12.2 ± 0.6^{a}	162.9 ± 2.8^{c}	10.6 ± 0.6^{a}	4.8 ± 1.1^{a}	99.2 ± 6.9^{a}
	UV25	4.60 ± 0.33^{a}	2.53 ± 0.25^{a}	13.0 ± 0.3^{a}	129.6 ± 10.3^{b}	13.6 ± 0.1^{a}	3.3 ± 1.1^{a}	129.6 ± 10.3^{b}
	UV45	4.75 ± 0.02^{a}	2.53 ± 0.04^{a}	13.7 ± 0.5^{a}	109.3 ± 0.04^{a}	16.5 ± 2.1^{a}	2.8 ± 0.4^{a}	109.3 ± 0.7^{ab}

		Colorimetric parameters		
Peach variety	Treatment	*L**	*a**	*b**
Baby Gold	Control	28.52 ± 1.69^{a}	7.01 ± 0.30^{b}	17.63 ± 0.57^{b}
	UV25	26.65 ± 1.17^{a}	5.83 ± 0.07^{a}	15.01 ± 0.53^{a}
	UV45	24.51 ± 0.11^{a}	5.57 ± 0.13^{a}	13.39 ± 0.04^{a}
Calanda	Control	21.18 ± 2.09^{a}	10.82 ± 0.53^{b}	8.30 ± 0.20^{b}
	UV25	20.54 ± 0.68^{a}	8.69 ± 0.23^{a}	5.46 ± 0.28^{a}
	UV45	21.40 ± 7.36^{a}	8.27 ± 0.43^{a}	4.51 ± 0.16^{a}
Planet Top	Control	20.92 ± 0.25^{a}	9.19 ± 0.11^{c}	9.54 ± 0.25^{b}
	UV25	21.37 ± 0.06^{a}	8.31 ± 0.02^{b}	8.79 ± 0.15^{a}
	UV45	20.68 ± 0.04^{a}	8.79 ± 0.15^{a}	7.57 ± 0.24^{a}

Mean value ± standard deviation. Different superscript letters (for each parameter) indicate significant differences from Tukey Test. TA = Titratable acidity expressed as g·L^{-1} malic acid. SS = soluble solids (ºBrix), TP = total phenols expressed as mg·L^{-1} gallic acid, FI = formol index expressed as mL NaOH 0.1N/100 mL, AA = ascorbic acid content (mg·L^{-1}), TS = total sugar content (g·L^{-1}).

It also can be seen that the soluble solids content tended to increase after the treatments in the three peach juises studied, although, this variations were not statistically significant. This phenomenon was also observed for a nectarine juice irradiated at 45ºC (Section 5.3.2). In a similar way, this increase could be due to the evaporation of water above room temperature.

The phenolic content was preserved in the Baby Gold and Calanda varieties, while a reduction was observed for the Planet Top juices. Falguera *et al.* (2012) found that the phenolic content can decrease after UV-Vis irradiation of grape juice. However, this phenomenon is still unclear, possibly being caused by photochemical degradation or by residual enzymatic activity.

The formol index did not vary significantly after processing of the Baby Gold and Planet Top varieties. Conversely, the juices from the Calanda variety showed an unexpected decrease of this parameter at both temperatures. As the formol index is related to the amino acid content in fruit juices, it looks like this juice variety losses its amino acid content. This loss could be a consequence of the Maillard reaction between the amino acids and sugars in the juice to produce a polymer blend called melanoidins. This reaction was reported many times in fruit derivatives without undergoing high temperatures (Ibarz *et al.*, 2011). It is possible that the Maillard reaction could be favoured by the high acidity and formol index observed for the Calanda variety.

The total sugar content was not varied after the treatments for the Baby Gold and the Calanda varieties. However, slight variations on this attribute were registered for the Planet Top variety. This particular behaviour could be due to different slight changes in juice composition taking place during processing, such as water evaporation as well as sugar degradation reactions, probably because of the high concentration of dissolved solids in this juice. The distribution of sugar between sucrose and hexoses (glucose plus fructose) for the three samples studied after irradiation is graphed in Figure 39. Non-irradiated juices were used as control, and their sugar distribution is also shown. The values in the graph are expressed as percentages of total sugar content (see Table 19). For the Baby Gold and Calanda varieties, the sugar distribution seems to be constant after the treatment at 25ºC, but the sucrose percentage appears to decrease at 45 ºC (Fig. 38). This behaviour was also observed for nectarine juices and can be related to sucrose hydrolysis. For the Planet Top variety, the decrease in the sucrose content is noticeable for both temperatures. Nevertheless, these variations were not significant for any of the peach

juices studied. This indicates that, from the practical point of view, the sugar content was not modified after the treatments.

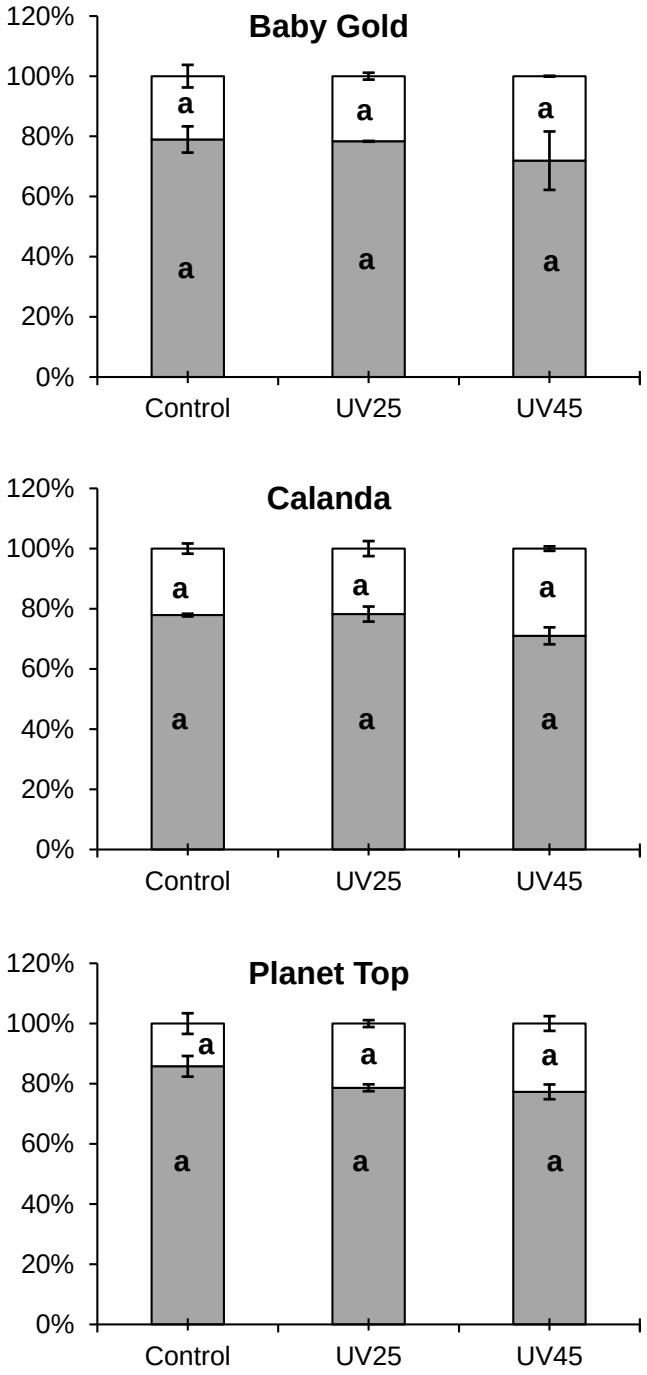

Figure 39. Sugar distribution into sucrose (grey) and hexoses (white) in peach juices processed by UV-Vis irradiation. Equal letters mean non-significant differences ($p < 0.05$) from statistical analysis.

The evolution of lightness (L^*) during the UV-Vis treatment of peach juices is shown in Figure 40. As can be seen, this colorimetric parameter did not change

significantly. Ibarz *et al.* (2005) concluded that the brightness (*L**) increases when the soluble solid content decreases. As the soluble solids content hardly changed, the brightness was also almost constant during irradiation.

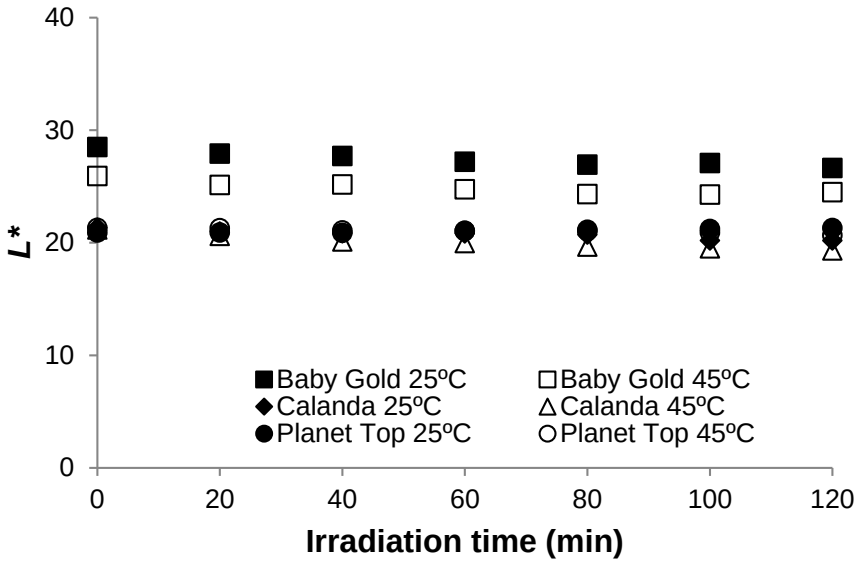

Figure 40. Evolution of the lightness with irradiation time for peach juices.

The evolution of the colour was also monitored with the other two colorimetric parameters: *a** (green-red) and *b** (blue-yellow). Figure 41 shows how both parameters *a** and *b** decrease with irradiation time. This trend indicates the degradation of some pigments in the juice, either initially present or formed later by the rapid action of polyphenol oxidase (melanins) in addition to the Maillard reaction between sugars and amino acids (melanoidins), as found for nectarine juices as well as in previous works (Ibarz *et al.*, 2005; Falguera *et al.*, 2011 and 2014).

5.3.4 Enzymatic activities

Figure 42 shows the evolution of the relative PPO activity at 25 and 45 ºC for the two nectarine juices studied. The effect of UV-Vis irradiation on PPO activity was similar for both varieties studied. Treatments performed at 45ºC completely inactivated the enzyme after 100 min in both juice samples, but at 25ºC a reduction of about 60% was only achieved after 120 min. Manzocco *et al.* (2009) demonstrated the effectiveness of UV-C at inactivating PPO. The higher the irradiance the greater the reduction in PPO activity. Meanwhile, a not significant effect was found in the absence of light. By UV-irradiation treatments, the initial activity of PPO in a clear apple juice was reduced up to

70% after 100 min at 4ºC. This achievement was very close to the total inactivation achieved by Falguera *et al.* (2011d) with UV-Vis light in the same period of time.

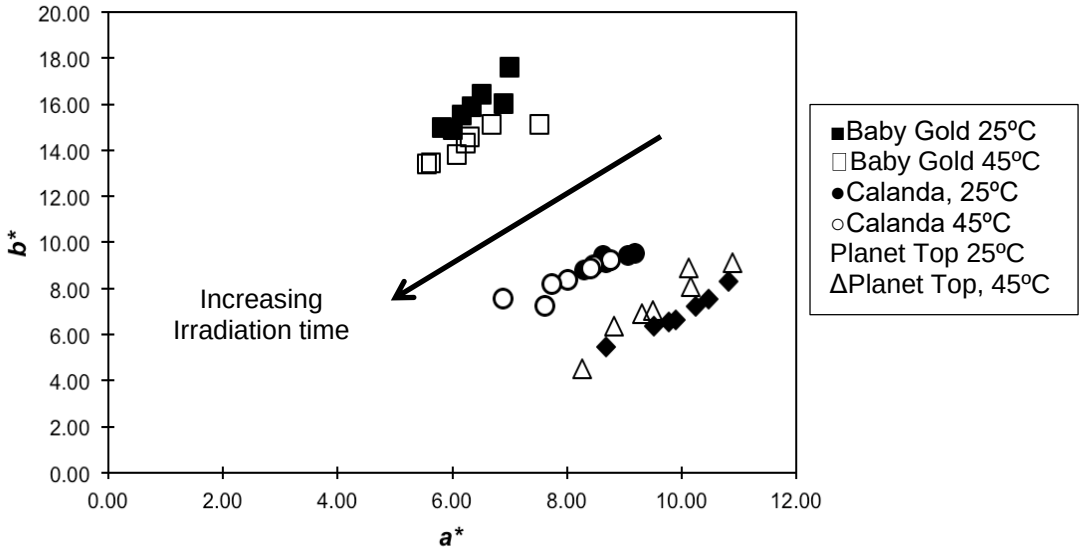

Figure 41. Evolution of the *a**-*b** parameters with irradiation time for peach juices.

Table 20 displays the parameters obtained by fitting the experimental data to the first-order model. The fitted values for the first-order kinetic constant (*k*) confirm that the higher the temperature the faster the inactivation, according to the results reported by Sampedro and Fan (2014). Those authors attributed the main inactivation of PPO and POD to UV radiation, since no effect at 25ºC or minimal effects at 45ºC were observed with the lamp off, when model systems were treated.

Figure 43 shows the evolution of the relative POD activity at both temperatures and for both nectarine juices. This behaviour depended largely on the temperature. At 25ºC, the POD activity increased for the Big Top variety. A hypothesis to explain this phenomenon could be that this enzyme has a globular structure that is altered by the absorption of UV light, leaving the active sites of the enzyme exposed. On the contrary, at 45ºC, both nectarine juice samples showed a fast decrease. In fact, for the Big Top variety the total inactivation of the enzyme was achieved before 20 min of treatment. The POD inactivation for the Luciana variety was slower than that observed for the Big Top variety and 120 min were required to totally inactivate the enzyme. Kinetics matched first-order models (Table 21).

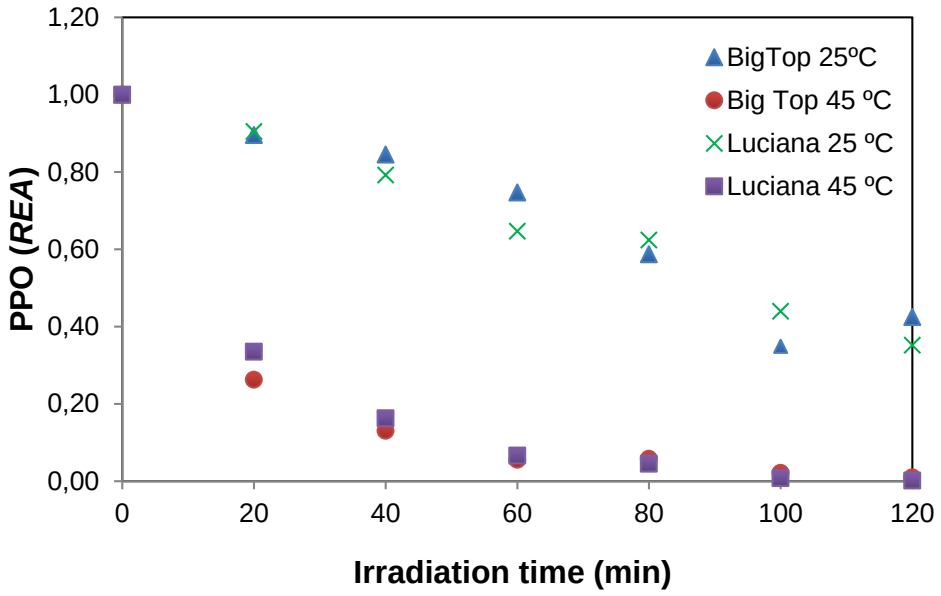

Figure 42. Evolution of PPO activity with irradiation time in nectarine juices.

Table 20. Estimated values of parameters obtained from the exponential fitting of PPO residual activity of nectarine juices as a function of irradiation time.

$$REA(t_{UV}) = \exp(-kt_{UV})$$

Nectarine variety	T (ºC)	k (min^{-1})	R^2
Big Top	25	0.008 ± 0.001	0.8821
	45	0.060 ± 0.004	0.9902
Luciana	25	0.008 ± 0.001	0.9589
	45	0.050 ± 0.002	0.9950

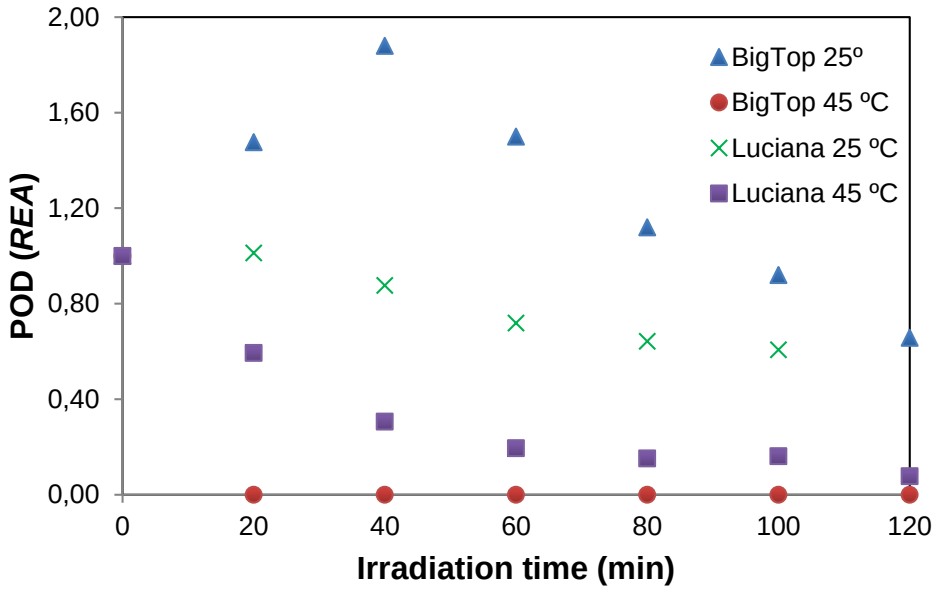

Figure 43. Evolution of POD activity with irradiation time in nectarine juices.

Table 21. Estimated values of parameters obtained from the exponential fitting of POD residual activity of nectarine juices as a function of irradiation time.

$$REA(t_{UV}) = \exp(-kt_{UV})$$

Nectarine variety	T (ºC)	k (min^{-1})	R^2
Big Top	25	0.0235 ± 0.0057	0.9722
	45	*	*
Luciana	25	0.0115 ± 0.0009	0.9877
	45	0.0250 ± 0.0048	0.8731

* Completely inactivated during the first 20 min of irradiation.

Likewise, Figure 44 shows the evolution of the relative enzymatic activities of PPO for peach juices processed by UV-Vis irradiation. It can be seen that the PPO activity was almost totally eliminated for all the peach juices studied after 60 min at 45ºC. At 25ºC, the activity was only totally eliminated after 120 min for the Planet Top variety, whereas the Calanda and Baby Gold varieties maintained a relative activity of about 40%. Falguera *et al.* (2013a and 2014) also found different rates of inactivation depending on the fruit variety when they irradiated grape and pear juices, respectively. Such differences can be due to the initial enzymatic activity or to the initial juice colour. Peach juices had initial activities of 0.001 (Calanda), 0.03 (Baby Gold) and 0.06 (Planet Top) U·mL^{-1}. As these juices had similar initial colorimetric parameters, the fast inactivation in the Calanda juices could be explained by their lower initial activity.

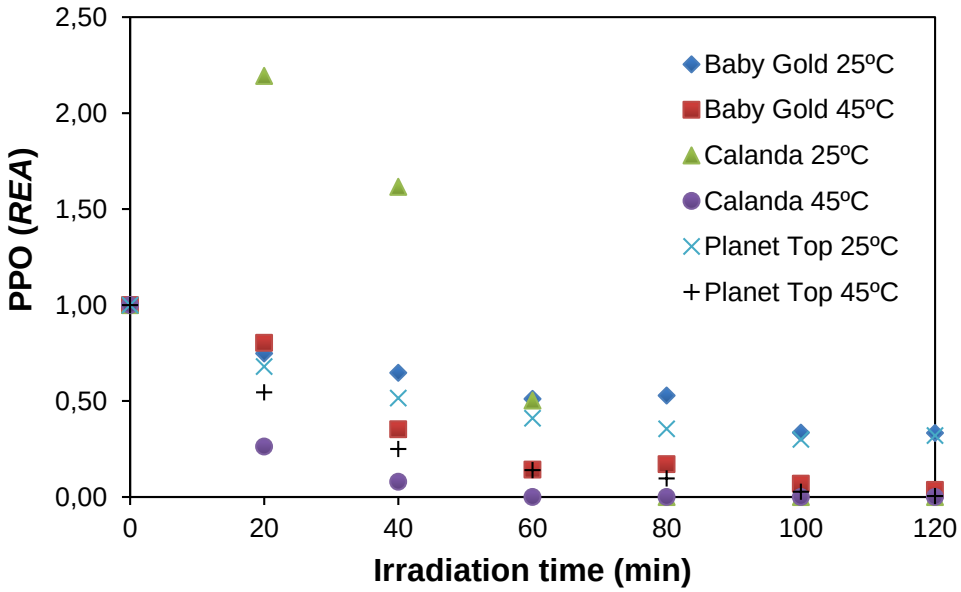

Figure 44. Evolution of PPO activity with irradiation time in peach juices.

It is worth remarking that, at 25ºC, the Calanda variety showed an initial activation

stage, reaching over 200% of the initial value after 20 min followed by an inactivation stage causing final relative activity similar to that in the other varieties at the same temperature. Manzocco *et al.* (2009) also found an initial activation phase followed by a decrease in PPO activity for prolonged exposure times when they irradiated a model solution with visible light (11.7 and $9.4 \cdot 10^{-4}$ $W \cdot cm^{-2}$). As previously mentioned, non-ionizing radiation promotes photo-oxidation processes that modify the native structure of the protein such as side-chain oxidation and backbone fragmentation. Consequently, the active sites become more accessible for the substrate. The first stage of activation was followed by a second stage of inactivation. This mechanism could be due to competitive reactions of activation and inactivation and is discussed below together with the even bigger activation stage found for POD activity.

In all cases, the temperature improved the inactivation of PPO in peach juices. Consequently, the enzymatic activity was lower than 5% after 120 min of irradiation at 45ºC. With high-pressure treatments, the maximum rate of inactivation was 80% in peach juices (Rao *et al.*, 2014). Table 22 shows the fitting parameters for the first-order kinetic model. The data for Calanda variety were excluded because of the initial activation at 25ºC and the very high rate at 45ºC. Correlation coefficients indicated that the first-order kinetic model is acceptable to describe the inactivation of PPO for the Baby Gold and Planet Top variety peach juices. The kinetic constant values indicated a greater inactivation rate as the temperature increased, matching the data shown in Figure 42 and Table 20.

Table 22. Estimated values of parameters obtained from the exponential fitting of PPO residual activity of peach juices as a function of irradiation time.

$$REA(t_{UV}) = \exp(-kt_{UV})$$

Variety	T (ºC)	RA_0	k (min^{-1})	R^2
Baby Gold	25	0.96 ± 0.80	0.009 ± 0.001	0.9551
	45	0.98 ± 0.21	0.028 ± 0.003	0.9669
Planet Top	25	0.70 ± 0.80	0.008 ± 0.001	0.9028
	45	1.31 ± 0.51	0.043 ± 0.004	0.9624

Figure 45 shows that the POD activity was not fully eliminated for any variety and temperature after 120 min, although the value was reduced by between 20 and 60% in most cases. The Calanda and Baby Gold varieties showed an initial activation of POD activity at both temperatures. At 25 ºC, the Calanda variety showed an activation of up to

almost 500% of the initial value after 60 min of irradiation, and this value remained almost constant for the following 60 min.

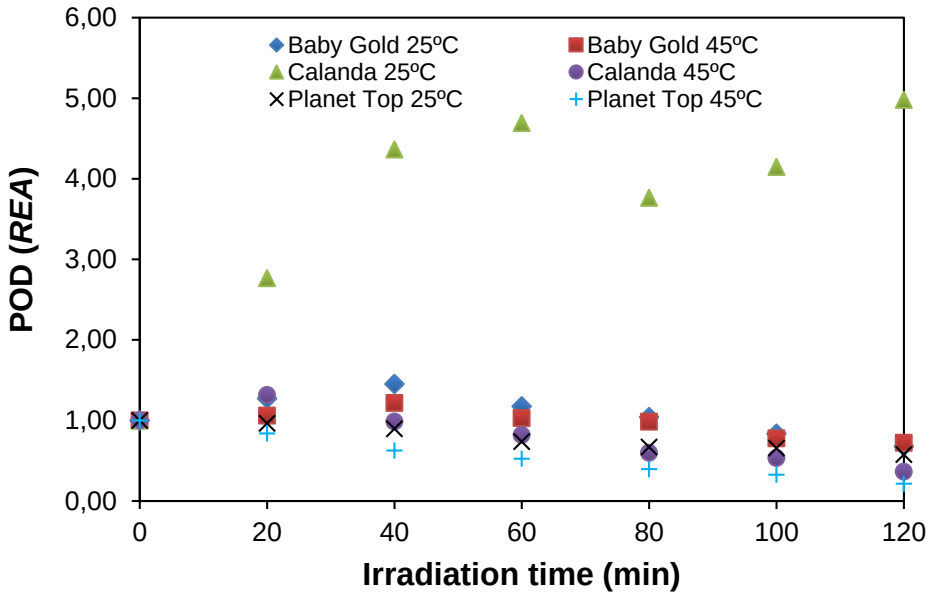

Figure 45. Evolution of POD activity with irradiation time in peach juices.

The initial activation of POD observed in both nectarine and peach juices was also found during the UV-Vis irradiation of a buffer solution of peroxidase from horseradish (Falguera *et al.*, 2013b). On the contrary, Sampedro *et al.* (2014) did not find POD activation in synthetic solutions of POD also from horseradish. In that case, the irradiation used wavelengths exclusively from 185 to 254 nm. Comparing the conclusions obtained by both groups of researchers, it seems that the UV wavelengths that produce the activation of POD are above 254 nm.

Augusto *et al.* (2015) proposed that the reason for the initial activation by UV irradiation is the partial molecular unfolding of the enzyme, because these configuration changes can expose the enzyme active sites better, increasing their enzymatic activity. The activation could be explained by the serial inactivation process described by Equation 64, when the intermediate enzyme form has more activity than the native form. However, the initial inactivation was not observed during the UV-Vis irradiation of apple, grape and pear juices (Falguera *et al.*, 2011d, 2013a and 2014, respectively). A possible explanation is that the serial inactivation process could always take place, even when the intermediate enzyme form has lower activity, thus without initial activation. Besides the range of wavelengths, the difference between the studies that showed initial activation

and those that did not could be explained by the presence of other substances, like sugars and salts. Matsui *et al.* (2007) found that salts and sugars significantly affected enzyme stability during POD and PPO microwave-thermal inactivation.

After 120 min, total inactivation of peroxidase was not achieved for any variety. These results are different to those in Falguera *et al.* (2011d), who fully inactivated the enzyme in apple juices after 15 min of UV-Vis irradiation. This variation could be due to variations in the colorimetric characteristics between juices. A protective effect of coloured substances (melanoidins) for inactivating POD in model solutions by multi-wavelength irradiation treatments has been demonstrated (Falguera *et al.*, 2013b).

Table 23 shows the fitting parameters for the first-order kinetic. In the case where previous activation was found, the first-order equation only fitted to the decay stage. The high correlation coefficient values indicated that the model is adequate for the inactivation of POD, at least for its decay stage, when previous activation was found. The kinetic constant values increased with the temperature, as expected. These values were lower than those for nectarine juices (Table 21), probably due to a higher content of pigments in peach juices (See Tables 18 and 19). The fitting parameters for the model in Giner-Seguí *et al.* (2006) were not included because the correlation coefficients were not good enough.

Table 23. Estimated values of parameters obtained from the exponential fitting of POD residual activity of peach juices as a function of irradiation time.

$$REA(t_{UV}) = \exp(-kt_{UV})$$

Peach variety	Temperature (ºC)	RA_0	k (min^{-1})	R^2
Baby Gold	25	2.43 ± 0.35	0.010 ± 0.001	0.9636
	45	1.51 ± 0.19	0.006 ± 0.001	0.9615
Calanda	25	*	*	*
	45	1.64 ± 0.16	0.012 ± 0.001	0.9771
Planet Top	25	1.05 ± 0.05	0.005 ± 0.001	0.9534
	45	1.11 ± 0.10	0.013 ± 0.001	0.9724

* No inactivation was observed after 120 min of irradiation.

5.4 Ascorbic acid degradation during UV-Vis processing

5.4.1 Absorption spectrum

The absorption spectrum of the L-ascorbic acid molecule in aqueous solutions (pH =3) is graphed in Figure 46. This spectrum shows a radiation band in the wavelength

range between 230 and 290 nm whereas the molecules barely absorb radiation in the range between 290 and 335 nm. The lamp used in this work has two emission peaks in the interval from 255 to 345 nm. Contrasting both spectra, it is noted that the interval of wavelengths where the emission and absorption match is located between 255 and 335 nm. However, the most powerful UV-C light is emitted at 295 and 335 nm. At both wavelengths, the absorption of light by the ascorbic acid molecules is minimal, suggesting a low probability of inducing a photo-chemical change. This is an interesting result, considering that this compound is intended to be preserved during the processing of fruit juices.

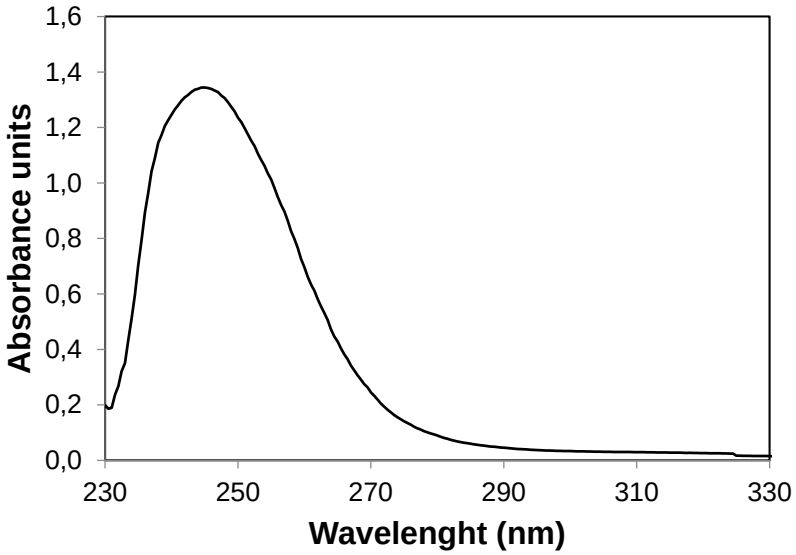

Figure 46. Absorption spectrum of an aqueous solution of AA (pH 3, 25 mg·L^{-1}).

The absorption spectrum was also obtained for pH=6. At wavelengths equal or higher than 255 nm, the curves matched Figure 46. This means that the pH of the solution does not influence the absorption of light at the conditions considered in this study.

The values of absorbance for ascorbic acid at the wavelength range between 255 and 335 nm were copied to a datasheet in order to calculate the absorption coefficients at each wavelength. These data are displayed in Table 24. It can be noted that the maximum absorbance of HMF in the interval considered is at 255 nm. This value is lower than the maximum obtained for HMF (see section 5.2.3, Table 7). Moreover, it is confirmed that the radiation emitted by the lamp is hardly absorbed by the AA molecules.

Table 24. Absorption coefficients and molar extinction coefficients of L-ascorbic acid at different wavelengths.

λ (nm)	μ_λ (cm^{-1}), C_{AA}^0 = 100 mg·L^{-1}	ε_λ (L·mol^{-1}·cm^{-1})
255	2.331	4105
265	0.986	1737
275	0.325	573
285	0.138	243
295	0.085	150
305	0.072	126
315	0.065	114
325	0.039	69
335	0.032	57

5.4.2 Incident radiation

Taking the data in Table 24, and using the Simpson integration method to solve Equation 12, the incident spectral radiation (from 255 to 335 nm) at the liquid surface of the reactor ($P(0)$) was calculated. Likewise, the incident radiation at the bottom of the reactor ($P(C)$ containing a 100-mg·L^{-1} AA solution was calculated. The distributions of both $P(0)$ and $P(C)$ in the upper and lower surfaces of the parallelepiped (12.5x10.5x10cm) are graphed in Figure 47. It can be appreciated that a considerable part of the incident radiation at the surface reaches the bottom. This behaviour is clearly different to that observed for HMF at the same concentration, where the incident radiation was almost totally absorbed by the solution in the tank.

The total spectral radiation reaching the liquid reactor surface, in the interval between 235 and 335 nm, was 0.75W ($5.71 \cdot 10^{-3}$ W·cm^{-2}), whereas the total radiation that reached the bottom of the reactor resulted in 0.39 W ($2.97 \cdot 10^{-3}$ W·cm^{-2}). This means that from the radiation power incident at the liquid surface of the sample, approximately 50 % reaches the reactor bottom, the rest being absorbed by the solution or exiting through the walls of the tank.

5.4.3 Absorbed radiation power

As with HMF, the spectral absorbed radiation power absorbed by the whole solution (P_{abs}) was calculated with Equation 14. The values obtained for different concentrations are shown in Figure 48. Similarly to HMF, P_{abs} increases with the AA concentration in a non-linear way. However, the curve drawn is far from reaching the asymptote and hence, a considerable difference exists between the incident and the absorbed radiation under the conditions assayed. This behaviour reinforces the idea that the L-ascorbic acid barely absorbs the light emitted by the lamp.

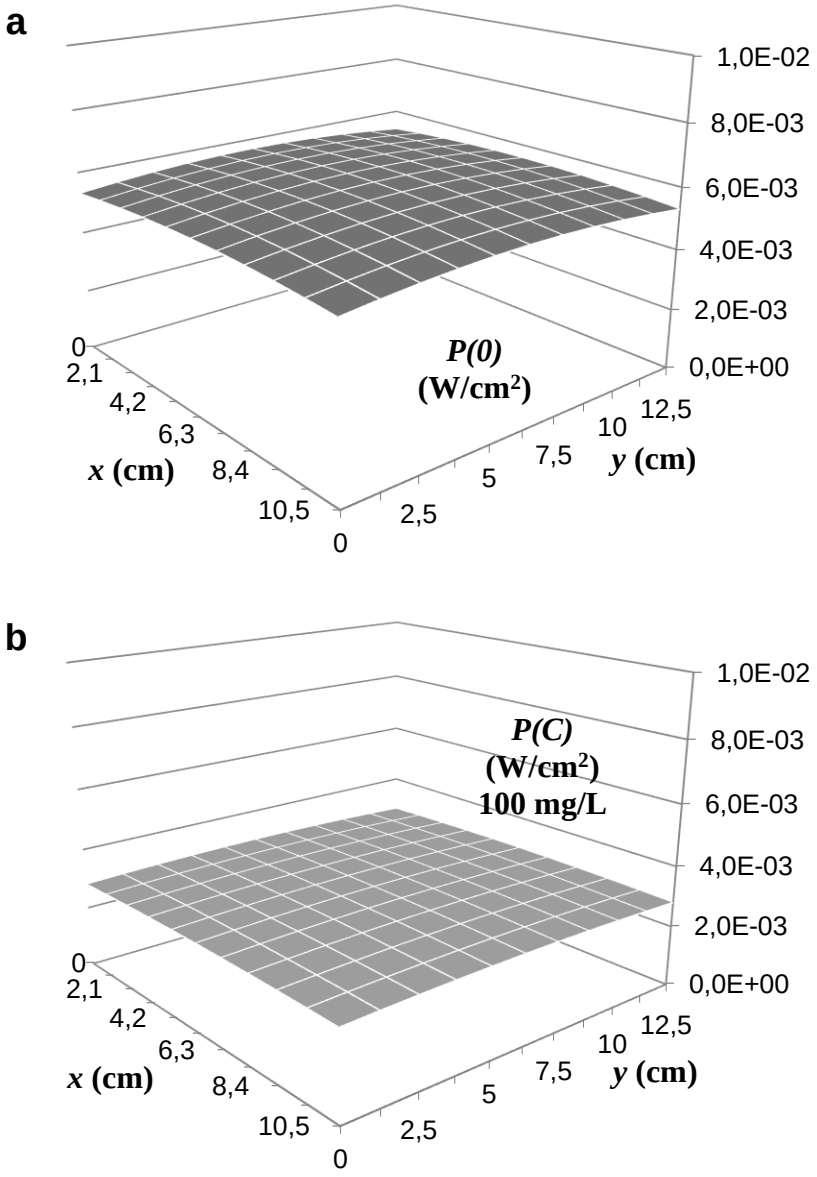

Figure 47. Incident spectral radiant power (255-335 nm) (a) at the reactor surface ($P(0)$) (b) at the reactor bottom ($P(C)$) considering a 100-mg·L^{-1} AA solution.

In order to obtain an equation to define the relation between P_{abs} and C_{AA}, the data of the absorbed radiation, in the range of concentrations from 50 to 250 mg·L^{-1}, were represented in a scatter plot (Fig. 49). This range includes all the concentration values measured during the irradiation of the AA solutions. A linear fitting was performed and the results of this calculation are also shown in this figure. Looking at the correlation coefficient, it can be said that the data can be related by a linear equation. On undertaking an analogy of the mechanism proposed for HMF and applying the mathematical models

developed, it can be elucidated that the photo-degradation of ascorbic acid, if it took place, would follow a pseudo-first-order model.

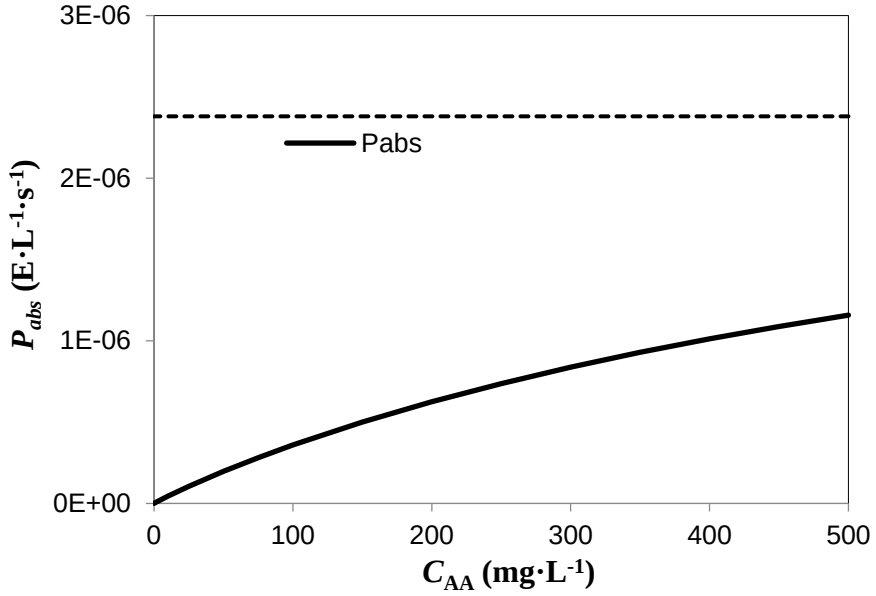

Figure 48. Spectral radiant power absorbed as a function of AA concentration.

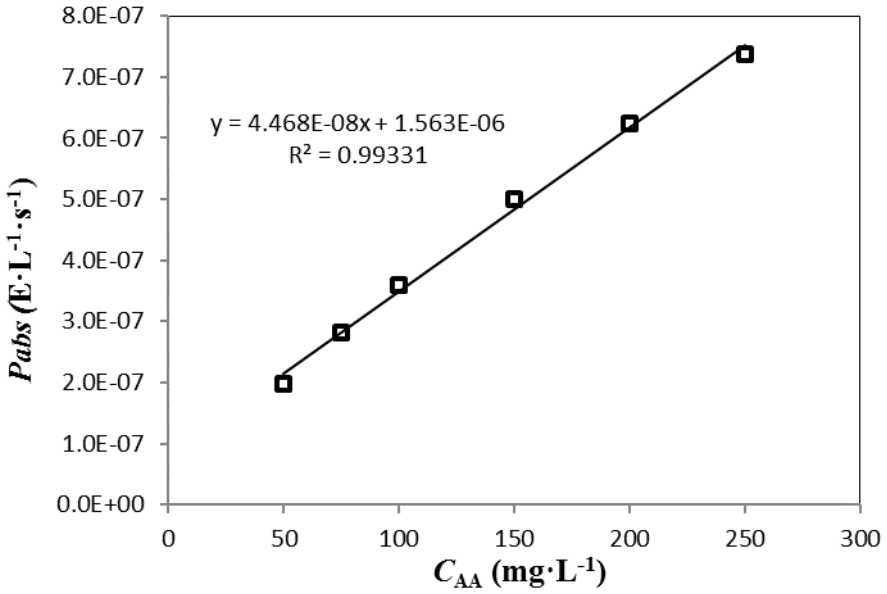

Figure 49. Spectral radiant power absorbed as a function of AA concentration in the interval between 50 and 250 mg·L^{-1}. Fitting equation and correlation coefficient.

5.4.4 AA degradation kinetics

Figure 50 shows the evolution of the ascorbic acid content in aqueous solutions (pH = 3) irradiated at 25 and 45 ºC. In the same graph, the results for control treatments (with the lamp off) are included. It can be appreciated that the content of ascorbic acid is reduced even under dark conditions regardless of the temperature in the sample. Overall,

Figure 50 shows that, under the temperature and pH conditions, the decrease in the ascorbic acid content as a function of the processing time is very similar for irradiated and not irradiated materials. At 25ºC, the two curves overlap each other, whereas at 45ºC, they are very close. Looking at the errors bars representing the standard deviation of two replicates, it can be supposed that there are not significant differences between the ascorbic acid content in aqueous solutions processed with and without ultraviolet irradiation.

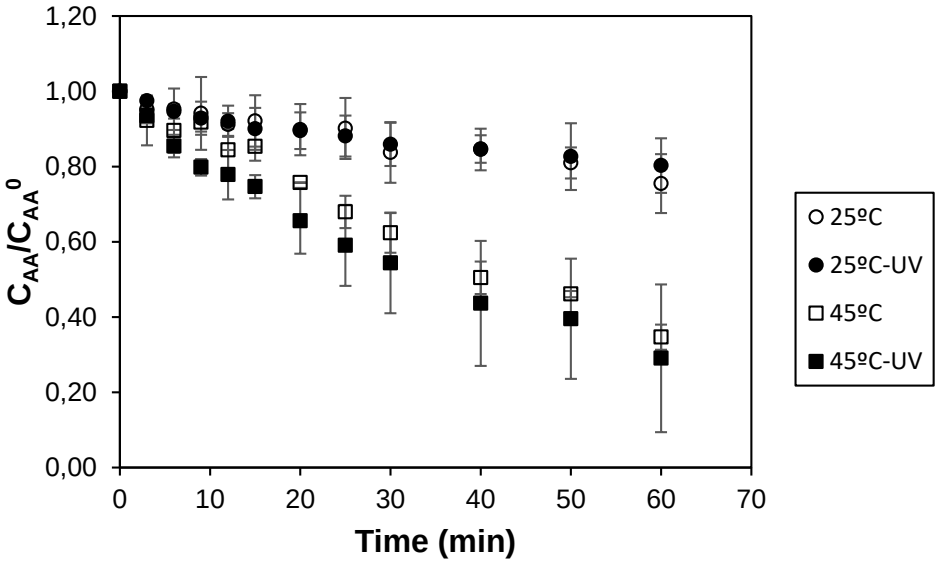

Figure 50. Evolution of AA content in irradiated and non-irradiated aqueous solutions at 25 and 45 ºC (pH = 3, $C_{AA}^0 \approx 250$ mg·L^{-1}).

With the aim of proving that AA decay during UV-treatments is similar than during control treatments, values of the residual ascorbic acid content (C_{AA}/C_{AA}^0) at different irradiation times were compared (Table 25). Then, a comparison of means was performed for each pair of values - irradiated and non-irradiated- under the same conditions. According to the p-values (< 0.05), it cannot be said that the means of the AA levels in irradiated solutions are different to those in solutions maintained in dark conditions. This means that the difference between the AA content in irradiated and non-irradiated samples are due to experimental error. In other words, the AA reduction was very similar in irradiated and non-irradiated aqueous solutions. This behaviour was also observed for solutions at pH 4, 5 and 6.

Table 24. Relative concentrations of ascorbic acid after different processing times in irradiated and non-irradiated aqueous solutions (pH = 3, $C_{AA}^0 \approx 250$ mg·L^{-1}). p-values resulting from comparison of means tests.

T (ºC)	Processing time (min)	C_{AA}/C_{AA}^0		p-value
		UV-Vis processed	Control	
25	30	0.86 ± 0.06	0.84 ± 0.08	0.6065
25	60	0.80 ± 0.07	0.76 ± 0.08	0.5122
45	30	0.55 ± 0.13	0.63 ± 0.05	0.5122
45	60	0.29 ± 0.20	0.35 ± 0.04	0.7362

As widely known, the ascorbic acid molecule is very unstable and is readily oxidized under the influence of light, heat, oxygen and metallic ions. The temperatures used during the treatments are relatively low compared to those employed in traditional thermal treatments for liquid food products. However, the results indicate that ascorbic acid oxidation occurred even at low temperatures and without direct incident radiation. Therefore, it can be supposed that ascorbic acid oxidation was possible due to the presence of metal ions or due to the oxygen dissolved in the solutions. Despite deionized water being used to wash the material and prepare the solutions, it is possible that traces of metal ions remained in the system. According to Gregory (2008), the degradation of AA in the absence of these species hardly takes place in aqueous systems. Moreover, the fact that the solutions were not degasified is a key to explaining the AA degradation observed.

The behaviour revealed in this study disagrees with that reported in similar research. For instance, Tikekar *et al* (2011) did not observe reductions in the ascorbic acid content in model systems mantained in the dark for 200 min. The model systems consisted of aqueous solutions of AA (25-250 mg·L^{-1}) and malic acid (0.5% w/v) at pH of 3.3. In another study, Tran and Farid (2004) detected an incipient degradation of AA in orange juice processed in a descendent film photoreactor with the lamp off. In contrast, the AA degradation in the absence of light observed in this work may be due to the continuous agitation of the samples, which continuously incorporate oxygen into the liquid.

On the contrary, both referred studies concluded that the UV-irradiation greatly influenced the AA degradation. The difference between the results of this work and those reported in the literature may be attributed to the use of a polychromatic emission lamp. Whereas single emission lamps mostly emit at 255 nm, the highest radiant power emitted by the mid-pressure lamp used in this work is close to 410 nm. In addition, the photo-degradation of AA may be enhanced by the presence of other compounds in the systems, e.g. malic acid (Tikekar *et al.*, 2011).

From Figure 51, the effect of the pH on the AA content in aqueous solutions during UV-Vis irradiations can be analysed for the two temperatures assayed. As can be seen, at 25ºC, the degradation increased with the increase in the pH value. Meanwhile, at 45ºC, the reduction in the AA content was similar for the four pH values studied. In addition, a higher degradation can be noted with the increase in the temperature, except for pH=6.

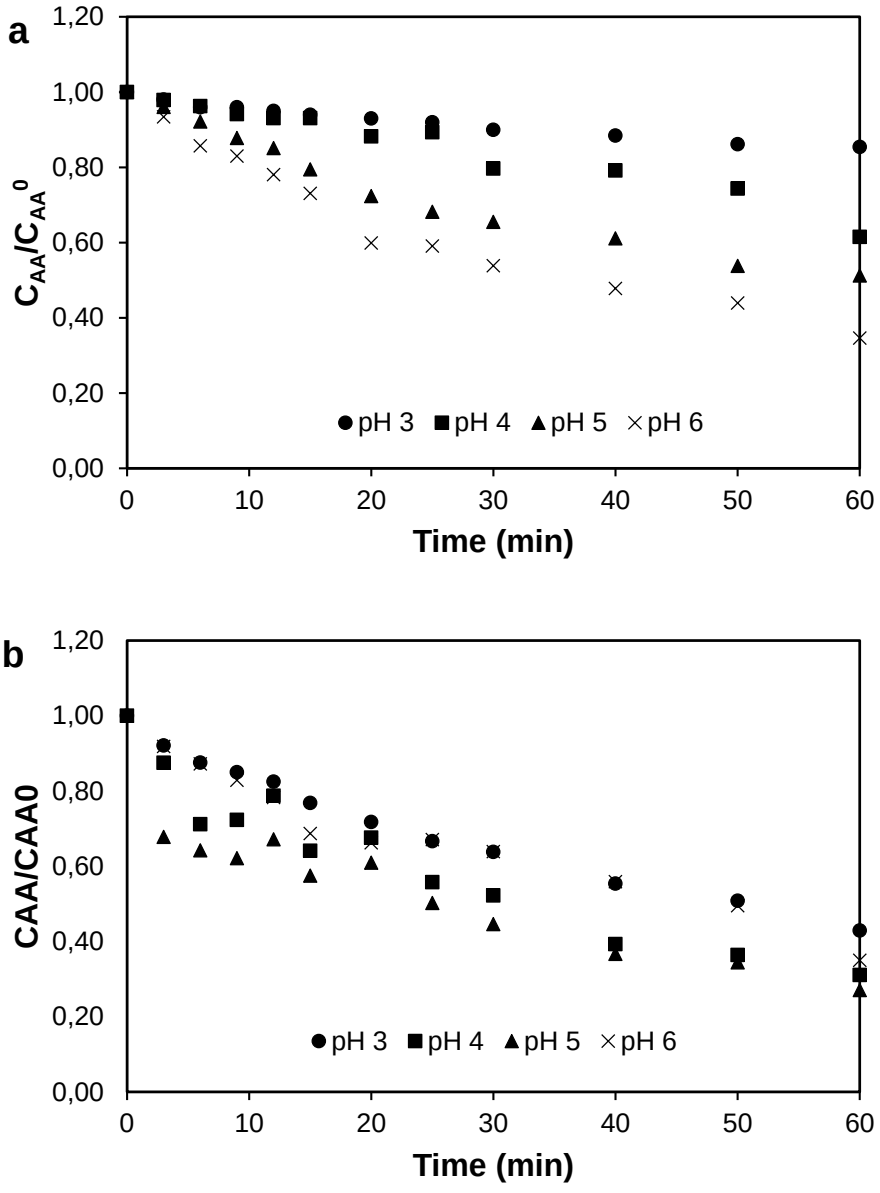

Figure 51. Evolution of AA content in aqueous solutions at different pH values irradiated (a) at 25ºC and (b) at 45ºC.

After 60 min of processing, AA losses between 15 and 65% were reached at 25ºC. Meanwhile, losses between 57 and 73% were reached at 45ºC. The whole decrease in the

AA content with the UV-Vis treatment at room temperature can be compared with the results reported for different fruit juices treated with a similar process. For instance, Falguera *et al.*, (2011d) processed fresh apple juices from different varieties by UV-Vis irradiation. After 120 min, the content of Vitamin C decreased by up to 70% of the initial value. The highest loss was registered for the juice from the King David variety, which showed a pH = 3.48 ± 0.03. On the other hand the vitamin was almost totally retained in juices from the Fuji variety, which showed a pH = 4.29 ± 0.02.

This inconsistency between our results and those in the literature proves that, the AA degradation in fruit juices, induced either by UV-irradiation or by oxidation, is affected by the presence of other compounds. Tikekar *et al.* (2011) proved that the concentration of organic acids, as well as the fructose levels, influence the AA degradation during UV processing of apple juice. Besides, Falguera *et al*. (2011d) suggest that the presence of pigments in juice samples may block the absorption of UV light by other solutes like vitamin C. In addition, the presence of other substances reactive to oxygen like polyphenols could consume part of this gas, reducing the quantity available for the ascorbic acid oxidation.

The decays in the AA content shown in Figure 51a seem to be linear for pH values of 3 and 4, and non-linear for values of 5 and 6. On the other hand, when the temperature in the solutions was maintained at 45ºC, the fall seems to deviate from the linearity for all the pH values assayed. Considering that the degradation was mostly attributed to AA oxidation and not to photo-chemical processes, the empirical models documented for the AA oxidation reaction were used to fit the experimental data. Thus, the first-order kinetic model (Eq. 64) and the fractionate conversion kinetic model (Eq. 65) were assessed. The parameters resulting from these fittings are shown in Table 25 and 26, respectively.

Table 25. Fitting parameters for the first-order kinetic to model AA degradation during UV-Vis irradiation of aqueous solutions under different temperature and pH conditions.

$$\frac{C_{AA}}{C_{AA}^{0}} = e^{-k_O \cdot t}$$

T(ºC)	pH	$k_O \cdot 10^3$ (min^{-1})	R^2
25	3	2.96 ± 0.18	0.8695
	4	6.65 ± 0.36	0.9469
	5	13.19 ± 0.86	0.8990
	6	20.60 ± 1.36	0.9254
45	3	15.13 ± 0.58	0.9691
	4	23.21 ± 2.39	0.7736
	5	28.57 ± 3.52	0.6374
	6	16.85 ± 2.53	0.4806

Table 26. Fitting parameters for the fractionate conversion kinetic to model AA degradation during UV-Vis irradiation of aqueous solutions under different temperature and pH conditions.

$$\frac{C_{AA} - C_{AA}^{\infty}}{C_{AA}^{0} - C_{AA}^{\infty}} = e^{-k_O t}$$

T(ºC)	pH	C_{AA}^{0} (mg·L^{-1})	C_{AA}^{∞} (mg·L^{-1})	$k_O \cdot 10^{-2}$ (min^{-1})	R^2
25	3	255.00 ± 0.90	206.35 ± 5.90	2.16 ± 0.44	0.9889
	4	247.73 ± 4.80	48.92 ± 160.63	0.91 ± 0.98	0.9436
	5	266.93 ± 3.11	108.53 ± 9.21	2.97 ± 0.36	0.9936
	6	252.43 ± 4.64	67.88 ±13.08	3.30 ± 0.52	0.9894
45	3	239.33 ± 2.46	58.55 ± 14.63	2.15 ± 0.31	0.9950
	4	203.86 ± 10.76	35.29 ± 38.02	2.71 ± 1.21	0.9307
	5	214.87 ± 14.43	60.39 ± 31.63	3.79 ± 1.81	0.8695
	6	206.72 ± 10.03	44.79 ± 43.54	2.25 ± 1.10	0.9430

From the fitting parameters listed in Table 25, it can be discussed wether the first-order kinetic model is suitable to describe the decrease in AA content during the treatments. First, it can be seen that the correlation coefficients for solutions processed at 25ºC were equal to or higher than 0.90 at pH values of 4, 5 and 6. This indicates that the AA degradation follows first-order kinetic in that range of pH values. The R^2 at pH = 3 was lower than 0.90, probably because of the small conversion achieved during the 60 min assayed. When the ascorbic acid concentrations are very similar in the aliquots, the measurement error is enhanced. In addition, the rate constants are consistent with the trend in Figure 50a, where the decay is increased with the increase in the pH value.

On the contrary, at 45ºC, the values for R^2 were markedly lower than 0.90 for the pH values of 4, 5 and 6 (Table 25). Meanwhile, for pH=3, the correlation coefficient was higher than 0.98, meaning that the first-order kinetic fitted the AA degradation well under this condition. Despite the low correlation coefficients, the values of the kinetic constants are highly consistent with the trend in the graph. The deviations from the first-order model could be due to the ionization of the L-ascorbic acid molecule at pH conditions higher than the pKa (pK1 = 4.2) (Tikekar et al., 2011). It has been documented that the L-ascorbic oxidation mechanism is initiated with a dissociation of the ascorbate and the oxidation of two electrons, thus, converting L-ascorbic acid into L-dehydroascorbic acid (DHAA) (Gregory, 2008).

On attending the resulting fitting parameters for the fractionate conversion kinetic model (Table 26), it can be seen that the correlation coefficients were higher than those calculated for the first-order model. The other parameters in the mathematical expression can also be discussed. C_{AA}^{0} is the fitted initial concentrations, C_{AA}^{∞} indicates the AA content at equilibrium and k_O is the rate constant. Regarding the kinetic constants at 25ºC, it can be seen that the speed of degradation increases with the pH, except pH = 4.

However, the highest value for C_{AA}^{∞} was obtained under this pH condition, meaning that a high degradation of the vitamin will be achieved after long periods of time. Unfortunately, this pH value close to 4 has been reported in many fruit juices (Falguera *et al.*, 2012b). For that reason, long processing times should be avoided, in addition to performing a deaeration step to limit the oxidation of the ascorbic acid.

On analyzing the kinetic constants at 45ºC in Table 26, the highest values are observed for pH values of 4 and 5. A possible hypothesis to explain this behaviour is that the mild-heating of the samples slightly accelerates the ionization of the L-ascorbic molecule. This hypothesis could also explain the fast initial decrease shown in Figure 50b in the initial period assessed. On the other hand, the values of C_{AA}^{∞} were very similar in all cases. It means that, at 45ºC, the oxidation rate practically hardly depends on the pH. Moreover, the kinetic constants for this kinetic model trend to increase with the increase in the temperature. Nevertheless, the fitting values for C_{AA}^{0}, at 45ºC, are lower than the initial concentration measured (≈250 $mg \cdot L^{-1}$), which indicates a slight deviation from the fractionate conversion kinetic model. In order to obtaine a more accurate mathematical model, the mechanistic model developed by Serpen and Gökmen (2007) could be used. However, the higher simplicity of the fractionate conversion kinetic model would justify its selection to be used to describe the oxidation of ascorbic acid during UV-Vis processing.

5.5 Effect of US processing on the ascorbic acid content

In order to improve the effectiveness of non-thermal technologies used to inactivate microorganisms and enzymes of liquid fruit juices, food technologist have proposed coupling non-thermal methods with mild heating as well as combining different non-thermal methods. Some examples include the use of UV at mild temperatures (Gayán *et al.*, 2013; Sampedro and Fan, 2014), ultrasound at mild temperatures –thermosonication- (Aabid *et al.*, 2013 and 2014; Martínez-Flores *et al.*, 2015; Saeedudin *et al.*, 2015), as well as UV and US as hurdle concept (Santhirasegaram *et al.*, 2015). With the aim of complementing the investigation of the effect of UV irradiation on quality parameters of fruit juices, ultrasound technology was initially explored as an assistant technology for UV processing. Therefore, an experiment was designed to evaluate the effect of a sonication process on the ascorbic content, in both model solutions and real fruit juices. The results obtained are included and discussed below.

First, the relative concentrations of AA obtained in the model solutions at different processing times are plotted in Figure 52. It is interesting that the ascorbic acid content seems to be constant in all cases. In fact, according to the statistical analysis, the processing time showed no significant effect ($p < 0.05$) on the AA concentration for any of the treatments studied. These results indicate that the variations observed may be due to experimental errors and not to processing. As the ascorbic acid content was stable throughout the treatments, including the most severe one (at 55 °C for 60 min), it can be affirmed that neither sonication, the thermal processing at 55ºC, nor thermosonication, were sufficient to degrade a representative number of AA molecules in the degassed aqueous systems.

The AA stability observed in the control treatment (US at 25 °C) was expected, given the low temperature and previous degassing of the solutions. According to the literature, the anaerobic degradation of ascorbic acid is too slow to be significant in the majority of foods (Gregory, 2008). Lima *et al.* (2010) observed that the AA content of degassed samples of cashew apple puree only decreased by 30 % after 120 min of thermal processing at 100 °C. Since AA degradation is more influenced by oxygen concentration than by temperature (Pátkai *et al.*, 2002), the prior degassing of the samples can limit the oxidation reaction, even at high temperatures.

In fact, when non-degassed solutions were subjected to constant agitation (see previous section) an extended decrease of the AA content was observed. This proves that the degradation of this compound in juices is heavily influenced by the presence of air, and this is why the industrial process is set to remove it. On the other hand, this removal is complicated on the laboratory scale, in such a way that many scientific studies cannot do it (in fact, many works even ignore this information), thus compromising their results.

Likewise, the AA stability shown during ultrasound processing may be attributed to the degassing of the preliminary samples. In a previous study, Portenlänger and Heusinger (1992) found that AA degradation by US in aqueous solutions is higher in the presence of air than in its absence. These authors proposed a degradation mechanism based on the reaction of this compound with free radicals ($H^{\bullet}$ and $OH^{\bullet}$), formed by the sonolysis of water.

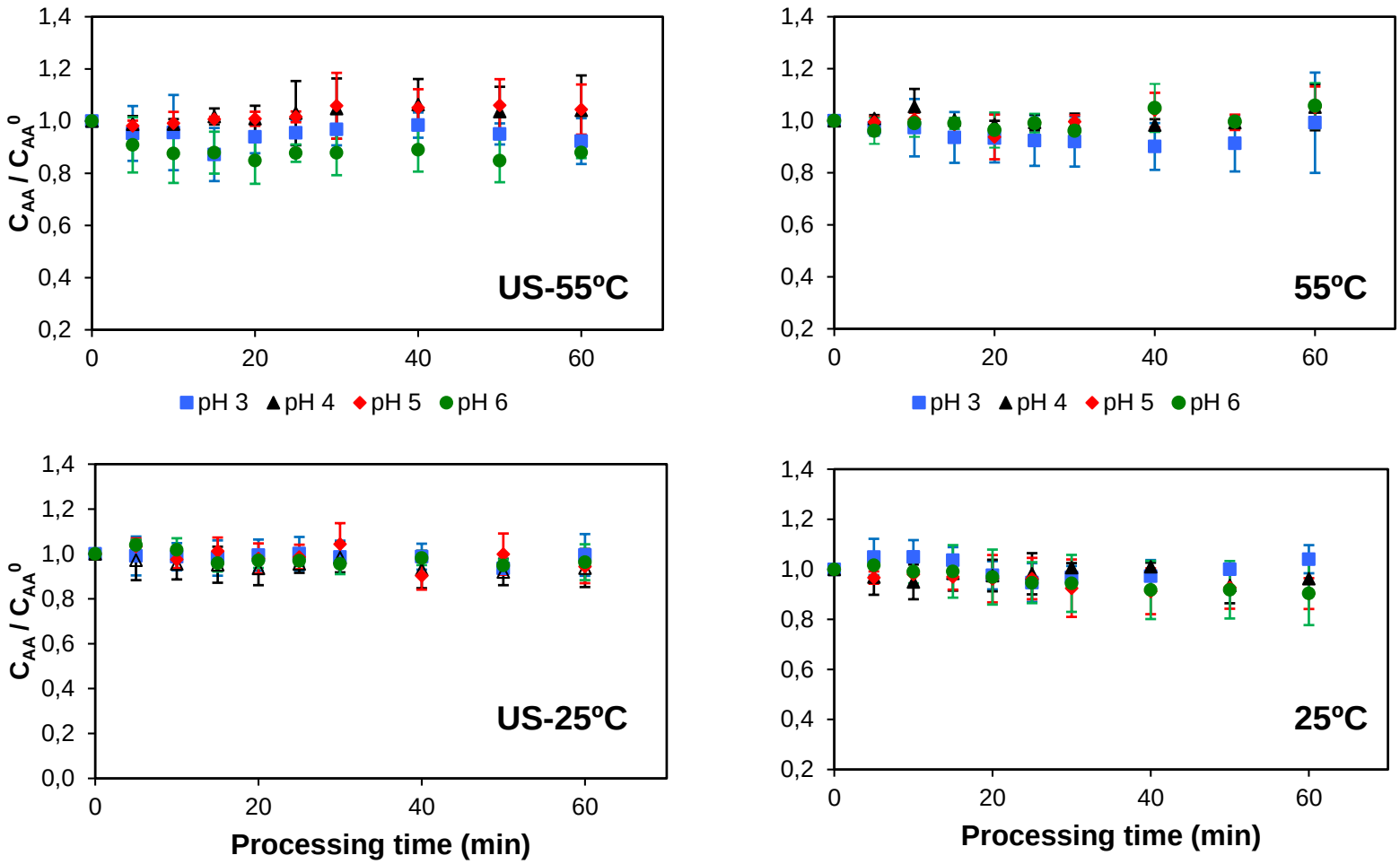

Figure 52. Relative concentrations of ascorbic acid in aqueous solutions at different times of thermosonication (US-55ºC), thermal processing (55ºC), sonication (US-25ºC), or control treatment (25ºC). Mean and standard deviation.

The sono-chemical activity is a consequence of the acoustic cavitation (Mead *et al.*, 1976), i.e. a phenomenon that takes place when sound waves propagate through a liquid, imposing cycles of alternating high and low pressure (Zinoviadou *et al.*, 2015). During the low-pressure periods, the liquid is vaporized and, during the high-pressure periods, it undergoes compression and condenses. The result is the uninterrupted formation of micro-bubbles, the size of which increases thousands of times during the alternation of the pressure cycles. The bubbles that reach a critical size implode violently. Merouani *et al.* (2015) explain that this collapse is quick enough to be nearly adiabatic, rendering each individual bubble a micro-reactor with localized temperatures of up to 5000 K and pressures of up to 50,000 kPa. Under such conditions, molecules trapped in the bubble (water vapour, gases and vaporized solutes) can dissociate and form such reactive species as $H^{\bullet}$, $OH^{\bullet}$, $HO_2^{\bullet}$, $O^{\bullet}$ and H_2O_2.

Thus, it has been shown that the generation of radicals is more intense in air-saturated systems than in those previously degassed by vacuum pressure, ultrasound, or saturation with argon (Yanagida, 2008; Okada *et al.*, 2009; Merouani *et al.*, 2015). This means that, although sonication induces degassing by cavitation of air-saturated systems, this process leads to enhanced free radical production and the consequent oxidation of the ascorbic acid. On the contrary, the radical formation is attenuated in degassed solutions due to the reduced content of air and oxygen, thus explaining the results obtained in this study.

Therefore, prior degassing or deaeration of fruit juices would help to prevent the degradation of ascorbic acid, which could be induced by ultrasound and/or thermal processing. The results obtained also highlight that ultrasound technology can be successfully used for food processing, with or without heating, and for different reasons -including microbial and enzyme inactivation (Abid *et al.*, 2014; Jabbar *et al.*, 2015; Saeeduddin *et al.*, 2015ts), and also promoting desirable changes in the physical properties (Rojas *et al.*, 2016) - without a large impact on the ascorbic acid content. Indeed, this is a very interesting result from an industrial perspective.

With the aim of confirming the stability of ascorbic acid during thermosonication in real liquid food products, two different juices were processed at 55°C, with and without ultrasound. The results from the determination of the ascorbic acid, before and after thermosonication, are graphed in Figure 53. It can be seen that both food products followed the same behaviour observed for the model solutions. The retention of AA

during the treatments was corroborated by the statistical analysis, where the processing time showed no significant effect ($p < 0.05$) on the AA content for any treatment.

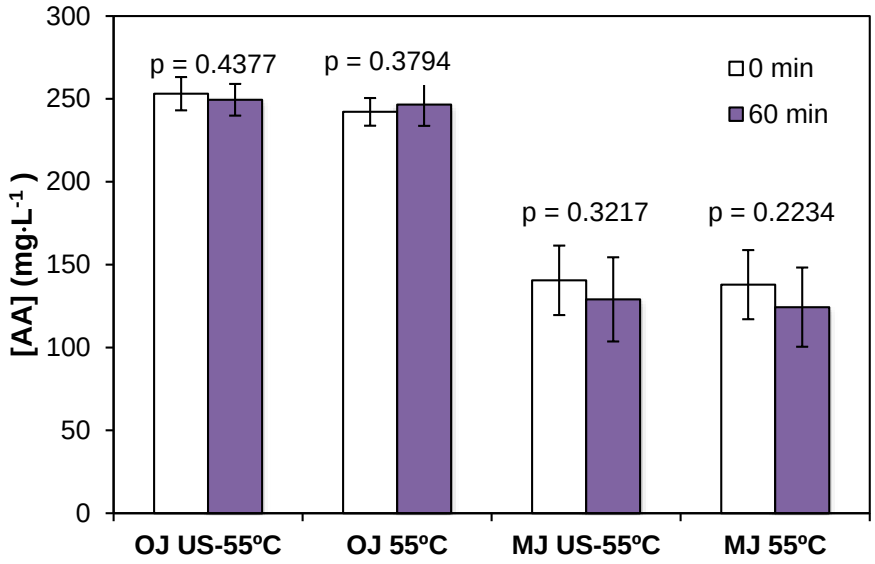

Figure 53. Initial ascorbic acid (AA) content in orange (OJ) and mandarin (MJ) juices, and after thermal (55 °C) or thermosonication processing (US-55 °C) for 60 min. Mean values and standard deviation; p-values from the one-way ANOVA (C_{AA} vs. t).

It is remarkable that the AA stability observed in this study disagrees with the trends observed in some other works (Table 25). According to previous reports, the AA content may increase or decrease depending on the food matrix (Khandpur and Gogate, 2015) or processing conditions (Abid *et al.*, 2014). Even so, it is noteworthy that some of the variability (increase or decrease) is less than 10 %, similar to the results of the present work. The variability in the AA behaviour suggests that different mechanisms act concurrently during processing and that these should be taken into account in order to explain the data collected from the experimental work. These mechanisms are discussed in the following paragraphs.

Release of bioactive components and other intracellular contents. - A number of researchers have reported an increase in the content of bioactive components after the US processing of fruit juices (Zinoviadou *et al.*, 2015). As these bioactive molecules are not synthetized during processing, this effect may be attributed to disruption of the juice cells caused by cavitation, leading to the release of intracellular components (Rojas *et al.*, 2016). In other words, the molecular content does not increase, but its extractability does, increasing the value obtained in the assays. This effect was not observed in the mandarin

and orange juices processed by sonication in this work. Other authors who sonicated orange juice did not report this effect (Tiwari *et al.*, 2009; Valdramidis *et al.*, 2010), probably because this food product has a low content of whole cells.

Table 27. Examples of works describing the effect of sonication or thermosonication on the ascorbic acid content for different fruit juices. Conditions and results reported in the literature.

Fruit juice	Processing conditions	Results	Reference
Orange	US probe (19 mm ∅), 1500 W 20 kHz, 0.30 – 0.81 W·mL^{-1} 25º C, 10 min pulsed	Degradations lower than 5%	Tiwari *et al.*, 2009
Tomato	US probe (19 mm ∅), 1500 W 20 kHz, volumetric power NR 32-45 ºC, 10 min pulsed	Decreased 32%	Adekunte *et al.*, 2010
Watermelon	US probe (19 mm ∅), 1500 W 20 kHz, volumetric power NR 20-45 ºC, 10 min pulsed	Decreased between 8 and 26%	Rawson *et al.*, 2011
Mango	US bath, 130 W 40 kHz, volumetric power NR 25 ºC, 15-60 min	Decreased between 13 and 28%	Santhirasegaram *et al.*, 2013
Orange Sweet lime	US probe (10 mm ∅), 100 W 20 kHz, 0.4 W·mL^{-1} Below 30 ºC, 15 min	Decreased 6% Decreased 36%	Khandpur and Gogate, 2015
Guava	US bath, nominal power NR 35 kHz, volumetric power NR 20 ºC, 30 min	Increased 8%	Cheng *et al.*, 2007
Grapefruit	US bath, 600 W 28 kHz, volumetric power NR 20 ºC, 30-90 min	Increased 14-29%	Aadil *et al.*, 2013
Apple	US bath, nominal power NR 25 kHz, 0.06 W·mL^{-1} 20 ºC, 90 min	Increased 34%	Abid *et al.*, 2013
Apple	US bath, nominal power NR 25 kHz, 0.06 W·mL^{-1} 20 and 60 ºC, 30 min US probe (12.7 mm ∅), 750 W 20 kHz, 0.30 W·mL^{-1} 20 and 60 ºC, 10 min pulsed	Increased 2% at 20ºC Decreased 10% at 60ºC Increased 12% at 20ºC Decreased 7% at 60ºC	Abid *et al.*, 2014
Pear	US probe (12.7 mm ∅), 750 W 20 kHz, volumetric power NR 25 and 65ºC, 10 min	Increased 13% at 25 ºC Decreased 9% at 65 ºC	Saeedudin *et al.*, 2015

US = ultrasound; ∅ = diameter; NR = not reported.

Although the release of bioactive compounds is perceived as a positive effect of sonication in fruit juices, it can result in the oxidation of ascorbic acid. Rojas *et al.* (2016)

describe the cell disruption induced by US on the structure of a peach juice (Fig. 54). The first step of this process leads to the disruption of intracellular structures like plastids, resulting in the release of the intracellular compounds. Under this condition, the contact between AA and the O_2 stored in the cell is favoured by the dispersion of these molecules in the cytoplasm. Thus, it is possible that the AA degradation in fresh juices is initiated from this stage of cell disruption. The degradation can continue when the cell walls break, allowing the dispersion of bioactive compounds into the juice serum, which contains air incorporated during extraction and further handling. In the opposite sense, the industrial deaeration of juices reduces this possibility, which explains why the ascorbic acid in the commercial juices sonicated in this work was not affected.

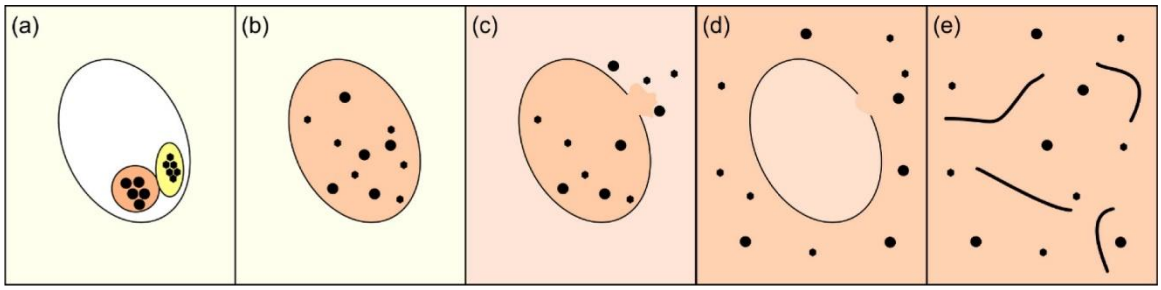

(a) Intact whole cell. (b) Rupture of intracellular structures, such as plastids, with consequent dispersion of molecules into the cytoplasm. (c) Cell wall rupture. (d) Release of intracellular components. (e) Dispersion of components into the serum.
Figure 54. Changes induced by US processing on the structure of cells content in fruit juices (according to Rojas *et al.*, 2016).

Reaction of AA with free radicals.- The sono-chemical degradation of AA has been attributed to the reaction of this compound with free radicals (mainly hydroxyl) (Portenlänger and Heusinger, 1992), whose production is influenced by a number of factors, such as the presence of dissolved gasses (mainly O_2), acoustic power and temperature (Merouani *et al.*, 2015). Tiwari *et al.* (2009) evaluated AA degradation during the sonication of orange juices, relating the degradation rate to the acoustic density power ($W \cdot mL^{-1}$). However, the largest reduction was lower than 5% of the initial value. Furthermore, it is known that the acoustic power, and hence the production of free radicals, decreases with increasing temperature (Raso *et al.*, 1999). Therefore, the retention of ascorbic acid in the mandarin and orange juices (Fig. 50) may be due to a low sono-chemical activity, taking into account the operating temperature (55 °C) and low oxygen concentration in packaged juices.

Aerobic degradation. - The aerobic oxidation of ascorbic acid is a reaction influenced by oxygen and temperature (Pátkai *et al.*, 2002). In fresh juices, oxygen is incorporated during extraction and handling. When these juices are sonicated, this gas may be released inside the cells after the disruption of organelles, or in the serum after whole cell disruption. Therefore, "regular" aerobic oxidation could explain the AA losses described in a number of fresh fruit juices processed by ultrasound (Table 25). It may also explain the greater decreases reported at increasing sonication temperatures (Valdramidis *et al.*, 2010; Abid *et al.*, 2014; Jabbar *et al.*, 2015; Saeeduddin et al., 2015). Despite this, a maximum degradation of 10% was reported after the thermosonication of fresh juices (Table 25), probably due to the US degassing effect. Once again, the stability of AA observed in this work may be related to the low oxygen content in commercial liquid food products.

To sum up, all the ideas presented converge in support of the hypothesis that the preliminary deaerating or degassing of the juice samples avoids the degradation of AA, whether induced by aerobic reactions or by the interaction with free radicals. The deaeration of fruit juices does not represent a technological hindrance, since it is a regular practice in the food industry, carried out either by vacuum deaeration or live steam injection (Nagy, 1980; Belitz *et al*., 2009). Ultrasound degassing, widely used in the laboratory, is obviously not recommended for this purpose, since the AA can be released and degraded when the oxygen content is high. Indeed, it is suggested that US processing should be performed in juices that have already been degassed, in order to reproduce the AA stability observed in this work.

The findings obtained from this study constitute a positive contribution to the US technology, showing that this treatment can be combined with mild thermal processing or other non-thermal technologies in order to inactivate microorganisms and enzymes without altering the ascorbic acid content in liquid fruit products.

CHAPTER 6. CONCLUSIONS

Multi-wavelength UV irradiation, as an emerging technology used to inactivate microorganisms in liquid food products, does not produce 5-hydroxymethylfurfural (HMF) and is a suitable method for its degradation. As HMF absorbs from 230 to 330 nm, any lamp emitting in this wavelength range could produce some degree of photo-degradation regardless of the initial concentration of this compound.

A mechanism for the photo-degradation of 5-hydroxymethylfurfural consisting of a three-stage reaction was proposed. In this mechanism, the magnitude of the photo-chemical change is based on the amount of radiation absorbed by the reactants. The radiation absorbed by an aqueous solution of HMF depends on the concentration of this compound. It increases when the HMF concentration also increases, achieving an asymptotic value that coincides with the incident radiation reaching the surface of the reactor.

Therefore, the photo-degradation kinetic depends on the relation between the absorbed radiation power and the concentration of the solute. For low HMF concentrations, this relation is linear and the kinetic model is of a first-order. For higher concentrations, the relation is also linear but with an origin ordinate different to zero, so the kinetic model becomes a pseudo-first-order. If the slope is significantly lower than the origin ordinate, the absorbed radiation can be assumed as constant and a zero-order kinetic model can be considered.

For concentrations bellow 1 $mg \cdot L^{-1}$, the photo-degradation of HMF fitted to a first-order kinetic model. On the contrary, the degradation fitted well to both zero-order and pseudo-first-order kinetic models when solutions of initial HMF concentrations of 25 were irradiated. For higher concentrations of this compound – between 40 and 100 $mg \cdot L^{-1}$ - the values of the absorbed radiant power barely varied and the results followed a zero-order kinetic.

The photo-degradation of HMF was enhanced with the increase in temperature and pH -at the ranges studied. The optimal conditions were 45ºC and pH=5, reaching a 60% reduction in the initial HMF content after 120 min. Although 45ºC is lower than the traditional temperature used in thermal pasteurization, the formation of by-products should be considered.

The kinetic compensation determined from the Arrhenius equation, and the thermodynamic equation based on the transition state theory, showed that the photo-degradation of HMF is entropy controlled. Therefore, the elimination of 5-

hydroxymethylfurfural can be improved by applying non-thermal treatments like agitation to modify the barriers of the system.

The UV-Vis installation used for juice processing provided an irradiation flux equal to $4.49 \cdot 10^{-2}$ W·cm^{-2}. Part of this radiation corresponds to the germicidal interval (250 to 300 nm), being $2.8 \cdot 10^{-3}$ W·cm^{-2}. Therefore, after 2 h of irradiation, a UV-C radiation dose of 20.16 J·cm^{-2} was provided to the juice samples, this dose being higher than the one needed to achieve the required microbial inactivation in clear juices.

The UV-Vis processing was effective at inactivating the enzymes polyphenol oxidase (PPO) and peroxidase (POD) in nectarine and peach juices. However, the inactivation was partial in the majority of cases when the treatments were performed at room temperature. The inactivation rate of the enzymes studied was increased with the temperature. Consequently, PPO was completely inactivated in all the juices irradiated at 45 ºC whereas considerable reductions of POD were achieved under the same conditions.

Hence, the UV-Vis processing of peach and nectarine juices is useful to prevent enzymatic browning. At the same time, the irradiation process is capable of destroying brown coloured compounds in these juices if the brown substances were formed in a prior juice heating. Moreover, after the ultraviolet processing of nectarine and peach juices, the physicochemical properties -pH, soluble solids content, acidity, formol index and sugar composition- were practically unaltered in the majority of cases. However, when the irradiation was combined with a mild thermal process, slight changes were observed such as small increases in the soluble solids content or incipient degradation of sugars.

Even though not significant variation were observed in the polyphenols content in the majority of the juices irradiated, the effect of UV-light on these bioactive compounds is still unclear and further studied it is recommended.

The rate of degradation of ascorbic acid caused by UV-Vis irradiation was insignificant compared to the oxidation occurring in dark conditions, which followed a fractionate conversion kinetic. On the contrary, sonication did not affect the ascorbic acid content in degassed samples even when the samples were processed at 55ºC. Previous deaeration of fruit juices is recommended in order to prevent vitamin C losses when these products are processed by ultraviolet, ultrasound, mild-heat, or a combination of these treatments.

The UV-Vis processing has been shown to be effective inactivating enzymes in peach and nectarine juices without considerable alterations to their physicochemical and

nutritional attributes and without the formation of undesirable compounds. Therefore, the performance of further experiments at pilot scale in continuous systems is suggested, in order to scale up the findings of this research work.

REFERENCES

A

Abid, M., Jabbar, S., Wu, T., Hashim, M.M., Hu, B. Lei, S. Zhang, X., & Zeng, X. (2013). Effect of ultrasound on different quality parameters of apple juice. *Ultrasonic Sonochemistry*, 20, 1182–1187.

Abid, M., Jabbar, S., Hu, B., Hashim, M.M., Wu, T., Lei, S., Khan, M.A., & Zheng, X. (2014). Thermosonication as a potential quality enhancement technique of apple juice. *Ultrasonic Sonochemistry*, 21, 984–990.

Aadil, R.M., Zeng, X.A., Han, Z., & Sun, D.W. (2013). Effects of ultrasound treatments on quality of grapefruit juice. *Food Chemistry*, 141, 3201–3206.

Adekunte, A.O., Tiwari, B.K., Cullen, P.J., Scannell, A.G.M., & O'Donnell, C.P. (2010). Effect of sonication on color, ascorbic acid and yeast inactivation on tomato juice. *Food Chemistry*, 122, 500–507.

AIJN (Association of the Industry of Juices and Nectars from Fruits and Vegetables of the European Union) (2001). *Code of Practice for Evaluation of Fruit and Vegetables Juices.*

AIJN (European Fruit Juice Association) (2016). *Liquid Fruit Market Report*.

Akillioglu, H.G., Mogol, B.A., Gökmen, V. (2011). Degradation of 5-hydroxymethylfurfural during yeast fermentation. *Food Additives and Contaminants*, 28(12), 1629-1635.

AOAC (2007) International, *Official Methods of Analysis*. 8th ed. AOAC International, Gaithersburg, MD.

Ashurst, P.R. (1999). *Chemistry and Technology of Soft Drinks and Fruit Juices*. Sheffield: Academic Press Ltd.

Augusto, P.E.D., Ibarz, R., Garvín, A., & Ibarz, A. (2015). Peroxidase (POD) and polyphenol oxidase (PPO) photo-inactivation in a coconut water model solution using ultraviolet (UV). *Food Research International*, 74, 151–159.

Awad. T.S., Moharram, H.A., Shaltout, O.E., Asker, D., & Youssef, M.M. (2012). Applications of ultrasound in analysis, processing and quality control of food: A review. *Food Research International*, 48, 410-427.

Azuara, E., & Beristain, C.I. (2006). Enthalpic and entropic mechanisms related to water sorption of yogurt. *Drying Technology*, 24(11), 1501–1507.

Azuara, E., & Beristain, C.I. (2007). Thermodynamic and kinetic study of water adsorption on whey protein. *Revista Mexicana de Ingeniería Química*, 6(3), 359–365.

B

Baltacioğlu, H., Bayindirli, A., & Severcan, F. (2017). Secondary structure and conformational change of mushroom polyphenol oxidase during thermosonication treatment by using FTIR spectroscopy. *Food Chemistry*, 214, 507–514.

Barnes, R., Vogel, H., & Gordon, J. (1969). Temperature of compensation: significance for virus inactivation. *Proceedings of the National Academy of Sciences* (U.S.A.), 62, 263.

Basaran, N., Quintero-Ramos, A., Moake, M. M., Churey, J.J., & Worobo, R.W. (2004). Influence of apple cultivars on inactivation of different strains of *Escherichia coli* O157:H7 in apple cider by UV irradiation. *Applied and Environmental Microbiology*, 70(10), 6061-6065.

Belitz, H.-D., Grosh, W., Schieberle, P. (2009). *Food Chemistry.* Springer-Verlag Berlin Heidelberg.

Beristain, C.I., García, H.S., & Azuara, E. (1996). Enthalpy-entropy compensation in food vapor adsorption. *Journal of Food Engineering*, 30(3), 405–415.

Beristain, C.I., Vernon-Carter, E.J., & Azuara, E. (2011). Thermodynamic and kinetic criteria to study the stability of dried foods. In: *New topics in food engineering*. New York: Nova Science Publishers, Inc.

Bintsis, T., Litopoulou-Tzanetaki, E., & Robinson R.K. (2000). Existing and potential applications of ultraviolet light in the food industry – a critical review. *Journal of the Science of Food and Agriculture*, 80, 637–645.

Brauns, F. (2014). Health aspects of juice consumption. In: *Liquid Fruit Market Report 2014*. AIJN (European Fruit Juice Association).

Burdurlu, H.S., Koca, N., & Karadeniz, F. (2006). Degradation of vitamin C in citrus juice concentrates during storage. *Journal of Food Engineering*, 74(2), 211-216.

C

Chandler, D. (2002). Two faces of water. *Nature*, 417, 491.

Chen, S., Yang, D., Chen, H., & Liu, S. (2009) Effect of hot acidic fructose solution on caramelisation intermediates including colour, hydroxymethylfurfural and antioxidative activity changes. *Food Chemistry*, 114 (2), 582–588.

Cheng, L.H., Soh, C., Liew, S.C., & Teh, F.F. (2007) Effects of sonication and carbonation on guava juice quality. *Food Chemistry*, 104, 1396–1401.

Codex STAN 247–2005. Codex General Standard for Fruit Juices and Nectars.

Chodera, J.D., & Mobley, D.L. (2013). Entropy–enthalpy compensation: role and ramifications in biomolecular ligand recognition and design. *Annual Review of Biophysics*, 42(1), 1–19.

E

EFSA (European Food Safety Authority) (2011).Report of the scientific panel on contaminants in the food chain on provisional findings on furan in food. *EFSA Journal*, 137, 1 –20.

El-Moselhy, M.M. (2009). Photo-degradation of acid red 44 using Al and Fe modified silicates. *Journal of Hazardous Materials*, 169, 498–508.

Esplugas, S., & Vicente, M. (1991). An easy equation to evaluate the direct radiation between a linear source and a plane photoreactor. *Afinidad*, 436, 371-372.

F

Falguera, V., Esplugas, S., Vicente, M., & Ibarz, A. (2011a). Modelling of absorbed radiation profiles in a system composed by a plane photoreactor and a single lamp. *Food Research International*, 44(9), 3111-3114.

Falguera, V., Pagán, J., Garza, S., Garvín, A., & Ibarz, A. (2011b). Ultraviolet processing of liquid food: a review. Part 1: fundamental engineering aspects. *Food Research International*, 44, 1571 –1579.

Falguera, V., Pagán, J., Garza, S., Garvín, A., & Ibarz, A. (2011c). Ultraviolet processing of liquid food: a review. Part 2: effects on microorganisms and on food components and properties. *Food Research International*, 44, 1580 –1588.

Falguera, V., Pagán, J., & Ibarz, A. (2011d). Effect of UV irradiation on enzymatic activities and physicochemical properties of apple juice from different varieties. *LWT – Food Science and Technology*, 44, 115-119.

Falguera, P.V. (2012). *Polyphenol oxidase: Activity, properties of its products and inactivation by innovative technologies*. Doctoral Thesis. Universitat de Lleida. Lleida, Catalonia, Spain.

Falguera, V., Pagán, J., Garza, S., Garvín, A., & Ibarz, A. (2012a). Inactivation of polyphenol oxidase by ultraviolet irradiation: protective effect of melanins. *Journal of Food Engineering*, 110(2), 305– 309.

Falguera, V., Sánchez-Riaño, A.M., Quintero-Cerón, J.P., Rivera-Barrero, C.A., Méndez-Arteaga, J.J., & Ibarz, A. (2012b). Characterization of polyphenol oxidase activity in juices from 12 underutilized tropical fruits with high agroindustrial potential. *Food and Bioprocess Technology*, 5(7), 2921-2927.

Falguera, V., Garza, S., Pagán, J., Garvín, A., & Ibarz, A. (2013a). Effect of UV-Vis irradiation on enzymatic activities and physicochemical properties of four grape musts from different varieties. *Food and Bioprocess Technology*, 6(8), 2223-2229.

Falguera, V., Moulin, A., Thevenet, L., & Ibarz, A. (2013b). Inactivation of peroxidase by ultraviolet-visible irradiation: Effect of pH and melanoidin content. *Food and Bioprocess Technology*, 6(12), 3627-3633.

Falguera, V., Garvín, A., Garza, S., Pagán, J., & Ibarz, A. (2014). Effect of UV-vis photochemical processing on pear juices from six different varieties. *Food and Bioprocess Technology*, 7(1), 84-92.

FDA (Food and Drug Administration) (2000). Irradiation in the production, processing and handling of food. Federal Register – Rules and Regulation, 65, 230.

Flores-Andrade, E, Beristain, C.I., Vernon-Carter, E.J., Gutiérrez, G.F., & Azuara, E. (2009). Enthalpy–entropy compensation and water transfer mechanism in osmotically dehydrated agar gel. *Drying Technology*, 27(9), 999–1009.

G

García, C. F., Moyano, P. C., & Pedreschi, F. (2008). Enthalpy-entropy compensation for water loss of vegetable tissues during air drying. *Drying Technology*, 26(12), 1563–1569.

Garvín, A., Ibarz, R., & Ibarz, A. (2015). Modelling of UV absorption in a plane photoreactor for solutions with high patulin concentration. *Food Research International*, 69, 266–273.

Gayán, E., Monfort, S., Álvarez, I., & Condón, S. (2011). UV-C inactivation of Escherichia coli at different temperatures. *Innovative Food Science and Emerging Technologies*, 12(4), 531-541.

Gayán, E., Serrano, M.J., Monfort, S., Álvarez, I., & Condón, S. (2013) Pasteurization of apple juice contaminated with Escherichia coli by a combined UV-mild temperature treatment. *Food Bioprocess and Technology*, 6, 3006–3016.

Guerrero-Beltrán, J.A., & Barbosa-Cánovas, G.V. (2004). Review: Advantages and limitations on processing foods by UV-light. *Food Science and Technology International*, 10 (3), 137–147.

Guerrero-Beltrán, J.A., Welti-Chanes, J., & Barbosa-Cánovas, G.V. (2009). Ultraviolet-C light processing of grape, cranberry and grapefruit juices to inactivate saccharomyces cerevisiae. *Journal of Food Process Engineering*, 32(6), 916-932.

Guerrero-Beltrán, J.A., & Barbosa-Cánovas, G.V. (2011). Ultraviolet-C light processing of liquid food products. In: *Nonthermal processing technologies for food*. IFT Press & Wiley Blackwell.

Giner-Seguí, J., Bailo-Ballarín, E., Gorinstein, S., & Martín-Belloso, O. (2006). New kinetic approach to the evolution of polygalacturonase (EC 3.2.1.15) activity in a commercial enzyme preparation under pulsed electric fields. *Journal of Food Science*, 71, 262-269.

Gregory III, J.F. (2008). Vitamins. In: *Food Chemistry*, London: CRC Press, Boca Raton.

H

Haddouche, L., Phalak, A., & Tikekar, R.V. (2015). Inactivation of polyphenol oxidase using 254nm ultraviolet light in a model system. *LWT - Food Science and Technology*, 62(1), 97-103.

Hammond, D.A. (1999). Analysis of soft drinks and fruit juices. In: *Chemistry and Technology of Soft Drinks and Fruit Juices*. Sheffield: Academic Press Ltd.

Health Canada (2003). Novel food decisions: ultraviolet light treatment of apple juice/cider using the CiderSure 3500. Ottawa, Ontario, Canada.

Horváth-Kerkai, E., & Stéger-Máté, M. (2012). Manufacturing fruit beverages and concentrates. In: *Handbook of fruits and fruit processing: Second edition.* Willey-Blackwell.

I

Ibarz, A., & Pagán, J. (1986) Calidad de una lámpara para tratamiento de contaminantes en alimentos líquidos. *Alimentaria*, 53–58.

Ibarz, A., Casero, T., Miguelsanz, R., & Pagán, J. (1989). Cinéticas de formación de hidroximetilfurfural en concentrado de zumo de pera almacenado a diferentes temperaturas. *Alimentaria*, 199, 81–84.

Ibarz, A., Panadés, R., Tejero, J.M. (1996). Fotodescomposición de benomilo en solución acuosa. *Afinidad*, 54(461), 53-56.

Ibarz, A., Pagán, J., Panadés, R., & Garza, S. (2005). Photochemical destruction of color compounds in fruit juices. *Journal of Food Engineering*, 69(2), 155–160.

Ibarz, A., Garza, S., Garvín, A., & Pagán, J. (2011). Degradation of mandarin juice concentrates treated at high temperatures. *Journal of Food Process Engineering*, 34(3), 682-696.

Ibarz, A., Garvín, A., & Falguera, V. (2015a) Ultraviolet in food preservation and processing. In: *Conventional and Advanced Food Processing Technologies*. Oxford: Wile Blackwell.

Ibarz, R., Garvín, A., Falguera, V., Pagán, J., Garza, S., & Ibarz, A. (2014). Modelling of patulin photo-degradation by a UV multiwavelength emitting lamp. *Food Research International*, 66, 158 – 166.

Ibarz, R., Garvín, A., Azuara, E., & Ibarz, A. (2015b). Modelling of ochratoxin A photo-degradation by a UV multi-wavelength emitting lamp. *LWT- Food Science and Technology*, 61, 385 –392.

Ibarz, M.R. (2016). *Degradación fotoquímica de compuestos tóxicos en fluidos alimentarios*. Doctoral Thesis. Universitat de Lleida. Lleida, Catalonia, Spain.

Ibarz, R., Garvín, A., Aguilar, K., & Ibarz, A. (2016). Kinetic study and modelling of the UV photo-degradation of thiabendazole. *Food Research International*, 81, 133-140.

ifu-fruitjuice.com/list-of-methods. Consulted on March 9th 2017.

IFU (1986) IFUMA30. Determination of formol number. International federation of fruit juice producers. *Methods of analysis*. Zug-Switzerland, 2001.

IFU (1996a) IFUMA03. Determination of tritratable acidity. International federation of fruit juice producers. *Methods of analysis*. Zug-Switzerland. 2001.

IFU (1996b) IFUMA67. Determination of sugars and sorbitol (HPLC). International federation of fruit juice producers. *Methods of analysis*. Zug-Switzerland. 2001.

Imai, T., & Hirata, F. (2005). Hydrophobic effects on partial molar volume. *Journal of Chemical Physics*, 122(9), 094509.

J

Jabbar, S., Abid, M., Hu, B., Hashim, M.M., Lei, S., Wu, T., & Zeng, X. (2015) Exploring the potential of thermosonication in carrot juice processing. *Journal of Food Science and Technology*, 52, 7002–7013.

Jacob, S.M., & Dranoff, J.S. (1970). Light intensity profiles in a perfectly mixed photoreactor. *AiChE Journal*, 16, 359-363.

Jiménez-Sánchez, C., Lozano-Sánchez, J., Segura-Carretero, A., & Fernández-Gutiérrez, A. (2017). Alternatives to conventional thermal treatments in fruit-juice processing. Part 1: Techniques and applications. *Critical Reviews in Food Science and Nutrition*, 57(3), 501-523.

K

Kaya, Z., Yildiz, S., Ünlütürk, S. (2015). Effect of UV-C irradiation and heat treatment on the shelf life stability of a lemon-melon juice blend: multivariate statistical approach. *Innovative Food Science and Emerging Technologies*, 29, 230-239.

Keklik, N.M., Krishnamurthy, K., & Demirci, A. (2012). Microbial decontamination of food by ultraviolet (UV) and pulsed UV light. In: *Microbial decontamination in the food industry: Novel methods and applications.* Woodhead Publishing.

Keyser, M., Müller, I.A., Cilliers, F.P., Nel, W., & Gows, P.A. (2008) Ultraviolet radiation as a non-thermal treatment for the inactivation of microorganisms in fruit juice. *Innovative Food Science and Emerging Technologies*, 9 (3), 348–354.

Khandpur, P., & Gogate, P.R. (2015). Effect of novel ultrasound based processing on the nutrition quality of different fruit and vegetables juices. *Ultrasonic Sonochemistry*, 27, 125–136.

Koutchma, T., Keller, S., Chirtel, S. & Parisi, B. (2004). Ultraviolet disinfection of juice products in laminar and turbulent flow reactors. *Innovative Food Science and Emerging Technologies*, 5, 179–189.

Koutchma, T. (2009) Advances in ultraviolet light technology for non-thermal processing of liquid foods. *Food and Bioprocess Technology*, 2 (2), 138–155.

Koutchma, T., Popović, V., Ros-Polski, V., Popielarz, A. (2016). Effects of ultraviolet light and high-pressure processing on quality and health-related constituents of fresh juice products. *Comprehensive Reviews in Food Science and Food Safety*, 15, 844-867.

Kraus, A., & Popek, S. (2013). Structural model of fruit juice quality determining factors in product design and development. *British Food Journal*, 115(6), 865-875.

Krug, R., Hunter, W.G., & Grieger, R.A. (1976). Enthalpy-entropy compensation.2—Separation of the chemical from the statistical effect. *Journal of Physical Chemistry*, 80(21), 2341–2351.

Kwak, S.S., Kim, S.K., Lee, M.S. Jung, K.H., Park, I.H., & Liu J.R. (1995) Acidic peroxidases from suspension-cultures of sweet potato. *Phytochemistry*, 39 (5), 981–984.

L

Lee, T.P., Sakai, R., Manaf, N.A., Rodhi, A.M., & Saad, B. (2014). High performance liquid chromatography method for the determination of patulin and 5-hydroxymethylfurfural in fruit juices marketed in Malaysia. *Food control*, 38 (1881), 142–149.

Leffler, J.E. (1955). The enthalpy-entropy relationship and its implications for organic chemistry. *Journal of Organic Chemistry*, 20(9), 1202–1231.

Li, X., & Farid, M. (2016). A review on recent development in non-conventional food sterilization technologies. *Journal of Food Engineering*, 182, 33-45.

Lima, J.R., Elizondo, N.J., & Bohuon, P. (2010) Kinetics of ascorbic acid degradation and colour change in ground cashew apples treated at high temperatures (100–180 °C). International. *Journal of Food Science and Technology*, 45, 1724–1731.

Ling, B., Tang, J., Kong, K., Mitchman, E.J., & Wang, S. (2015) Kinetics of food quality changes during thermal processing: a review. *Food Bioprocess Technology*, 8, 258-343.

Lum, K., Chandler, D., & Weeks, J. D. (1999). Hydrophobicity at small and large length scales. *Journal of Physical Chemistry B*, 103(22), 4570–4577.

M

Manzocco, L., Quarta, B., & Dri, A. (2009). Polyphenoloxidase inactivation by light exposure in model systems and apple derivatives. *Innovative Food Science and Emerging Technologies*, 10, 506–511.

Martínez-Flores, H.E., Garnica-Romo, M.G., Bermúdez-Aguirre, D., Pokhrel, P.R., & Barbosa-Cánovas, G.V. (2014). Physico-chemical parameters, bioactive compounds and microbial quality of thermo-sonicated carrot juice during storage. *Food Chemistry*, 172, 650-656.

Matsui, K.N., Granado, L.M., De Oliveira, P.V., Tadini, C.C. (2007). Peroxidase and polyphenol oxidase thermal inactivation by microwaves in green coconut water simulated solutions. *LWT-Food Science and Technology*, 40, 852-859.

McIlvaine, T.C. (1921) A buffer solution for colorimetric comparison. *Journal of Biology and Chemistry*, 49, 183-186.

McLellan, M.R., & Padilla-Zakour, O.I. (2005). Chapter 4. Juice processing. In: *Processing fruits Science and Technology*. London: CRC Press.

Mead, E.L., Sutherland, R.G., & Verrall, R.E. (1976). The effect of ultrasound on water in the presence of dissolved gases. *Canadian Journal of Chemistry*, 54, 1114–1120.

Mikheev, Y.A., Guseva, L.N., Davydov, E.Y., & Ershov, Y.A. (2007). The hydration of hydrophobic substances. *Russian Journal of Physical Chemistry A*, 81(12), 1897–1913.

Missen, R.W., Mims, C.A., & Saville, B.A. (1999). *Introduction to chemical reaction engineering and kinetics.* New York: Wiley.

Merouani, S., Ferkous, H., Hamdaoui, O., Rezgui, Y., & Guemini, M. (2015). New interpretation of the effects of argon-saturating gas toward sonochemical reactions. *Ultrasonic Sonochemistry*, 23, 37–45.

Morales, F.J. (2009). Hydroxymethylfurfural (HMF) and related compounds. In: *Process-induced Food Toxicants*, New York: John Wiley & Sons, Inc.

Müller, A., Noack, L., Greiner, R., Stahl, M.R., Posten, C. (2014). Effect of UV-C and UV-B treatment on polyphenol oxidase activity and shelf life of apple and grape juices. *Innovative Food Science and Emerging Technologies*, 26, 498–504.

N

NACMCF (National Advisory Committee on Microbiological Criteria for Foods) (2004). Requisite Scientific Parameters for Establishing the Equivalence of Alternative Methods of Pasteurization, Washington, D.C., U.S.A.

Nagy, S. (1980) Vitamin C contents of citrus fruit and their products: a review. *Journal of Agriculture and Food Chemistry*, 28, 8–18.

National Aeronautics and Space Administration, Science Mission Directorate. (2010). Ultraviolet Waves. Retrieved *[March 10th, 2016]*, from NASA Science website: http://science.nasa.gov/ems/10_ultravioletwaves.

O

Official Journal of The European Union (2012). 2001L0112 — EN — 27.04.2012 — 005.001 — 1.

Okada, K., Kudo, N., Hassan, M.A., Kondo, T., Yamamoto, K. (2009). Threshold curves obtained under various gaseous conditions for free radical generation by burst ultrasound – Effects of dissolved gas, microbubbles and gas transport from the air. *Ultrasonic Sonochemistry*, 16, 512–518.

Oke, M., Jacob, J.K., & Paliyath, G. (2012). Biochemistry of fruit processing. In: *Food biochemistry and food processing: Second edition.* Willey-Blackwell.

Oms-Oliu, G., Odriozola-Serrano, I., Soliva-Fortuny, R., Elez-Martínez, P., & Martín-Belloso, O. (2012). Stability of health-related compounds in plant foods through the application of non thermal processes. *Trends in Food Science and Technology, 23*(2), 111-123.

P

Pascual-Pineda, L.A., Flores-Andrade, E., Alamilla-Beltrán, L., Chanona-Pérez, J.J., Beristain, C.I., Gutiérrez-López, G.F., & Azuara, E. (2014). Micropores and their relationship with carotenoids stability: a new tool to study preservation of solid foods. *Food and Bioprocess Technology*, 7(4), 1160–1170.

Pátkai, G., Kormendy, I., & Kormendy-Domján, A. (2002). Vitamin C decomposition kinetics in solutions, modelling citrus juices. *Acta Alimentaria*, 31 (2002), pp. 125–147.

PBH (Products for Better Health Foundation) (2015). State of the Plate, 2015 Study on American Consumption of Fruit & Vegetables.

Piyasena, P., Mohareb, E., & McKellar, R.C. (2003). Inactivation of microbes using ultrasound: a review. *International Journal of Food Microbioogy*, 87(3), 207-216.

Portenlänger, G., & Heusinger, H. (1992). Chemical reactions induced by ultrasound and γ-rays in aqueous solutions of L-ascorbic acid. *Carbohydrate Research*, 232, 291–301.

Pysiak, J., & Sabalski, B. (1979). Compensation effect and isokinetic temperature in thermal dissociation reactions of the type: Asolid ↔ Bsolid+Cgas. *Journal of Thermal Analysis*, 17, 287-290.

Q

Quintero-Ramos, A., Churey, J.J., Hartman, P., Barnard, J., & Worobo, R.W. (2004). Modeling of *Escherichia coli* inactivation by UV irradiation at different pH values in apple cider. *Journal of Food Protection*, 67(6), 1153-1156.

R

Rao, L., Guo, X., Pang, X., Tan, X., Liao, X., Wu, J. (2014). Enzyme Activity and Nutritional Quality of Peach (prunus persica) Juice: Effect of High Hydrostatic Pressure. *International Journal of Food Properties*, 17, 1406-1417.

Raso, J., Mañas, P., Pagán, R., & Sala, F.J. (1999). Influence of different factors on the output power transferred into medium by ultrasound. *Ultrasonic Sonochemistry*, 5, 157–162.

Rawson, A., Tiwari, B.K., Patras, A., Brunton, N., Brennan, C., Cullen, P.J., & O'Donnell, C. (2011). Effect of thermosonication on bioactive compounds in watermelon juice. *Food Research International*, 44, 1168–1173.

Rojas, M.L., Leite, T.S., Cristianini, M., Alvim, I.D., & Augusto, P.E.D. (2015). Peach juice processed by ultrasound technology: Changes in its microstructure improves its physical and properties and stability. *Food Research International*, 82, 22–33.

Ryde, U. (2014). A fundamental view of enthalpy-entropy compensation. *Medicinal Chemistry Communications*, 5, 1324–1336.

S

Saeeduddin, M., Abid, M., Jabbar, S., Wu, T., Hashim, M.M., Awad, F.N., Hu, B., & Lei, S. (2015). Quality assessment of pear juice under ultrasound and commercial pasteurization processing conditions. *LWT- Food Science and Technology*, 64, 452–458.

Sampedro, F., & Fan, X. (2014). Inactivation kinetics and photoreactivation of vegetable oxidative enzymes after combined UV-C and thermal processing. *Innovative Food Science and Emerging Technologies*, 23, 107–113.

Santhirasegaram, V., Razali, Z., & Somasundram, C. (2013). Effects of thermal treatments and sonication on the quality of Chokanan mango (Mangifera indica L.) juice. *Ultrasonic Sonochemistry*, 20, 1276–1282.

Santhirasegaram, V., Razali, Z., & Somasundram, C. (2015). Effects of sonication and ultraviolet-C treatment as a hurdle concept on quality attributes of chokanan mango (mangifera indica L.) juice. *Food Science and Technology International*, 21(3), 232-241.

Sapei, L., & Hwa, L. (2014). Study on kinetics of vitamin C degradation in fresh strawberry juices. *Procedia Chemistry*, 9, 62-68.

Sastry, S.K., Datta, A.K., & Worobo, R.W. (2000). Ultraviolet light. *Journal of Food Science*, 65, s8, 90-92.

Serpen, A., & Gökmen, V. (2007). Reversible degradation kinetics of ascorbic acid under reducing and oxidizing conditions. *Food Chemistry*, 124, 721-725.

Shaghaghi, M., Manzoori, J.L., & Jouyban, A. (2008). Food Chemistry Determination of total phenols in tea infusions, tomato and apple juice by terbium sensitized fluorescence method as an alternative approach to the Folin – Ciocalteu spectrophotometric method. *Food Chemistry*, 108, 695–701.

Shama, G, C., Peppiatt, C. & Biguzzi, M. (1996). A novel thin film photoreactor. *Journal of Chemical Technology and Biotechnology*, 65, 56–64.

Soares, M.V.L., Alves Filho, E.G., Silva, L.M.A., Novotny, E.H., Canuto, K.M., Wurlitzer, N.J., Narain, N., & de Brito, E.S. (2017). Tracking thermal degradation on passion fruit juice through nuclear magnetic resonance and chemometrics. *Food Chemistry*, 219, 1-6.

Southgate, D.A.T., Johnson, I.T., & Fenwick, G.R. (1995). Nutritional value and safety of processed fruit juices. In: *Production and Packaging of Non-Carbonated Fruit juices and Fruit Beverages*. Second Edition. Glasgow: Chapman & Hall.

Starikov, E.B., Nordén, B. (2012). Entropy–enthalpy compensation as a fundamental concept and analysis tool for systematical experimental data. *Chemical Physics Letters*, 538, 118-120.

Sun, D., & Wicker, L. (1999). Kinetic compensation and the role of cations in pectinesterase catalysis. *Journal of Agricultural and Food Chemistry*, 47(4), 1471–1475.

T

Tikekar, R.V., Anantheswaran, R.C., & LaBorde, L.F. (2011). Ascorbic acid degradation in a model apple juice system and in apple juice during ultraviolet processing and storage. *Journal of Food Science*, 76(2), H62-H70.

Tiwari, B.K., Muthukumarappan, K., O'Donell, C.P., & Cullen, P.J. (2008). Effects of sonication on the kinetics of orange juice quality parameters. *Journal of Agricultural and Food Chemistry*, 56(7), 2423-2428.

Tiwari, B.K., O'Donnell, C.P., Muthukumarappan, K., Cullen, P.J. (2009). Ascorbic acid degradation kinetics of sonicated orange juice during storage and comparison with thermally pasteurised juice. *LWT- Food Science and Technology*, 42, 700–704.

Tomas-Barberán, F.A., & Espin, J.C. (2001). Phenolic compounds and related enzymes as determinants of quality in fruits and vegetables. *Journal of the Science of Food and Agriculture*, 81, 853-876.

Tran, T.T.M., & Farid M.M. (2004). Ultraviolet treatment of orange juice. *Innovative Food Science and Emerging Technologies*, 5, 495–502.

Tribst, A.A.L., De Souza Santana, A., & De Massaguer, P.R. (2009). Review: Microbiological quality and safety of fruit juices. Past, present and future perspectives microbiology of fruit juices. *Critical Reviews in Microbiology*, 35(4), 310-339.

U

Unluturk, S.K., Arastoopour, H., Koutchma, T. (2004). Modeling of UV dose distribution in a thin-film UV reactor for processing of apple cider. *Journal of Food Engineering*, 65, 125-136.

Unluturk, S., & Atilgan, M.R. (2015). Microbial safety and shelf life of UV-C treated freshly squeezed white grape juice. *Journal of Food Science*, 80(8), M1831-M1841.

V

Valdramidis, V.P., Cullen, P.J., Tiwari, B.K., & O'Donnell, C.P. (2010). Quantitative modelling approaches for ascorbic acid degradation and non-enzymatic browning of orange juice during ultrasound processing. *Journal of Food Engineering*, 96, 449–454.

Vieira, M., Teixeira, A.A., Silva, C.L.M. (2000). Mathematical modeling of the thermal degradation kinetics of vitamin C in cupuaçu (*Theobroma grandiflorum*) nectar. *Journal of Food Engineering*, 43, 1-7.

Vinatoru, M. (2015). Ultrasonic assisted extraction (UAE) of natural products some guidelines for good practice and reporting. *Ultrasonic Sonochemistry*, 25, 94-95.

W

Walking-Ribero, M., Noci, F., Riener, J., Cronin, D.A., Lyng, J.G., & Morgan, D.J. (2009). The impact of thermosonication and pulsed electric fields on *Staphylococcus aureus* inactivation and selected quality parameters in orange juice. *Food and Bioprocess Technology*, 2, 422-430.

Wardle, B. (2009). *Principles and Applications of Photochemistry*. Sussex: John Wiley & Sons, Ltd.

Wibowo, S., Grauwet, T., Santiago, J.S., Tomic, J., Vervoort, L., Hendrickx, M., & Loey, A.V. (2015). Quality changes of pasteurised orange juice during storage: A kinetic study of specific parameters and their relation to colour instability. *Food Chemistry*, 187, 140-151.

Wilfong, E.M., Kogiso, Y., Muthukrishnan, S., Kowatz, T., Du, Y., Bowie, A., Naismith, J.H., Hadad, C.M., Toone, E.J., & Gustafson, T.L. (2011). A multidisciplinary approach to probing enthalpy-entropy compensation and the interfacial mobility model. *Journal of the American Chemical Society*, 133, 11515–11523.

Williams, D.H., O'Brien, D.P., & Bardsley, B. (2001). Enthalpy/entropy compensation as a competition between dynamics and bonding: the relevance to melting of crystals and biological aggregates. *Journal of American Chemical Society*, 123(4), 737–738.

Wright, J.R., Sumner, S.S., Hackney, C.R., Pierson, M.D., & Zoecklein, B.W. (2000). Efficacy of ultraviolet light for reducing *Escherichia coli* O157:H7 in unpasteurized apple cider. *Journal of Food Protection*, 63(5), 563-567.

Y

Yi, J., Kebede, B.T., Dhang, D.N., Buvé, C., Grauwet, T., Loey, A.V., Hu, X., Hendrickx, M. (2017). Quality change during high-pressure processing and thermal processing of cloudy apple juice. *LWT- Food Science and Technology*, 75, 85-92.

Yanagida, H. (2008). The effect of dissolve gas concentration in the initial growth stage of multi cavitation bubbles. Differences between vacuum degassing and ultrasound degassing. *Ultrasonic Sonochemistry*, 15, 492–496.

Yerlitürk, F.Ü., Arslan, O., Sinan, S., Gencer, N., Özenzoy, G.O. (2008). Characterization of polyphenoloxidase from wild pear (*Pyrus elaegrifolia*). *Journal of Food Biochemistry*, 32, 368–383.

Z

Zinoviadou, K., Galanakis, C., Brnčić, M., Grimi, N., Boussetta, N., Mota, M.N., Saraiva, J.A., Patras, A., Tiwari, B., & Barba, F.J. (2015). Fruit juice sonication: Implications on food safety and physicochemical and nutritional properties. *Food Research International*, 77, 743–752.

Zsako, J. (1976). The kinetic compensation effect. *Journal of Thermal Analysis*, 9, 101-108.

AGRADECIMIENTOS

Ya que un trabajo de investigación así como su conclusión en forma de tesis requieren de la colaboración de otros científicos, quisiera agradecer a los doctores que contribuyeron a la revisión y discusión de las ideas presentadas en este trabajo.

En primer lugar a los profesores Albert Ibarz Ribas y Alfonso Garvín Arnés, por la precisa dirección de este trabajo, por la paciencia para indicarme mis errores y vicios, por valorar mi esfuerzo, reconocer mis logros y sobre todo por su disposición para compartir su conocimiento.

Al Profesor Pedro Esteves Duarte Augusto, por ser un buen colega, orientador, anfitrión y amigo. Por alentarme a buscar nuevas metas profesionales, compartir su particular punto de vista sobre el quehacer científico y sobre todo por compartir una taza de café.

A los expertos externos que evaluaron esta tesis, Ebner Azuara Nieto y Raúl Siche Jara, por evaluar mi trabajo y su tiempo invertido en la revisión.

A los doctores Víctor Falguera Pascual, Manoel Divino Mata, Cyndia Azucena González Arias, Janeth Rodríguez Roque, Rogelio Sánchez Vega y Harry Barragán por su amistad y consejos.

También quisiera reconocer la colaboración de las colegas del laboratorio, Shirley Estefany Rojas Torres y la Maestra en Ciencias Maricela Santiago Santiago, por su compañía en las largas jornadas de laboratorio y por sus puntos de vista. De igual manera, a los doctorandos Guillermo Valdivia Nájer, Mariona Vendrell Pacheco y Mauro Junio de Vasconcelos por el intercambio de ideas y experiencias.

Además, quiero agradecer a Dios y a las personas que él puso en mi camino para alcanzar esta meta:

En primer lugar a mi madre, la Lic. Rosalba Lara Sagahón, por ser un ejemplo a seguir y apoyarme incansablemente en todos los aspectos de mi vida.

A los científicos de la familia, los doctores Alma Virginia Lara Sagahón, Enrique Núñez Lara, y sus cónyuges, por motivarme a seguir estudiando. Más a Vicky por inducirme a la ciencia desde mi niñez.

A los colegas que me ayudaron de alguna manera.

A las Mexicanas en Lleida, Liza, Rosa Ángela, Rosángela y Mary Paz, por su compañía en las buenas y en las malas.

Al personal administrativo, de limpieza y del bar de la ETSEA.

Así mismo quiero agradecer a las personas de Lleida que me recibieron con mucho cariño, en especial a Laura y a Carmen. También a todos los amigos que conocí durante esta aventura de cuatro años. A Esther-Harry, Martín, Rochelle-Mauro y Janeth-Rogelio por ser mi familia en estas tierras lejanas.

Finalmente, agradezco a España y Brasil por recibirme y mostrarme su cultura.